

One-loop central-emission vertex for two gluons in $\mathcal{N} = 4$ super Yang-Mills theory

Emmet P. Byrne,^a Vittorio Del Duca,^{b,c,1} Lance J. Dixon,^d Einan Gardi^a
and Jennifer M. Smillie^a

^a*Higgs Centre for Theoretical Physics, School of Physics and Astronomy, The University of Edinburgh, Edinburgh EH9 3FD, Scotland, UK*

^b*Institute for Theoretical Physics, ETH Zürich, 8093 Zürich, Switzerland*

^c*Physik-Institut, Universität Zürich, 8057 Zürich, Switzerland*

^d*SLAC National Accelerator Laboratory, Stanford University, Stanford, CA 94309, USA*

E-mail: Emmet.Byrne@ed.ac.uk, delducav@itp.phys.ethz.ch,
lance@slac.stanford.edu, Einan.Gardi@ed.ac.uk, J.M.Smillie@ed.ac.uk

ABSTRACT: A necessary ingredient for extending the BFKL equation to next-to-next-to-leading logarithmic (NNLL) accuracy is the one-loop central emission vertex (CEV) for two gluons which are not strongly ordered in rapidity. Here we consider the one-loop six-gluon amplitude in $\mathcal{N} = 4$ super Yang-Mills (SYM) theory in a central next-to-multi-Regge kinematic (NMRK) limit, we show that its dispersive part factorises in terms of the two-gluon CEV, and we use it to extract the one-loop two-gluon CEV for any helicity configuration within this theory. This is a component of the two-gluon CEV in QCD. Although computed in the NMRK limit, both the colour structure and the kinematic dependence of the two-gluon CEV capture much of the complexity of the six-gluon amplitudes in general kinematics. In fact, the transcendental functions of the latter can be conveniently written in terms of impact factors, trajectories, single-emission CEVs and a remainder, which is a function of the conformally invariant cross ratios which characterise the six-gluon amplitudes in planar $\mathcal{N} = 4$ SYM. Finally, as expected, in the MRK limit the two-gluon CEV neatly factorises in terms of two single-emission CEVs.

KEYWORDS: QCD, BFKL, Regge limit

¹On leave from INFN, Laboratori Nazionali di Frascati, Italy.

Contents

1	Introduction	1
2	The building blocks of the BFKL equation	5
2.1	Building blocks at LL accuracy	6
2.2	Building blocks at NLL accuracy	8
2.3	Building blocks at NNLL accuracy	11
3	The two-gluon central-emission vertex at tree level	12
3.1	A minimal set of variables	14
3.2	BCFW representations	16
3.3	Other colour orderings	19
3.4	The target-projectile exchange	22
4	The two-gluon central-emission vertex at one loop	23
4.1	Same-helicity vertex	27
4.2	Opposite-helicity vertex	35
4.3	NLO $gg \rightarrow gggg$ squared matrix element in the central NMRK limit	42
5	All-orders conjectures for amplitudes in a central NMRK limit	45
6	Conclusions	48
A	Kinematic regions	50
A.1	General multi-parton kinematics	50
A.2	Multi-Regge kinematics	52
A.3	Central next-to-multi-Regge kinematics	53
B	Lorentz invariant quantities in minimal coordinates	55
B.1	Cross ratios in the NMRK limit	56
C	The power-suppressed helicity configurations	58
D	NMHV amplitudes in general kinematics	59
D.1	Tree-level six-gluon NMHV amplitudes	59
D.2	One-loop six-gluon NMHV amplitudes in $\mathcal{N} = 4$ SYM	60
E	Additional forms of the opposite-helicity central-emission vertex	61
E.1	BCFW representation for the ordering $\sigma_{A'}$	62
F	Absorptive part of the one-loop six-gluon amplitude in NMRK	63

G	Kinematic limits of the two-gluon central-emission vertex	69
G.1	MRK limit	70
G.2	Soft limits	71
G.3	Collinear limits	76

1 Introduction

In the Regge limit, in which the squared centre-of-mass energy s is much larger than the momentum transfer $|t|$, $s \gg |t|$, any $2 \rightarrow 2$ scattering process is dominated by the exchange in the t channel of the highest-spin particle. In the case of QCD or $\mathcal{N} = 4$ Super Yang-Mills (SYM) theory, that implies the exchange of a gluon in the t channel. Contributions that do not feature gluon exchange in the t channel are power suppressed in t/s . Building upon this feature, the Balitsky-Fadin-Kuraev-Lipatov (BFKL) equation describes strong-interaction processes with two large and disparate scales, $s \gg |t|$, by resumming the radiative corrections to parton-parton scattering to all orders at leading logarithmic (LL) [1–4] and next-to-leading logarithmic (NLL) accuracy [5–8] in $\log(s/|t|)$. The resummation of large energy logarithms extends to higher-multiplicity final states in special kinematic limits and improves the description of scattering events where large rapidity intervals are spanned [9–15]. In the last decade or so, the Regge limit has been explored extensively in both $\mathcal{N} = 4$ SYM [16–21] and QCD [22–26] amplitudes and cross sections [27, 28]. Furthermore, owing to its relative simplicity, it has been used to constrain, compute or validate amplitudes in general kinematics [26, 29–36].

The BFKL equation [1–4] describes rapidity evolution in terms of an integral of the gluon propagator exchanged in the t channel over all transverse momenta. The kernel of this integral equation consists of two elements, which are described schematically in fig. 1 and which we review in section 2.1: a virtual component corresponding to the Regge trajectory, which first occurs in the one-loop $2 \rightarrow 2$ scattering amplitude at LL accuracy in $\log(s/|t|)$ (fig. 1(a)), and a real component involving the emission of a gluon into the final state. The latter involves a vertex termed the Lipatov or *central-emission vertex* (CEV), which first occurs in the tree-level $2 \rightarrow 3$ amplitude in multi-Regge kinematics (MRK) (fig. 1(b)), where the outgoing partons are strongly ordered in light-cone momentum, or equivalently in rapidity. Upon integrating the BFKL evolution equation one thus resums corrections in which all emissions are ordered in rapidity, forming the famous ladder graphs. At LL accuracy, each gluon emission along the ladder introduces a factor of $\mathcal{O}(\alpha_s \log(s/|t|))$ after rapidity integration. The impact factors, eq. (2.2), are not part of the gluon ladder, but sit at its ends. In fig. 1, they are represented by the green blobs. When they are squared, they constitute the jet impact factors and contribute to jet cross sections at LL accuracy [9–12, 14].

The $2 \rightarrow 2$ scattering amplitudes at LL accuracy are real-valued, and the terms of $\mathcal{O}(\alpha_s^n \log^n(s/|t|))$ exponentiate, manifesting the phenomenon of *gluon Reggeization* [37]. The hard scattering is effectively mediated by the t -channel exchange of a *single* Reggeized

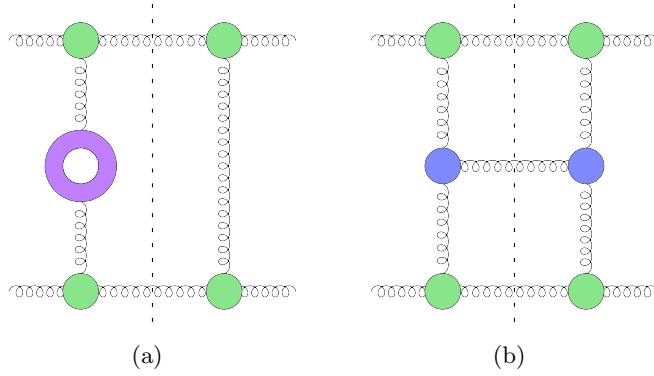


Figure 1. Interference diagrams which contain the building blocks required for constructing the BFKL equation at LL accuracy: (a) gluon Regge trajectory at one loop; (b) one-gluon central emission vertex at tree level. Tree-level impact factors (shown in green) are required for the computation of cross sections, but are not required to determine the evolution of the t -channel Reggeon.

gluon, or Reggeon, carrying an octet colour charge, just as at tree level, and it gives rise to a Regge pole in the complex angular momentum plane.

The BFKL equation has been extended to next-to-leading logarithmic (NLL) accuracy [5–8], allowing one to resum the terms of $\mathcal{O}(\alpha_s^n \log^{n-1}(s/|t|))$ [38, 39]. This generalization involves next-to-leading-order corrections to the BFKL kernel, consisting of three elements, which are depicted schematically in fig. 2: two-loop corrections to the Regge trajectory [40–44] (fig. 2(a)), one-loop corrections to the central emission vertex [45–49] (fig. 2(b)), which we review in section 2.2, and a new tree-level vertex function for the emission of two gluons (fig. 2(c)) (or of a quark-antiquark pair) that are *not* strongly ordered in rapidity [50–54], which we review in section 3. The latter requires the evaluation of a

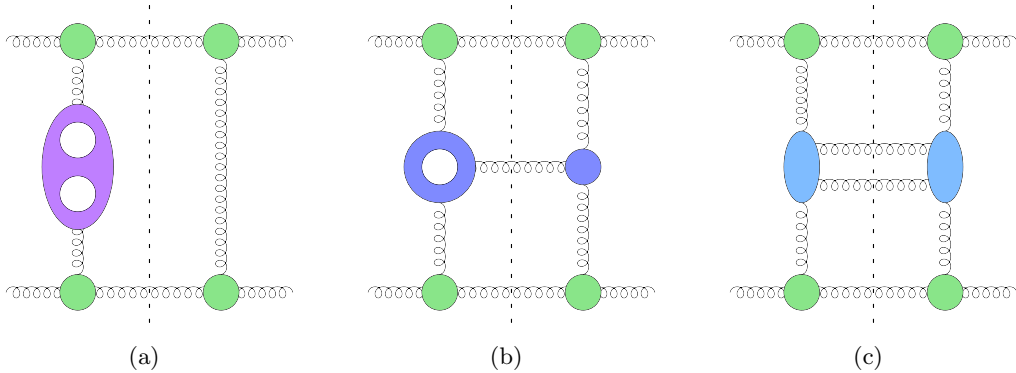


Figure 2. Interference diagrams which contain the building blocks required for constructing the BFKL equation at NLL accuracy: (a) gluon Regge trajectory at two loops; (b) one-gluon central-emission vertex at one loop; (c) two-gluon central emission vertex at tree level.

six-parton tree-level amplitude in the so-called next-to-multi-Regge kinematics (NMRK), in which the outgoing partons are strongly ordered in rapidity except for two gluons (or a quark-antiquark pair) emitted centrally off the gluon ladder. When these are integrated in

rapidity, they yield a factor of $\mathcal{O}(\alpha_s^2 \log(s/|t|))$, thus contributing at NLL accuracy. Crucial to carrying out the BFKL program at NLL accuracy is the fact that the real part – or more precisely, the $s \leftrightarrow u$ signature-odd part – of the $2 \rightarrow 2$ amplitude is still described by the exchange of a single Reggeized gluon [38, 39]. Note that the same is not true for the imaginary (signature even) part of the amplitude, which is governed by the exchange of a pair of Reggeized gluons [22, 24, 25].

In order to compute jet cross sections at NLL accuracy [13, 15] through the BFKL equation, jet impact factors at next-to-leading order (NLO) in α_s [55, 56] are required. They are based on the one-loop impact factor [45, 49, 57–59], eq. (2.18), and the impact factor for the emission of two gluons or of a quark-antiquark pair [50–54, 60], evaluated in the NMRK in which the gluons are strongly ordered in rapidity except for two partons emitted at one end of the ladder.

Extending the BFKL equation to next-to-next-to-leading logarithmic (NNLL) accuracy faces additional challenges¹. Chief amongst these is the fact that starting at this logarithmic order, the real part of $2 \rightarrow 2$ amplitudes is not anymore governed by a single Reggeized gluon. Instead, it also involves contributions from three Reggeon exchange [24, 26, 44, 64–66] and the mixing of the latter with a single Reggeon. These give rise to a Regge cut as well as a Regge pole in the complex angular momentum plane. This makes the determination of the three-loop Regge trajectory, characterizing the Regge-pole term, a subtle problem, as it requires to disentangle Regge pole and cut contributions, see e.g. [24, 64, 67]. Recently this problem has been resolved [26, 68] and the three-loop Regge trajectory in QCD has been determined [36, 68, 69]. This gives some hope that the analytic structure of amplitudes in the Regge limit can be understood beyond NLL accuracy also in the multi-leg case, and indeed that the BFKL programme could eventually be extended to NNLL and beyond.

Carrying out the BFKL program at NNLL accuracy one needs, in addition to the three-loop Regge trajectory (fig. 3 (a)), which has recently been determined [36, 68, 69], various corrections to the central emission vertex. These are described schematically in fig. 3 and include the following elements: the emission vertex of three partons along the gluon ladder [60, 70, 71] (fig. 3 (e)), which have been obtained by evaluating seven-parton tree-level amplitudes in next-to-next-to-multi-Regge kinematics (NNMRK); the square of the one-loop correction to the emission vertex of one gluon (fig. 3 (c)); the one-loop correction to the emission vertex of two gluons (fig. 3 (d)) or of a quark-antiquark pair along the gluon ladder; and the two-loop correction to the central-emission vertex of one gluon (fig. 3 (b)). The latter two contributions are yet to be determined. In this paper, we compute the one-loop corrections to the central-emission vertex of two gluons in $\mathcal{N} = 4$ SYM. Utilizing the supersymmetric decomposition of QCD loop amplitudes [72–74], the $\mathcal{N} = 4$ result is a first step toward the determination of the same quantity in QCD. To this end we use the one-loop six-gluon amplitudes in $\mathcal{N} = 4$ SYM based on refs. [73, 74]. By considering the appropriate NMRK kinematic limit of these amplitudes and comparing the result with a Regge-factorized form, we extract the two-gluon central-emission vertex in both the same

¹The BFKL equation has been extended to NNLL [61, 62] and to N³LL accuracy [63] in planar $\mathcal{N} = 4$ SYM theory.

helicity and opposite helicity configurations.

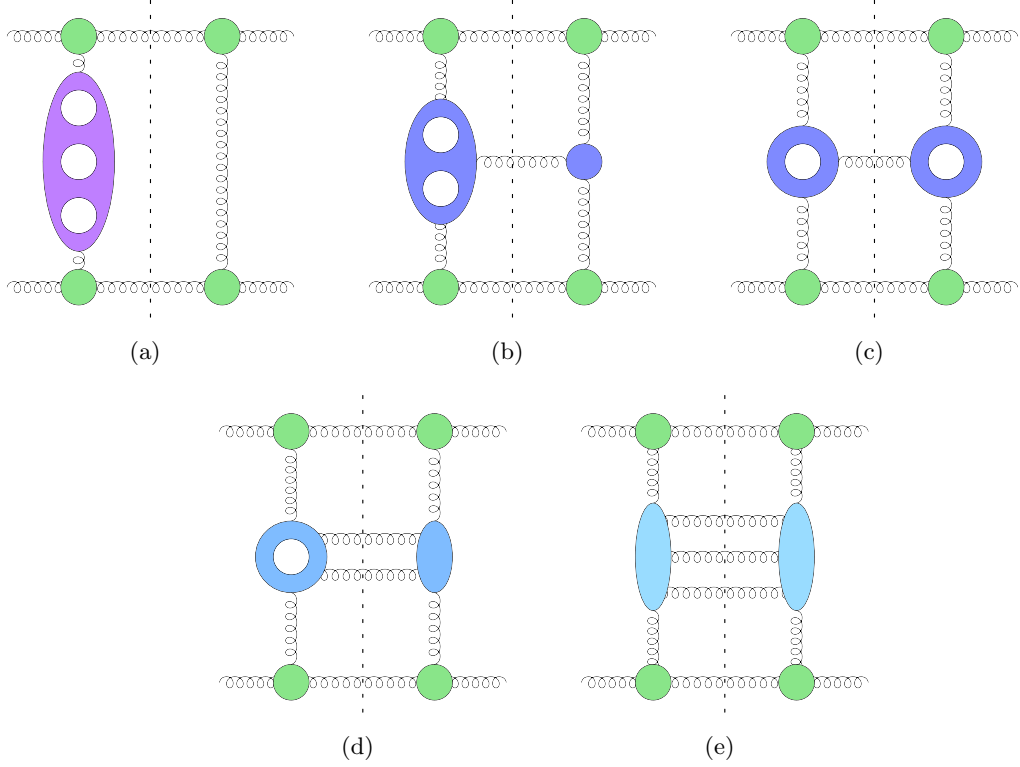


Figure 3. Interference diagrams which contain the building blocks required for constructing the BFKL equation at NNLL accuracy: (a) gluon Regge trajectory at three loops; (b) one-gluon CEV at two loops; (c) self-interference of one-gluon CEV at one loop; (d) two-gluon CEV at one loop; (e) three-gluon CEV at tree level.

An important motivation for our investigation, besides the extension of the BFKL program, stems from the potential of the NMRK limit to unravel the analytic structure (as well as the colour structure) of multi-leg amplitudes. Indeed, direct analytical evaluation of multi-leg amplitudes in general kinematics at one-loop level is highly demanding, and the extension to two loops and beyond is ever more so. Even when such amplitudes are known, bringing them to a compact form and evaluating them efficiently are in general unsolved problems, which are of high interest both from a theoretical perspective and because of their immediate relevance to precision collider physics. Understanding the behaviour of amplitudes in various limits, where drastic simplifications occur, is a key strategy towards understanding them in general kinematics. Specifically, in the MRK limit one-loop amplitudes are very simple indeed: they are proportional to the tree amplitude, and involve simple kinematic dependence on the transverse momenta of the emitted gluons. We shall see that the NMRK limit of six gluon amplitudes (already in $\mathcal{N} = 4$ SYM) features several new aspects compared to MRK, including new colour structures as well as rational functions that depart from the tree-level amplitude, making it closer in complexity to the amplitude in general kinematics, while still more tractable.

We find that a useful way to organise the one-loop amplitudes in $\mathcal{N} = 4$ SYM is by separately considering the dispersive and absorptive parts of the amplitude. We find that in the NMRK limit, the dispersive part of the one-loop amplitude factorises in terms of a one-loop two-gluon CEV, while the absorptive part admits no such simple factorisation. However, upon considering the helicity-summed interference of the one-loop amplitude with the tree-level amplitude, we observe that only the dispersive part of the amplitude contributes at NNLL accuracy, which is a promising result for the prospect of extending the BFKL kernel to this logarithmic accuracy. We also find that simplifications occur when considering the interference of the dispersive part of the one-loop amplitude with the tree-level amplitude: While, as mentioned above, the one-loop two-gluon CEV has an additional, fully symmetric colour structure which does not feature at tree level, this new colour structure does not contribute at NNLL accuracy. It does however, contribute to cross sections at N³LL accuracy, where one must consider the square of the one-loop two-gluon CEV, giving rise to a quartic Casimir invariant.

The structure of this paper is as follows. In section 2 we review the factorised structure of amplitudes at LL and NLL accuracy. In section 3 we review the properties of the tree-level two-gluon central-emission vertex and we obtain new representations of this vertex. In section 4 we take the central NMRK limit of the one-loop six-gluon amplitude in $\mathcal{N} = 4$ SYM. We find that the dispersive part of the amplitude factorises in terms of a one-loop two-gluon CEV. We obtain this CEV for the case of same-helicity gluons in section 4.1 and for the case of opposite-helicity gluons in section 4.2. In section 4.3 we consider the NLO $gg \rightarrow gggg$ squared matrix element and show that several simplifications occur in this context. We discuss the implications of these results for the NNLL BFKL kernel. In section 5 we speculate how the behaviour we have observed for six-gluon one-loop amplitudes may be extended to higher multiplicity and loop order. Finally, we conclude in section 6. Several appendices are included: in appendices A and B we display the kinematic regions and invariants of interest; in appendix C we list the power-suppressed helicity configurations; in appendix D we list the tree-level and one-loop six-gluon NMHV amplitudes in $\mathcal{N} = 4$ SYM in general kinematics; in appendix E we include alternative forms of the tree-level opposite-helicity CEV; in appendix F we display the absorptive part of the one-loop six-gluon amplitude in $\mathcal{N} = 4$ SYM in the NMRK limit; in appendix G we compute the MRK, soft and collinear limits of the one-loop two-gluon CEV.

2 The building blocks of the BFKL equation

In this section we review the factorized structure of four and five gluon amplitudes in the Regge limit. We define the elements which appear in this factorization, which are also the building blocks of the BFKL equation, as shown schematically in figs. 1, 2 and 3. We will need these when discussing the more involved two-gluon central emission vertex in $\mathcal{N} = 4$ SYM, which we determine from the six-gluon amplitude in the following sections. As high-energy factorization properties are universal, that is independent of the particular gauge theory being considered, our discussion in the present section will be entirely general. Note however that the functions appearing in the factorized amplitudes, such as impact

factors, Regge trajectory and central emission vertices, do depend on the theory under consideration starting from one loop.

2.1 Building blocks at LL accuracy

In the Regge limit, one can write the tree-level $2 \rightarrow 2$ amplitudes in a factorised way. For example, the amplitude for gluon-gluon scattering $g_1 g_2 \rightarrow g_3 g_4$ at tree level and at fixed helicities may be written as [1, 2],

$$\mathcal{M}_{4g}^{(0)} = \left[g_S (F^{a_3})_{a_2 c} C^{g(0)}(p_2^{\nu_2}, p_3^{\nu_3}) \right] \frac{s}{t} \left[g_S (F^{a_4})_{a_1 c} C^{g(0)}(p_1^{\nu_1}, p_4^{\nu_4}) \right], \quad (2.1)$$

with the incoming momenta p_1 and p_2 parametrised as in eq. (A.2), and with $s = (p_1 + p_2)^2$, $q = -(p_2 + p_3)$, $t = q^2 \simeq -|q_\perp|^2$ and $(F^c)_{ab} = i\sqrt{2}f^{acb}$, and where the superscript ν_i labels the helicity of gluon g_i . We consider all the momenta as outgoing, so the helicities for incoming partons are reversed, see appendix A.1. As is apparent from the colour coefficient $(F^{a_3})_{a_2 c} (F^{a_4})_{a_1 c}$, in eq. (2.1) only the antisymmetric octet $\mathbf{8}_a$ is exchanged in the t channel.

Since the four-gluon amplitude is a maximally helicity-violating (MHV) amplitude, eq. (2.1) describes $\binom{4}{2} = 6$ helicity configurations. However, at leading power in t/s , helicity is conserved along the s -channel direction, so in eq. (2.1) four helicity configurations are leading, two for each tree impact factor, $g^* g \rightarrow g$, with g^* an off-shell gluon [75],

$$C^{g(0)}(p_2^\ominus, p_3^\oplus) = 1, \quad C^{g(0)}(p_1^\ominus, p_4^\oplus) = \frac{p_{4\perp}^*}{p_{4\perp}}, \quad (2.2)$$

with complex transverse coordinates p_\perp as in eq. (A.1). At this order, the impact factors are just overall phases, and they transform under parity into their complex conjugates,

$$[C^g(p^\nu, p'^{\nu'})]^* = C^g(p^{-\nu}, p'^{-\nu'}). \quad (2.3)$$

The helicity-flip impact factor $C^{g(0)}(p^\oplus, p'^\oplus)$ and its parity conjugate $C^{g(0)}(p^\ominus, p'^\ominus)$ are power suppressed in t/s . In eq. (2.2), and in what follows, we encircle the helicity index to avoid any confusion with the light-cone direction labelling.

The tree amplitudes for quark-gluon or quark-quark scattering have the same form as eq. (2.1), up to replacing one or both gluon impact factors $C^{g(0)}$ (2.2) with quark impact factors $C^{q(0)}$, and the colour factors $(F^c)_{ab}$ in the adjoint representation with the colour factors T_{ij}^c in the fundamental representation of $SU(N_c)$, which we normalise as $\text{tr}(T^a T^b) = T_F \delta^{ab}$, with $T_F = 1$. So in the Regge limit, $2 \rightarrow 2$ scattering amplitudes factorise into gluon or quark impact factors and a gluon propagator in the t channel, and are uniquely determined by them.

At LL accuracy in $\log(s/|t|)$, the four-gluon amplitude is given to all orders in α_s by Reggeizing the gluon, i.e. by dressing the gluon propagator in eq. (2.1) as [1, 2]

$$\frac{1}{t} \rightarrow \frac{1}{t} \left(\frac{s}{\tau} \right)^{\alpha(t)}, \quad (2.4)$$

where $\tau > 0$ is a Regge factorisation scale, which is of order of $|t|$, and much smaller than s . The function $\alpha(t)$ is the gluon Regge trajectory which is related to the loop transverse-momentum integration. The latter is infrared divergent, and in dimensional regularization

with $d = 4 - 2\epsilon$, it can be written as

$$\alpha(t) = \frac{\alpha_s}{4\pi} \alpha^{(1)}(t) + \mathcal{O}(\alpha_s^2), \quad \text{with} \quad \alpha^{(1)}(t) = N_c \frac{2}{\epsilon} \left(\frac{\mu^2}{-t} \right)^\epsilon \kappa_\Gamma, \quad (2.5)$$

where for brevity we omit the dependence of $\alpha(t)$ on μ^2 . In eq. (2.5), $\alpha_s \equiv g_s^2/(4\pi)$ is the bare coupling, and the $\mathcal{O}(\alpha_s^2)$ term indicates the presence of higher corrections which become relevant beyond LL accuracy, N_c is the number of colours, and

$$\kappa_\Gamma \equiv (4\pi)^\epsilon \frac{\Gamma(1+\epsilon) \Gamma^2(1-\epsilon)}{\Gamma(1-2\epsilon)}. \quad (2.6)$$

It is said that in the Regge limit, the four-gluon amplitude of eq. (2.1) with the dressing in eq. (2.4), is determined by the t -channel exchange of a single Reggeized gluon, or Reggeon.

In five-gluon scattering $g_1 g_2 \rightarrow g_3 g_4 g_5$, the multi-Regge kinematics (MRK) are defined as a strong ordering in the light-cone momenta,

$$p_3^+ \gg p_4^+ \gg p_5^+, \quad |p_{3\perp}| \simeq |p_{4\perp}| \simeq |p_{5\perp}|. \quad (2.7)$$

or equivalently in the rapidities, of the produced gluons, eq. (A.14). In MRK, appendix A.2, the tree five-gluon amplitude takes the factorised form (fig. 1 (b)),

$$\begin{aligned} \mathcal{M}_{5g}^{(0)} = & s \left[g_s(F^{a_3})_{a_2 c_1} C^{g(0)}(p_2^{\nu_2}, p_3^{\nu_3}) \right] \frac{1}{t_1} \\ & \times \left[g_s(F^{a_4})_{c_1 c_2} V^{g(0)}(q_1, p_4^{\nu_4}, q_2) \right] \frac{1}{t_2} \left[g_s(F^{a_5})_{a_1 c_2} C^{g(0)}(p_1^{\nu_1}, p_5^{\nu_5}) \right], \end{aligned} \quad (2.8)$$

with $q_1 = -(p_2 + p_3)$, $q_2 = q_1 - p_4$, and $t_i = q_i^2 \simeq -q_{i\perp} q_{i\perp}^*$ ($i = 1, 2$). The impact factors are given in eq. (2.2), while the emission vertex of a real gluon from the t -channel gluon, which is termed the CEV, is [1, 76]

$$V^{g(0)}(q_1, p_4^\oplus, q_2) = \frac{q_{1\perp}^* q_{2\perp}}{p_{4\perp}}, \quad (2.9)$$

which transforms under parity into its complex conjugate,

$$\left[V^{g(0)}(q_1, p^\nu, q_2) \right]^* = V^{g(0)}(q_1, p^{-\nu}, q_2). \quad (2.10)$$

The one-loop gluon Regge trajectory, eq. (2.5), and the tree-level central-emission vertex (CEV), eq. (2.9), are the building blocks of an iterative structure, in the sense that a tree six-gluon amplitude in MRK, $g_1 g_2 \rightarrow g_3 g_4 g_5 g_6$, will display two CEVs along the gluon ladder, with the four outgoing gluons separated by three large rapidity gaps. At LL accuracy, each of the corresponding t -channel gluons Reggeizes according to eq. (2.4) with the one-loop trajectory of eq. (2.5). Similarly, a seven-gluon amplitude in MRK will display three CEVs, and at LL accuracy it will feature four Reggeized t -channel gluons across each of the rapidity gaps, and so on for higher-multiplicity amplitudes. This iterative structure is captured by the leading-order BFKL equation. It is depicted in figure 4, which is suggestive of an all-multiplicity, all-order generalization.

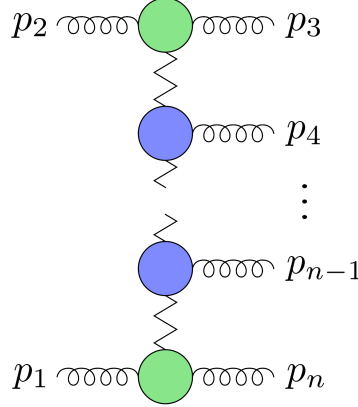


Figure 4. The factorised structure of gluon amplitudes in MRK. The zigzag line represents the Reggeized gluon propagator given in eq. (2.4). The coloured blobs represent impact factors, and one-gluon CEVs. At LL accuracy these elements are only required at tree level, but much like the gluon Regge trajectory $\alpha(t)$, they can be defined to all orders in perturbation theory (note that this interpretation departs from the previous figures where the blobs are specific to a given loop order).

2.2 Building blocks at NLL accuracy

As mentioned in the introduction, in order to extend the BFKL equation to NLL accuracy, as done in refs. [5–8], one needs three ingredients, which are described schematically by fig. 2. First, one needs one-loop corrections to the single-gluon CEV of eq. (2.9), which can be extracted from a five-gluon one-loop amplitude [45–49] (fig. 2 (b)), as we show later in this section. Second, one requires the tree-level CEV for two gluons, which are not ordered in rapidity. This object can be extracted from a tree-level six-gluon amplitude at NMRK [50–52, 54, 60] (fig. 2 (c)) and it will be again extracted and analysed in some detail in section 3 below. Finally, one needs two-loop corrections to the Regge trajectory $\alpha(t)$ [40–44]. The latter may be extracted from $2 \rightarrow 2$ amplitudes at two loops (fig. 2 (a)). This requires an operative prescription to disentangle the Regge trajectory from the impact factor. In what follows, we briefly present such a prescription following ref. [45].

We recall that in the Regge limit, $2 \rightarrow 2$ scattering amplitudes $g_1 g_2 \rightarrow g_3 g_4$, can be conveniently split into odd $\mathcal{M}_{4g}^{(-)}$ and even $\mathcal{M}_{4g}^{(+)}$ components under so-called signature symmetry, corresponding to a kinematic $s \leftrightarrow u$ interchange,

$$\mathcal{M}_{4g}(s, t) = \mathcal{M}_{4g}^{(-)}(s, t) + \mathcal{M}_{4g}^{(+)}(s, t), \quad \mathcal{M}_{4g}^{(\pm)}(s, t) = \frac{\mathcal{M}_{4g}(s, t) \pm \mathcal{M}_{4g}(u, t)}{2}, \quad (2.11)$$

with $u = -s - t \simeq -s$. In order to resum energy logarithms in $\mathcal{M}_{4g}(s, t)$ beyond LL accuracy it is useful to define a signature-symmetric logarithm,

$$L \equiv \log \left(\frac{s}{-t} \right) - \frac{i\pi}{2} = \frac{1}{2} \left[\log \left(\frac{-s - i0}{-t} \right) + \log \left(\frac{-u}{-t} \right) \right], \quad (2.12)$$

and expand the amplitude at leading power in the Regge limit as

$$\mathcal{M}_{4g}^{(\pm)} = g_s^2 \sum_{n=0}^{\infty} \left(\frac{\alpha_s}{4\pi} \right)^n \sum_{m=0}^n L^m \mathcal{M}_{4g}^{(\pm, n, m)}, \quad (2.13)$$

with $m = n$ yielding the coefficients at LL accuracy, $m = n - 1$ the coefficients at NLL accuracy, and so on. With eqs. (2.12) and (2.13) at work, one can show [23] that the coefficients of the odd (even) amplitude, $\mathcal{M}_{4g}^{(\mp, n, m)}$, are purely real (imaginary). Moreover, $\mathcal{M}_{4g}^{(-)}$ only receives contributions from t -channel exchange of an odd number of Reggeons, while $\mathcal{M}_{4g}^{(+)}$, from an even number.

Owing to Bose symmetry, also the colour factors of $\mathcal{M}_{4g}^{(-)}$ and $\mathcal{M}_{4g}^{(+)}$ are respectively odd and even under the interchange of the colour indices of the corresponding gluons g_2 and g_3 (or, instead, those of g_1 and g_4). The tree amplitude in eq. (2.1) is entirely odd under signature, and indeed, its colour structure is antisymmetric under interchanging a_2 and a_3 , corresponding to a pure t -channel octet exchange, $\mathbf{8}_a$. Higher-order contributions to this process involve in general additional colour structures, as dictated by the decomposition of the product $\mathbf{8}_a \otimes \mathbf{8}_a$ into irreducible representations,

$$\mathbf{8}_a \otimes \mathbf{8}_a = \{\mathbf{1} \oplus \mathbf{8}_s \oplus \mathbf{27}\} \oplus [\mathbf{8}_a \oplus \mathbf{10} \oplus \overline{\mathbf{10}}], \quad (2.14)$$

where the curly (square) brackets contain the representations which are even (odd) under signature. However, at NLL accuracy, the signature-odd component of the amplitude, i.e. $\mathcal{M}_{4g}^{(-, n, n-1)}$ for all n in eq. (2.13), is still governed by the exchange of a single Reggeon in the t channel, and eq. (2.4) generalises in a straightforward way to [45],

$$\mathcal{M}_{4g}^{(-)[8_a]} = \frac{1}{2} [g_s(F^{a_3})_{a_2c} C^g(p_2^{\nu_2}, p_3^{\nu_3})] \frac{s}{t} \left[\left(\frac{s}{\tau} \right)^{\alpha(t)} + \left(\frac{-s}{\tau} \right)^{\alpha(t)} \right] [g_s(F^{a_4})_{a_1c} C^g(p_1^{\nu_1}, p_4^{\nu_4})], \quad (2.15)$$

where the colour and kinematic parts of the amplitude are each odd under $g_2 \leftrightarrow g_3$ interchange.

In eq. (2.15), we expand the gluon Regge trajectory in α_s as

$$\alpha(t) = \frac{\alpha_s}{4\pi} \alpha^{(1)}(t) + \left(\frac{\alpha_s}{4\pi} \right)^2 \alpha^{(2)}(t) + \mathcal{O}(\alpha_s^3), \quad (2.16)$$

with $\alpha^{(1)}$ in eq. (2.5), and $\alpha^{(2)}$ is the two-loop Regge trajectory which enters the BFKL equation at NLL accuracy. Likewise, we expand the helicity-conserving impact factor,

$$C^g(p^\oplus, p'^\ominus) = C^{g(0)}(p^\oplus, p'^\ominus) + \frac{\alpha_s}{4\pi} C^{g(1)}(p^\oplus, p'^\ominus) + \mathcal{O}(\alpha_s^2), \quad (2.17)$$

with one-loop corrections,

$$C^{g(1)}(p^\oplus, p'^\ominus) = C^{g(0)}(p^\oplus, p'^\ominus) c^{g(1)}(t). \quad (2.18)$$

The same applies to the opposite helicity-conserving impact factor $C^g(p^\ominus, p'^\oplus)$. Note that the one-loop coefficients $c^{g(1)}$ are real and independent of the helicity configuration. The coefficient $c^{g(1)}$, and therefore also C^g , depend on the renormalisation and Regge-factorisation scales μ^2 and τ , but we omit this dependence for brevity.

The $2 \rightarrow 3$ scattering amplitudes, $g_1 g_2 \rightarrow g_3 g_4 g_5$, can be likewise split into odd and even components under signature symmetry,

$$\mathcal{M}_{5g} = \mathcal{M}_{5g}^{(+,+)} + \mathcal{M}_{5g}^{(+,-)} + \mathcal{M}_{5g}^{(-,+)} + \mathcal{M}_{5g}^{(-,-)}, \quad (2.19)$$

with

$$\begin{aligned} \mathcal{M}_{5g}^{(\sigma_a, \sigma_b)}(p_1^{\nu_1}, p_2^{\nu_2}, p_3^{\nu_3}, p_4^{\nu_4}, p_5^{\nu_5}) \\ = \frac{1}{4} \mathcal{M}_{5g}(p_1^{\nu_1}, p_2^{\nu_2}, p_3^{\nu_3}, p_4^{\nu_4}, p_5^{\nu_5}) + \frac{\sigma_a}{4} \mathcal{M}_{5g}(p_1^{\nu_1}, p_3^{\nu_3}, p_2^{\nu_2}, p_4^{\nu_4}, p_5^{\nu_5}) \\ + \frac{\sigma_b}{4} \mathcal{M}_{5g}(p_5^{\nu_5}, p_2^{\nu_2}, p_3^{\nu_3}, p_4^{\nu_4}, p_1^{\nu_1}) + \frac{\sigma_a \sigma_b}{4} \mathcal{M}_{5g}(p_5^{\nu_5}, p_3^{\nu_3}, p_2^{\nu_2}, p_4^{\nu_4}, p_1^{\nu_1}), \end{aligned} \quad (2.20)$$

where the two signature indices σ_a and σ_b can separately be $+1$ or -1 . By Bose symmetry, the upper and lower vertices (see fig. (11)) then acquire a corresponding colour symmetry: the upper vertex is symmetric/antisymmetric upon interchanging the colour indices a_2 and a_3 for $\sigma_a = +$ and $\sigma_a = -$, respectively. Similarly, the lower one is symmetric/antisymmetric upon interchanging a_1 and a_5 for $\sigma_b = +$ and $\sigma_b = -$, respectively. Specifically, the $\mathcal{M}^{(-,-)}$ amplitude, which we discuss below, is antisymmetric in colour in both the upper and lower vertices.

In MRK, eq. (2.20) is understood to involve the exchanges $s_{34} \leftrightarrow s_{24} = -s_{34}$ and $s_{45} \leftrightarrow s_{41} = -s_{45}$ along with the associated change in sign of $s = s_{12} = -s_{13} = -s_{52} = s_{35}$. At NLL accuracy, the signature odd-odd component of the amplitude, $\mathcal{M}^{(-,-)}$, is governed by an antisymmetric octet exchange, $\mathbf{8}_a$, in the t_1 and t_2 channels, corresponding to a single Reggeon. One can then generalise eq. (2.8),

$$\begin{aligned} \mathcal{M}_{5g}^{(-,-)[\mathbf{8}_a]} = \frac{1}{4} s [g_S(F^{a_3})_{a_2 c_1} C^g(p_2^{\nu_2}, p_3^{\nu_3})] \frac{1}{t_1} \left[\left(\frac{s_{34}}{\tau} \right)^{\alpha(t_1)} + \left(\frac{-s_{34}}{\tau} \right)^{\alpha(t_1)} \right] \\ \times [g_S(F^{a_4})_{c_1 c_2} V^g(q_1, p_4^{\nu_4}, q_2)] \frac{1}{t_2} \left[\left(\frac{s_{45}}{\tau} \right)^{\alpha(t_2)} + \left(\frac{-s_{45}}{\tau} \right)^{\alpha(t_2)} \right] \\ \times [g_S(F^{a_5})_{a_1 c_2} C^g(p_1^{\nu_1}, p_5^{\nu_5})], \end{aligned} \quad (2.21)$$

where the CEV now includes one-loop corrections

$$V^g(q_1, p_4^{\nu_4}, q_2) = V^{g(0)}(q_1, p_4^{\nu_4}, q_2) + \frac{\alpha_S}{4\pi} V^{g(1)}(q_1, p_4^{\nu_4}, q_2) + \mathcal{O}(\alpha_S^2), \quad (2.22)$$

which we express as

$$V^{g(1)}(q_1, p_4^{\nu_4}, q_2) = V^{g(0)}(q_1, p_4^{\nu_4}, q_2) v^{g(1)}(t_1, |p_{4\perp}|^2, t_2). \quad (2.23)$$

where $v^{g(1)}$ is real and helicity-independent. Similarly to $c^{g(1)}$, we omit the dependence on the scales μ^2 and τ in $v^{g(1)}$ and V^g .

Finally, we note that while the signature-odd NLL $gg \rightarrow gg$ amplitude is governed by a pure t -channel $\mathbf{8}_a$ exchange, leading to the simple resummation formula in eq. (2.15), the signature-even NLL amplitude $\mathcal{M}_{4g}^{(+)}$, which is purely imaginary, is governed by two-Reggeon exchange, leading to a more complex structure involving all t -channel representations that are compatible with the even signature in (2.14), namely the singlet $\mathbf{1}$, the

symmetric octet $\mathbf{8}_s$ and the $\mathbf{27}$. Such a contribution occurs already in the non-logarithmic signature-even one-loop term $\mathcal{M}_{4g}^{(+,1,0)}$, which is proportional to $i\pi$ [59]. More generally, the signature-even amplitude obeys the BFKL equation [2–4]: it is described by ladder graphs formed between two Reggeized gluons, which admits an all-order iterative solution [22, 24, 25], rendering both infrared-singular and finite corrections $\mathcal{M}_{4g}^{(+,n,n-1)}$ computable for all n for general colour. The signature-even gluon-gluon amplitude at NLL accuracy can only contribute to a squared amplitude, and thus to a cross section, at NNLL accuracy.

2.3 Building blocks at NNLL accuracy

As outlined in the introduction, computing the next-to-next-to-leading-order corrections to the BFKL kernel requires to determine five elements: the three-loop correction to the Regge trajectory [36, 68, 69] (fig. 3 (a)); the two-loop correction to the single-gluon CEV² (fig. 3 (b)); the square of the one-loop correction to the single-gluon CEV³ (fig. 3 (c)); the one-loop correction to the two-parton (two gluons or a quark-antiquark pair) CEV (fig. 3 (d)); the tree-level three-parton CEV (fig. 3 (e)), which is known for the case of three gluons [60, 70, 71]. We note in passing that the tree-level four-gluon CEV, which would occur at N³LL accuracy, is also known [60].

Computing the three-loop gluon Regge trajectory has required to tackle a new hurdle: starting at NNLL accuracy the signature-odd part of the $gg \rightarrow gg$ amplitude (namely its real part) cannot be described purely in terms of a single-Reggeon exchange [23, 26, 44, 64–66, 68, 82–85]. Instead, contributions from three Reggeon exchange occur, starting from two loops [23, 65, 85], and furthermore, three-Reggeon mixing with a single Reggeon kicks in starting at three loops [23]. As a consequence, a resummation formula of the form eq. (2.15), which corresponds to a pure Regge pole in the complex angular momentum plane, is insufficient. It must be supplemented by additional contributions which do not admit such simple factorization and exponentiation properties, and build up a Regge-cut in the complex angular momentum plane. Since t -channel $\mathbf{8}_a$ contributions, which are proportional to the tree amplitude, arise from both single and multiple Reggeon exchange, it had not been obvious how to disentangle Regge pole and cut contributions when working at fixed order.

Infrared factorisation shows that [83, 86], in addition to the usual diagonal terms of the colour octet exchange, also non-diagonal terms in the t -channel colour basis contribute to the real part of $M_{4g}^{(-,2,0)}$ [64, 84]. More recently, following the computation of NNLL corrections $\mathcal{M}_{4g}^{(-,n,n-2)}$ to the odd amplitude through four loops [26, 66], the structure of the NNLL tower has been understood [68], uncovering a deep connection to the non-planar origin of Regge cuts [87, 88]. Specifically, it has become clear that *planar* multi-Reggeon contributions at NNLL only occur at two and three loops. These contribute to the Regge pole, and factorise along with the single-Reggeon contribution as in eq. (2.15), while

²The two-loop correction to the single-gluon CEV is known in planar $\mathcal{N} = 4$ SYM theory [77].

³The one-loop correction to the single-gluon CEV is known in planar $\mathcal{N} = 4$ SYM theory to all orders of ϵ [77]. Beyond $\mathcal{O}(\epsilon^0)$, the one-loop single-gluon CEV requires the one-loop pentagon in $6 - 2\epsilon$ dimensions [78–81].

the *non-planar* multi-Reggeon contributions are precisely those that build up the Regge cut. Accordingly, the three-loop gluon Regge trajectory has been determined [36, 68, 69], providing the fully-virtual input, shown in fig. 3 (a), that is necessary for extending the BFKL equation to NNLL accuracy,

While the two-loop corrections to the single-gluon CEV (fig. 3 (b)) are yet to be determined, in this paper, we evaluate the one-loop corrections to the two-gluon CEV (fig. 3 (d)) in $\mathcal{N} = 4$ SYM, as a first step toward computing the same quantity in QCD.

Let us also note that in order to compute jet cross sections at NNLL accuracy through the BFKL equation, jet impact factors at next-to-next-to-leading order (NNLO) in α_s will be needed. Building blocks to evaluate the latter are the two-loop impact factors [64]; the one-loop impact factors for the emission of two gluons [89] or of a quark-antiquark pair, evaluated in NMRK; and the tree impact factor for the emission of three partons at one end of the ladder [70] evaluated in NNMRK. Further, one must include the square of the one-loop helicity-violating impact factor [59].

3 The two-gluon central-emission vertex at tree level

In this section we investigate several equivalent representations of the two-gluon CEV at tree level. In section 3.1 we introduce a new set of kinematic variables which, in particular, greatly simplifies the task of showing equivalence between the different representations of the CEV. In section 3.2 we obtain new representations for the opposite-helicity CEV from amplitudes that were derived via Britto-Cachazo-Feng-Witten (BCFW) recursion relations [90, 91]. Not only do these representations make clear the collinear structure of the tree-level CEV, the individual rational terms that comprise the BCFW amplitudes appear also in the one-loop six-gluon NMHV amplitudes of $\mathcal{N} = 4$ SYM. The study of these rational terms therefore also lays the groundwork for section 4, where we obtain the one-loop two-gluon CEV in $\mathcal{N} = 4$ SYM.

We begin by reviewing the factorisation properties of six-gluon amplitudes in the central NMRK. We consider the production of four gluons of momenta p_i , with $i = 3, 4, 5, 6$ in the scattering of two gluons of momenta p_1 and p_2 , with the momenta parametrised in terms of lightcone coordinates as in eq. (A.2). We suppose that the outgoing gluons are in a central NMRK configuration, as described in appendix A.3, where the rapidities and transverse momenta of the outgoing gluons satisfy

$$y_3 \gg y_4 \simeq y_5 \gg y_6; \quad |p_{3\perp}| \simeq |p_{4\perp}| \simeq |p_{5\perp}| \simeq |p_{6\perp}|. \quad (3.1)$$

In the NMRK region of eq. (3.1), the tree-level amplitude for the $g_1 g_2 \rightarrow g_3 g_4 g_5 g_6$ scattering process is [50–52, 54]:

$$\mathcal{M}_{6g}^{(0)} \Big|_{\text{NMRK}} = \sum_{\sigma \in S_2} g_s^4 (F^{a_3})_{a_2 c_1} (F^{a_{\sigma_4}} F^{a_{\sigma_5}})_{c_1 c_3} (F^{a_6})_{a_1 c_3} M_{6g}^{(0)}(p_1^{\nu_1}, p_2^{\nu_2}, p_3^{\nu_3}, p_{\sigma_4}^{\nu_{\sigma_4}}, p_{\sigma_5}^{\nu_{\sigma_5}}, p_6^{\nu_6}), \quad (3.2)$$

where the sum is over the two permutations of the gluon labels 4 and 5, and on the right-hand side an NMRK subscript on the colour-ordered amplitudes $M_{6g}^{(0)}$ is understood. The

latter factorise in this limit as

$$M_{6g}^{(0)}(p_1^{\nu_1}, p_2^{\nu_2}, p_3^{\nu_3}, p_4^{\nu_4}, p_5^{\nu_5}, p_6^{\nu_6}) = s C^{g(0)}(p_2^{\nu_2}, p_3^{\nu_3}) \frac{1}{t_1} A^{gg(0)}(q_1, p_4^{\nu_4}, p_5^{\nu_5}, q_3) \frac{1}{t_3} C^{g(0)}(p_1^{\nu_1}, p_6^{\nu_6}), \quad (3.3)$$

with $s = s_{12} = (p_1 + p_2)^2$, $q_1 = -(p_2 + p_3)$, $q_3 = p_1 + p_6$, $s_{23} = t_1 = q_1^2 \simeq -|q_{1\perp}|^2$, $s_{61} = t_3 = q_3^2 \simeq -|q_{3\perp}|^2$. Here $A^{gg(0)}(q_1, p_4^{\nu_4}, p_5^{\nu_5}, q_3)$ is the tree-level two-gluon central-emission vertex, which is the subject of this section. This quantity has been studied previously [50–52, 54] and our analysis here is primarily intended to prepare the grounds for the determination of this quantity at one loop in the next section.

Since the six-gluon amplitude can be in either a maximally helicity-violating (MHV) or next-to-maximally helicity-violating (NMHV) configuration, eq. (3.2) describes a total of $2\binom{6}{2} + \binom{6}{3} = 50$ helicity configurations. Out of these, 34 configurations are associated to amplitudes which have at least one helicity-flip impact factor, appendix C, and thus are power suppressed in t_i/s , with $i = 1, 3$. Conversely, at leading power in t_i/s , helicity is conserved along the s -channel direction in Minkowski space, so in eq. (3.2) 16 helicity configurations are leading. Two are associated to each tree impact factor, $g^* g \rightarrow g$, with g^* an off-shell gluon, eq. (2.2).

Multiplying the four helicity configurations associated to the impact factors, there are four helicity configurations associated to the central-emission vertex for the emission of two gluons, $g^* g^* \rightarrow g g$, which read⁴ [50–52, 54]

$$A^{gg(0)}(q_1, p_4^\oplus, p_5^\oplus, q_3) = \frac{q_{1\perp}^* q_{3\perp}}{p_{4\perp}} \sqrt{\frac{x_4}{x_5}} \frac{1}{\langle 45 \rangle}, \quad (3.4)$$

$$A^{gg(0)}(q_1, p_4^\oplus, p_5^\ominus, q_3) \Big|_1 = -\frac{p_{4\perp}^*}{p_{4\perp}} \left\{ -\frac{1}{s_{45}} \left[\frac{y_5 p_{5\perp} |q_{1\perp}|^2}{p_{5\perp}^*} + \frac{x_4 p_{4\perp} |q_{3\perp}|^2}{p_{4\perp}^*} + \frac{s_{234} p_{4\perp} p_{5\perp}}{p_4^- p_5^+} \right] + \frac{(q_{3\perp} + p_{5\perp})^2}{s_{234}} - \frac{q_{3\perp} + p_{5\perp}}{s_{45}} \left[\frac{p_{4\perp}}{y_4} - \frac{p_{5\perp}}{x_5} \right] \right\}, \quad (3.5)$$

where the kinematic invariants are given in eqs. (A.25), (A.27), and (A.30), and where we use the momentum fractions,

$$x_i = \frac{p_i^+}{p_4^+ + p_5^+}, \quad y_i = \frac{p_i^-}{p_4^- + p_5^-}, \quad i = 4, 5. \quad (3.6)$$

In eqs. (3.4)–(3.5), similarly to eq. (2.2), we have encircled the helicity index and we have appended the index $|_1$ to the opposite-helicity vertex (eq. (3.5)) in order to stress that this is the first amongst several equivalent representations we are going to consider for this quantity.

Note that the impact factors, eq. (2.3), and the central-emission vertex, eqs. (3.4)–(3.5), transform under parity into their complex conjugates,

$$\left[A^{gg(0)}(q_1, p_4^{\nu_4}, p_5^{\nu_5}, q_3) \right]^* = A^{gg(0)}(q_1, p_4^{-\nu_4}, p_5^{-\nu_5}, q_3), \quad (3.7)$$

⁴Note that having defined $(F^c)_{ab} = i\sqrt{2}f^{acb}$, the central-emission vertices, eqs. (2.9), (3.4) and (3.5), do not display the usual overall powers of $\sqrt{2}$.

allowing one to obtain $A^{gg(0)}(q_1, p_4^\ominus, p_5^\ominus, q_3)$ and $A^{gg(0)}(q_1, p_4^\ominus, p_5^\oplus, q_3)$ from those in eq. (3.5). If the further MRK limit is taken, i.e. further requiring $p_4^+ \gg p_5^+$, the two-gluon CEV factorises into a product of two Lipatov vertices times an intermediate t -channel pole. The MRK limit is discussed in appendix G.1.

In ref. [60] an alternative form of the opposite-helicity two-gluon CEV was found by using the CSW rules [92], eq. (E.1). This is a compact form of the vertex, consisting of only four rational terms, but unlike eq. (3.5), this representation appears to have unphysical poles e.g. at $p_{4\perp} + p_{5\perp} = 0$. This is a feature which is shared with the new representations we will obtain from the BCFW recursion relations in section 3.2. Before obtaining these new representations, we will first introduce a minimal set of independent variables which we will use throughout this paper. In particular, these variables will make it simple to analytically verify the equivalence of all the representations of the opposite-helicity vertex we will study, thereby proving that the apparent unphysical singularities in the CSW and BCFW representations are spurious.

3.1 A minimal set of variables

In MRK the central-emission vertex for the emission of one gluon can be expressed in terms of one independent transverse momentum, i.e. in terms of two real parameters. We expect that the emission of one more gluon out of the central-emission vertex will require the introduction of the variables of one more on-shell massless particle, i.e. three more real parameters, such that the central-emission vertex for the emission of n gluons will be expressed in terms of a set of $(3n - 1)$ independent real parameters. In particular, the central-emission vertex for the emission of two gluons will be given in terms of five real parameters.

We write $p_{4\perp}$ and $p_{5\perp}$ in terms of MRK t -channel transverse momenta,

$$p_{4\perp} = q_{1\perp} - q_{2\perp}, \quad p_{5\perp} = q_{2\perp} - q_{3\perp}. \quad (3.8)$$

In the sum of the equations above, $q_{2\perp}$ cancels such that transverse momentum conservation in NMRK is fulfilled. We parametrise the ratios of transverse momenta in eq. (3.8) in terms of two complex variables, w and z ,

$$\begin{aligned} \frac{p_{4\perp}}{q_{1\perp}} &= \frac{1}{1-z}, & \frac{q_{2\perp}}{q_{1\perp}} &= \frac{-z}{1-z}, \\ \frac{p_{5\perp}}{q_{3\perp}} &= \frac{-1}{1-w}, & \frac{q_{2\perp}}{q_{3\perp}} &= \frac{-w}{1-w}. \end{aligned} \quad (3.9)$$

Inverting these relations gives us

$$z = -\frac{q_{2\perp}}{p_{4\perp}}, \quad w = \frac{q_{2\perp}}{p_{5\perp}}. \quad (3.10)$$

Using complex parametrization of the transverse momenta (see appendix A.1), z and w are also complex. We will use \bar{z} and \bar{w} to denote their complex conjugates.

In summary, we may parametrise the central-emission vertex for the emission of two gluons, involving five real degrees of freedom, in terms of the set $\{w, z, X\}$, where X is a

real positive variable which depends on the rapidity difference between p_4 and p_5 ,

$$X \equiv \frac{p_4^+}{p_5^+} = \frac{x_4}{x_5}. \quad (3.11)$$

The MRK limit is reached by taking $X \rightarrow \infty$. When we use the acronym MRK, we will always mean this canonical MRK limit with the strict rapidity ordering $y_3 \gg y_4 \gg y_5 \gg y_6$. The multi-Regge regime with strict rapidity ordering $y_3 \gg y_5 \gg y_4 \gg y_6$ is also contained within the central NMRK limit of appendix A.3, and we will refer to this kinematic condition as MRK'. The MRK' limit is reached by taking $X \rightarrow 0$.

The leading NMRK behaviour of several Lorentz invariant quantities are listed in terms of the minimal set of variables in appendix B. In terms of this minimal set, eqs. (3.4)–(3.5) become

$$A^{gg(0)}(q_1, p_4^\oplus, p_5^\oplus, q_3) = \frac{q_{1\perp}^*}{q_{1\perp}} \frac{z(w-1)(z-1)X}{(w+Xz)}, \quad (3.12)$$

$$\begin{aligned} A^{gg(0)}(q_1, p_4^\oplus, p_5^\ominus, q_3) \Big|_1 &= \frac{\bar{w}^2 z^2 |z-1|^2 X^2}{|w+Xz|^2 (|w|^2 + X|z|^2)} + \frac{z^2 X}{(1+X|z|^2)} \\ &+ \frac{Xz}{|w+Xz|^2} \left(\frac{|w-1|^2 X \bar{z}}{(1+X)} + \bar{w}(1+X|z|^2) \right. \\ &\quad \left. - (|w|^2 + X|z|^2) - \bar{w}z(1+X) \right). \end{aligned} \quad (3.13)$$

We note that the same-helicity vertex, eq. (3.12), contains a remaining phase $q_{1\perp}^*/q_{1\perp}$, which cannot be expressed in terms of the minimal variables. From eq. (B.2) we see that the physical singularity of this vertex corresponds to

$$\langle 45 \rangle = 0 \quad \leftrightarrow \quad w + Xz = 0. \quad (3.14)$$

The opposite-helicity vertex, eq. (3.13), has a more complicated singularity structure. From eq. (B.3) we see that the further physical singularities of this vertex correspond to the vanishing of three-particle Mandelstam invariants,

$$\begin{aligned} s_{123} = 0 &\quad \leftrightarrow \quad 1 + X = 0, \\ s_{234} = 0 &\quad \leftrightarrow \quad 1 + X|z|^2 = 0, \\ s_{345} = 0 &\quad \leftrightarrow \quad |w|^2 + X|z|^2 = 0. \end{aligned} \quad (3.15)$$

The right-hand side of eq. (3.14) and eq. (3.15) define the physical-singularity surfaces of the minimal set $\{w, z, X\}$. However, in NMRK, if we require all transverse momenta to be non-vanishing, the only singularity surface which can be reached is the collinear limit $w = -zX$. This collinear limit is studied in appendix G.3. This agrees with the intuitive picture of NMRK where, for example, the large rapidity separation $y_3 \gg y_4$ means we cannot take the further collinear limit $p_3 \parallel p_4$. Relaxing the requirement of non-vanishing transverse momenta, eqs. (3.12) and (3.13) are singular in the soft limits $p_4 \rightarrow 0$ and $p_5 \rightarrow 0$, which are explored in appendix G.2.

3.2 BCFW representations

In ref. [54], the opposite-helicity vertex of eq. (3.5) was obtained from the tree-level six-gluon amplitude given in ref. [93]. Compact expressions for NMHV six-gluon amplitudes were later derived using the BCFW on-shell recursion relations [90, 91]. We present one of the amplitudes obtained in ref. [90] here, which we will use as an example in the following⁵:

$$\begin{aligned}
M_{(3.16)}^{(0)}(p_1^\oplus, p_2^\oplus, p_3^\ominus, p_4^\oplus, p_5^\ominus, p_6^\ominus) = & - \frac{\langle 3|1+2|4]^4}{\langle 12\rangle\langle 23\rangle[45][56]s_{123}\langle 1|2+3|4\rangle\langle 3|4+5|6\rangle} \\
& - \frac{\langle 56\rangle^4[24]^4}{\langle 56\rangle\langle 61\rangle[23][34]s_{234}\langle 5|6+1|2\rangle\langle 1|2+3|4\rangle} \\
& - \frac{\langle 35\rangle^4[12]^4}{[61][12]\langle 34\rangle\langle 45\rangle s_{345}\langle 3|4+5|6\rangle\langle 5|6+1|2\rangle}.
\end{aligned} \tag{3.16}$$

A complete set of six-gluon NMHV tree amplitudes are listed in eqs. (D.1)–(D.3). A second set of representations of the tree-level amplitudes are given by eqs. (D.6)–(D.8); these are discussed further in appendix D.2. As mentioned earlier, the individual terms of these BCFW-based amplitudes appear also in the six-gluon one-loop amplitudes in $\mathcal{N} = 4$ SYM. As an example, note that the rational coefficients that appear in the one-loop amplitude (D.10) consist of the individual rational terms that make up the tree-level amplitudes (D.2) and (D.7). In this section we are therefore interested not only in the NMRK limit of the tree-level amplitudes as a whole, but also in the NMRK behaviour of the individual rational terms which will appear outside the context of tree-level amplitudes in section 4.2.

BCFW-based representations have the additional advantage of making the collinear singularity structure of the tree amplitudes manifest. For example, eq. (3.16) has separate poles at $\langle 45\rangle = 0$ and $[45] = 0$, while eq. (3.5) only displays a pole at $s_{45} = 0$. The form in eq. (3.5) entangles the two types of contributions, from different helicity intermediate states; also, individual terms are more singular than the actual amplitude. The BCFW-based representations are therefore more amenable to the study of collinear limits, a property which is utilised in appendix G.3. In addition to physical singularities (spinor products of two cyclically adjacent momenta, and Mandelstam invariants of three cyclically adjacent momenta), the individual terms in these BCFW-based representations also contain unphysical singularities (which cancel in the sum of terms appearing in the amplitude). A simple example is provided by the spinor string

$$\langle 3|4+5|6\rangle \xrightarrow{\text{NMRK}} -q_{3\perp}^* \sqrt{\frac{p_3^+}{p_6^+}} (p_{4\perp} + p_{5\perp}) = |q_{1\perp}|^2 \sqrt{\frac{p_3^+}{p_6^+}} \frac{\bar{z}(\bar{w}-1)(w-z)}{|w|^2|z-1|^2} \tag{3.17}$$

which appears in the denominator of terms in eq. (3.16).

For six-particle kinematics there is a simple relationship between the square of such spinor strings and two- and three-particle Mandelstam invariants,

$$\langle 3|4+5|6\rangle\langle 6|4+5|3\rangle = s_{123}s_{345} \left(1 - \frac{s_{12}s_{45}}{s_{123}s_{345}} \right). \tag{3.18}$$

⁵This amplitude is equal to the complex conjugate of eq. (D.2) and we have expanded the D_i functions to display the physical and spurious poles of the amplitude.

The quantity appearing on the right-hand side, $s_{12}s_{45}/(s_{123}s_{345})$, is a conformally-invariant cross ratio [94]. In this way we see that each of the unphysical singularity surfaces of the rational terms in eqs. (D.1)–(D.3) corresponds to one of the following cross ratios equalling unity,

$$\begin{aligned} u_A &= \frac{s_{12}s_{45}}{s_{123}s_{345}} \xrightarrow{\text{NMRK}} \frac{s_{45}}{(p_4^+ + p_5^+)(p_4^- + p_5^-)} = \frac{|w + Xz|^2}{(1 + X)(|w|^2 + X|z|^2)}, \\ v_A &= \frac{s_{23}s_{56}}{s_{234}s_{123}} \xrightarrow{\text{NMRK}} \frac{(-t_1)p_5^+}{(|q_{2\perp}|^2 + p_4^- p_5^+)(p_4^+ + p_5^+)} = \frac{X|1 - z|^2}{(1 + X|z|^2)(1 + X)}, \\ w_A &= \frac{s_{34}s_{61}}{s_{345}s_{234}} \xrightarrow{\text{NMRK}} \frac{(-t_3)p_4^-}{(p_4^- + p_5^-)(|q_{2\perp}|^2 + p_4^- p_5^-)} = \frac{X|1 - w|^2|z|^2}{(|w|^2 + X|z|^2)(1 + X|z|^2)}. \end{aligned} \quad (3.19)$$

We use the label A to indicate that these are the cross ratios of the colour ordering $\{1, 2, 3, 4, 5, 6\}$, which we will refer to as σ_A . In the NMRK region these cross ratios lie in the range $[0, 1]$, and are studied further in appendix B.1. We choose to label the unphysical singularities of the BCFW representations by the cross ratio which tends to unity as this unphysical singularity surface is approached,

$$P_x^A = 0 \quad \Rightarrow \quad x_A = 1, \quad x \in \{u, v, w\}. \quad (3.20)$$

This notation will be helpful in section 4.2 for demonstrating that the NMHV one-loop six-gluon amplitudes in $\mathcal{N} = 4$ are free from unphysical singularities. We use the term P_x^A to generically refer to the unphysical-singularity surfaces of the terms in the BCFW representation of the amplitudes. We list these unphysical-singularity surfaces in NMRK in terms of both light-cone coordinates and the minimal variables,

$$\begin{aligned} \langle 1|2 + 3|4 \rangle = 0 & \quad \Leftrightarrow \quad P_v^A = 0 \quad \Leftrightarrow \quad q_{2\perp}^* - p_{4\perp}^* \frac{p_5^+}{p_4^+} = 0 \quad \Leftrightarrow \quad 1 + X\bar{z} = 0, \\ \langle 3|4 + 5|6 \rangle = 0 & \quad \Leftrightarrow \quad P_u^A = 0 \quad \Leftrightarrow \quad p_{4\perp} + p_{5\perp} = 0 \quad \Leftrightarrow \quad w - z = 0, \\ \langle 5|6 + 1|2 \rangle = 0 & \quad \Leftrightarrow \quad P_w^A = 0 \quad \Leftrightarrow \quad q_{2\perp}^* + p_{5\perp}^* \frac{p_4^-}{p_5^-} = 0 \quad \Leftrightarrow \quad w + X|z|^2 = 0, \end{aligned} \quad (3.21)$$

which provides intuition for the origin and nature of the unphysical singularities that appear in eqs. (3.22) and (3.24) below. Equations (A.31) and (B.4) list the full expressions for the NMRK limit of these spinor strings in lightcone and minimal coordinates respectively, from which the unphysical singularity surfaces of eq. (3.21) can be identified.

It is interesting to note that a given BCFW representation of a tree amplitude can give rise to different representations of the opposite-helicity two-gluon CEV. As an example, we can obtain a representation for this CEV from eq. (3.16) by taking the central NMRK limit of this amplitude and dividing by impact factors and t -channel propagators according in eq. (3.3). In this way we obtain

$$A^{gg(0)}(q_1, p_4^\oplus, p_5^\ominus, q_3) \Big|_2 = R_{uv}^A + R_{vw}^A + R_{wu}^A, \quad (3.22)$$

with

$$\begin{aligned}
R_{uv}^A &= \frac{X^3|w-1|^2(\bar{z}-1)|z|^2}{(X+1)(\bar{w}+X\bar{z})(w-z)(1+X\bar{z})}, \\
R_{vw}^A &= \frac{zX(w-1)(z-1)}{(1+X|z|^2)(1+X\bar{z})(w+X|z|^2)}, \\
R_{wu}^A &= -\frac{z^3X^3(\bar{w}-1)|z-1|^2|z|^2}{(w+Xz)(|w|^2+X|z|^2)(w+X|z|^2)(w-z)}.
\end{aligned} \tag{3.23}$$

Eq. (3.22) is our second representation for the opposite helicity vertex, equivalent to eq. (3.13) above. In addition to the physical singularities of eq. (3.14) and eq. (3.15), individual terms in eq. (3.22) feature the unphysical singularities of eq. (3.21). We denote the rational terms in (3.23) by their singularities, where R_{xy}^A features unphysical poles at $P_x^A = 0$ and $P_y^A = 0$.

We can obtain another equivalent representation for the opposite-helicity vertex from eq. (3.16) by taking the central NMRK limit of

$$M_{(3.16)}^{(0)}(p_3^\oplus, p_4^\ominus, p_5^\oplus, p_6^\oplus, p_1^\ominus, p_2^\ominus)^*.$$

This gives us our third representation of the CEV,

$$A^{gg(0)}(q_1, p_4^\oplus, p_5^\ominus, q_3) \Big|_3 = R_{\bar{u}\bar{v}}^A + R_{\bar{v}\bar{w}}^A + R_{\bar{w}\bar{u}}^A, \tag{3.24}$$

with

$$\begin{aligned}
R_{\bar{u}\bar{v}}^A &= \frac{X|w-1|^2(z-1)|z|^2}{(X+1)(w+Xz)(\bar{w}-\bar{z})(1+Xz)}, \\
R_{\bar{v}\bar{w}}^A &= \frac{X^3(\bar{w}-1)(\bar{z}-1)z^4\bar{z}}{(1+X|z|^2)(1+Xz)(\bar{w}+X|z|^2)}, \\
R_{\bar{w}\bar{u}}^A &= -\frac{Xz(w-1)\bar{w}^4|z-1|^2}{(\bar{w}+X\bar{z})(|w|^2+X|z|^2)(\bar{w}+X|z|^2)(\bar{w}-\bar{z})}.
\end{aligned} \tag{3.25}$$

The notation $R_{\bar{x}\bar{y}}^A$ indicates these rational terms have unphysical singularities at $\bar{P}_x^A = 0$ and $\bar{P}_y^A = 0$, where as usual, we use bar to denote complex conjugation. Of course, these six rational terms are not independent due to the relation,

$$R_{uv}^A + R_{vw}^A + R_{wu}^A = R_{\bar{u}\bar{v}}^A + R_{\bar{v}\bar{w}}^A + R_{\bar{w}\bar{u}}^A. \tag{3.26}$$

These rational terms, when divided by the appropriate MHV central-emission vertex, correspond to the NMRK limit of the dual-conformal-invariant R -invariants of $\mathcal{N} = 4$ SYM [95]. In this paper however, we do not normalise by the MHV vertex as this will avoid the introduction of the MHV phase, and will lead to simpler expressions when we take further kinematic limits of these rational terms.

Having studied the physical and spurious poles of the BCFW representation of the opposite-helicity CEV, we briefly return to the CSW representation of the vertex, eq. (E.1). We write this in terms of the minimal variables in eq. (E.2). We can now see that this representation has the expected physical singularities of eqs. (3.14) and (3.15), and also

spurious poles at $P_u^A = 0$ and $\bar{P}_v^A = 0$. In addition to these representations, one can find a compact representation of the central-emission vertex, eq. (E.3), which only has a single spurious pole at $P_u^A = 0$. We have checked analytically that the five representations of the opposite-helicity vertex in eqs. (3.13), (3.22), (3.24), (E.2) and (E.3) are all equivalent. The equivalence of these expressions shows that $P_x^A = 0$ are not true singularities of the central-emission vertex, and we say that they are spurious, or removable poles of this expression.

3.3 Other colour orderings

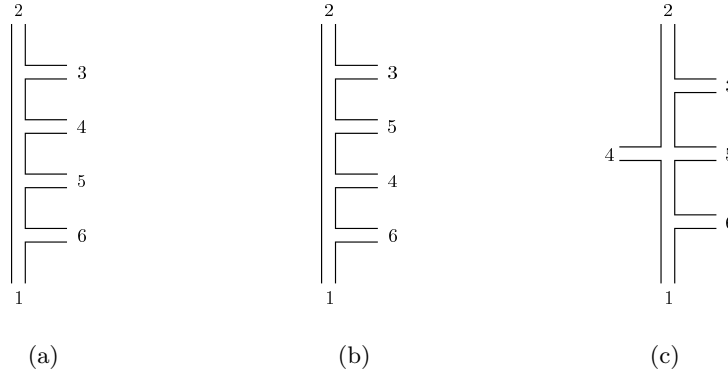


Figure 5. The colour connections of the three representative colour orderings we discuss in this paper, displayed on a two-sided rapidity plot: (a) σ_A ; (b) $\sigma_{A'}$; (c) σ_B , which uses 't Hooft graphical notation, with untwisted colour lines. Modulo cyclic permutations of the colour ordering, the gluons which fall between incoming gluons 2 and 1 are placed on the “front” side of the plot, while the gluons which fall between 1 and 2 are placed on the “back” side. In MRK, the gluons are ordered in rapidity both on the front and on the back sides, however the relative ordering between the two sides is immaterial [75, 96]. On the front side, colour and rapidity have the same ordering; on the back, the opposite ordering. In NMRK, the strict orderings may be relaxed on either side as appropriate [51].

So far we have only investigated a single colour ordering, which we termed σ_A . All colour orderings were studied in NMRK at tree-level in ref. [51]. There the leading behaviour was found to be given by colour orderings that have p_1 adjacent to p_6 and p_2 adjacent to p_3 . An interchange of $p_1 \leftrightarrow p_6$ or $p_2 \leftrightarrow p_3$ leads only to a change in the sign of the amplitude. In addition to σ_A we should therefore consider the representative orderings $\sigma_{A'} = \{1, 2, 3, 5, 4, 6\}$ and $\sigma_B = \{1, 4, 2, 3, 5, 6\}$, which are displayed in fig. 5 using the two-sided rapidity plot [75, 96]⁶. The ordering $\sigma_{A'}$, is related to the former by a simple interchange of $p_4 \leftrightarrow p_5$, which we may directly apply to the functions in eq. (3.5). In terms

⁶An earlier version of the two-sided rapidity plot, for which though colour was absent, was used in multiperipheral and dual models [97, 98].

of the minimal variables this operation is given by

$$\begin{aligned} z &\xrightarrow[p_4 \leftrightarrow p_5]{} 1 + w \frac{1-z}{z}, \\ w &\xrightarrow[p_4 \leftrightarrow p_5]{} 1 + z \frac{1-w}{w}, \\ X &\xrightarrow[p_4 \leftrightarrow p_5]{} \frac{1}{X}. \end{aligned} \tag{3.27}$$

Throughout this paper we will use a prime to refer to an interchange of $p_4 \leftrightarrow p_5$, for example

$$q_2 \equiv q_1 - p_4 = q_3 + p_5, \quad \text{so} \quad q_2' \equiv q_1 - p_5 = q_3 + p_4, \tag{3.28}$$

which is the relevant t -channel momentum for the MRK' limit. For example, the equal-helicity tree-level CEV in the minimal variables is given by

$$A^{gg(0)}(q_1, p_5^\oplus, p_4^\oplus, q_3) = \frac{q_{1\perp}^*}{q_{1\perp}} \frac{w(w-1)(z-1)}{(w+Xz)}. \tag{3.29}$$

For completeness, we list the full analysis of the BCFW representations of the opposite-helicity vertex for the ordering $\sigma_{A'}$ in appendix E.1.

In the central NMRK limit, the colour-ordered amplitude of the remaining ordering σ_B similarly factorises as

$$M_{6g}^{(0)}(p_1^{\nu_1}, p_4^{\nu_4}, p_2^{\nu_2}, p_3^{\nu_3}, p_5^{\nu_5}, p_6^{\nu_6}) = s C^{g(0)}(p_2^{\nu_2}, p_3^{\nu_3}) \frac{1}{t_1} B^{gg(0)}(q_1, p_4^{\nu_4}, p_5^{\nu_5}, q_3) \frac{1}{t_3} C^{g(0)}(p_1^{\nu_1}, p_6^{\nu_6}), \tag{3.30}$$

However, the tree-level CEV for the ordering σ_B is not independent to that of the orderings σ_A and $\sigma_{A'}$ due to the relationship [51],

$$A^{gg(0)}(q_1, p_4^{\nu_4}, p_5^{\nu_5}, q_3) + A^{gg(0)}(q_1, p_5^{\nu_5}, p_4^{\nu_4}, q_3) + B^{gg(0)}(q_1, p_4^{\nu_4}, p_5^{\nu_5}, q_3) = 0. \tag{3.31}$$

This relation follows [70] from the U(1) decoupling equation [99, 100], or as the leading contribution in NMRK to a Kleiss-Kuijf relation [101] which relates colour-ordered amplitudes at tree level [102]. Eq. (3.31) is simple to verify in the equal-helicity case using eqs. (3.12) and (3.29), and

$$B^{gg(0)}(q_1, p_4^\oplus, p_5^\oplus, q_3) = \frac{q_{1\perp}^* q_{3\perp}}{p_{4\perp} p_{5\perp}} = -\frac{q_{1\perp}^*}{q_{1\perp}} (w-1)(z-1). \tag{3.32}$$

To demonstrate the relationship given in eq. (3.31) for the opposite-helicity case, it will be easier to first obtain a representation of $B^{gg(0)}$ in the minimal variables. At tree level, there are therefore only two independent colour orderings in NMRK, as in eq. (3.2). However, in the one-loop MHV amplitudes of $\mathcal{N} = 4$ SYM, the tree-level amplitudes for σ_A , $\sigma_{A'}$ and σ_B will all be multiplied by distinct transcendental functions, so these colour orderings are independent beyond tree level. Furthermore, in the one-loop NMHV amplitudes for $\mathcal{N} = 4$ SYM, we encounter rational coefficients of transcendental functions which are not simply tree-level amplitudes. However, as mentioned in the outset of section 3, these rational coefficients consist of the individual terms in the BCFW representations of

the tree amplitudes. For this reason, we investigate the BCFW-based representation of the tree-level amplitudes for the σ_B ordering in this section, with an emphasis on the individual rational terms.

We now perform a study analogous to section 3.2 for the ordering σ_B . We first list the cross ratios for this colour ordering,

$$\begin{aligned} u_B &= \frac{s_{14}s_{35}}{s_{142}s_{235}} = \frac{p_4^+ p_5^-}{|q_{2\perp}'|^2 + p_4^+ p_5^-} = \frac{X|z|^2}{|w+z-wz|^2 + X|z|^2} \\ v_B &= \frac{s_{42}s_{56}}{s_{423}s_{142}} = \frac{p_4^- p_5^+}{|q_{2\perp}|^2 + p_4^- p_5^+} = \frac{1}{1 + X|z|^2} \\ w_B &= \frac{s_{23}s_{61}}{s_{235}s_{423}} = \frac{(-t_1)(-t_3)}{(|q_{2\perp}|^2 + p_4^- p_5^+)(|q_{2\perp}'|^2 + p_4^+ p_5^-)} = \frac{|w-1|^2|z-1|^2 X|z|^2}{(1 + X|z|^2)(|w+z-wz|^2 + X|z|^2)} \end{aligned} \quad (3.33)$$

which, like eq. (3.19), lie in the range $[0, 1]$ for our physical kinematic region. Returning to our example amplitude, the NMRK limit of $M_{(3.16)}^{(0)}(p_1^\oplus, p_4^\oplus, p_2^\ominus, p_3^\oplus, p_5^\ominus, p_6^\ominus)$ yields the representation,

$$B^{gg(0)}(q_1, p_4^\oplus, p_5^\ominus, q_3) = R_{uv}^B + R_{vw}^B + R_{wu}^B, \quad (3.34)$$

with

$$\begin{aligned} R_{uv}^B &= \frac{z|w-1|^2|z-1|^2}{\bar{z}(w+z-wz)}, \\ R_{vw}^B &= -\frac{z(w-1)(z-1)}{\bar{z}(1+X|z|^2)(w+z-wz+X|z|^2)}, \\ R_{wu}^B &= -\frac{(\bar{w}-1)X^2 z^3 (\bar{z}-1)\bar{z}}{(w+z-wz)(w+z-wz+X|z|^2)(|w+z-wz|^2 + X|z|^2)}, \end{aligned} \quad (3.35)$$

while the NMRK limit of $M_{(D.1)}^{(0)}(p_1^\ominus, p_4^\ominus, p_2^\ominus, p_3^\oplus, p_5^\oplus, p_6^\oplus)$ yields the representation,

$$B^{gg(0)}(q_1, p_4^\oplus, p_5^\ominus, q_3) = R_{u\bar{v}}^B + R_{v\bar{w}}^B + R_{\bar{w}\bar{u}}^B, \quad (3.36)$$

with

$$\begin{aligned} R_{u\bar{v}}^B &= 0, \\ R_{v\bar{w}}^B &= -\frac{(\bar{w}-1)(\bar{z}-1)|z|^2 z^2 X^2}{(1+X|z|^2)(\bar{w}+\bar{z}-\bar{w}\bar{z}+X|z|^2)}, \\ R_{\bar{w}\bar{u}}^B &= -\frac{z(w-1)(z-1)(\bar{w}+\bar{z}-\bar{w}\bar{z})^3}{\bar{z}(\bar{w}+\bar{z}-\bar{w}\bar{z}+X|z|^2)(|w+z-wz|^2 + X|z|^2)}. \end{aligned} \quad (3.37)$$

One can now verify the relation eq. (3.31) using the representations in eq. (3.34) or eq. (3.36) along with those obtained in section 3.2.

Recalling eq. (A.27) and eq. (B.3), the physical-singularity surfaces of this ordering are

$$\begin{aligned} s_{142} = 0 &\quad \leftrightarrow \quad p_3^+ p_6^- = 0, \\ s_{234} = 0 &\quad \leftrightarrow \quad |q_{2\perp}|^2 + p_4^- p_5^+ = 0 \quad \leftrightarrow \quad 1 + X|z|^2 = 0, \\ s_{235} = 0 &\quad \leftrightarrow \quad |q_{2\perp}'|^2 + p_4^+ p_5^- = 0 \quad \leftrightarrow \quad |w+z-wz|^2 + X|z|^2 = 0, \end{aligned} \quad (3.38)$$

where we note that there is no singularity in the collinear limit, eq. (3.14). In the NMRK limit $s_{142} \sim s_{12}$ which does not depend on the central degrees of freedom of the process. We therefore have not listed an entry for this Mandelstam invariant in terms of the minimal variables. With reference to eqs. (A.32) and (B.5), the unphysical-singularity surfaces are⁷

$$\begin{aligned}
\langle 1|4+2|3\rangle = 0 &\leftrightarrow P_v^B = 0 \leftrightarrow q_{2\perp}^* = 0, \\
\langle 2|3+5|6\rangle = 0 &\leftrightarrow P_u^B = 0 \leftrightarrow q'_{2\perp} = 0 \leftrightarrow w + z - wz = 0, \\
\langle 5|6+1|4\rangle = 0 &\leftrightarrow P_w^B = 0 \leftrightarrow \frac{q_{2\perp}^*}{p_{4\perp}^*} + \frac{q'_{2\perp}}{p_{5\perp}} \frac{p_5^+}{p_4^+} = 0 \leftrightarrow w + z - wz + X|z|^2 = 0.
\end{aligned} \tag{3.39}$$

We note that under the transformation in eq. (3.27) one obtains

$$u_B \xleftrightarrow[p_4 \leftrightarrow p_5]{} v_B, \quad w_B \xleftrightarrow[p_4 \leftrightarrow p_5]{} w_B, \tag{3.40}$$

and

$$\begin{aligned}
R_{uv}^B &\xleftrightarrow[p_4 \leftrightarrow p_5]{} (R_{uv}^B)^*, & R_{vw}^B &\xleftrightarrow[p_4 \leftrightarrow p_5]{} (R_{wu}^B)^*, \\
R_{\bar{u}\bar{v}}^B &\xleftrightarrow[p_4 \leftrightarrow p_5]{} (R_{\bar{u}\bar{v}}^B)^* = 0, & R_{\bar{v}\bar{w}}^B &\xleftrightarrow[p_4 \leftrightarrow p_5]{} (R_{\bar{w}\bar{u}}^B)^*.
\end{aligned} \tag{3.41}$$

These properties will be useful for organising the one-loop opposite-helicity amplitude in section 4.2.

3.4 The target-projectile exchange

The amplitude in eq. (3.2) is manifestly symmetric under the target-projectile exchange. The manifest symmetry is broken on the right-hand side of eq. (3.3) by the choice of impact factors in eq. (2.2), which is dictated by the momentum representation, eq. (A.5), of the spinor products. However, in transverse-momentum space the impact factors in (2.2) are just phases, and hence the central-emission vertex for the emission of two gluons is invariant under target-projectile exchange up to an overall phase. We may consider then the target-projectile map F , which interchanges

$$p_1 \xleftrightarrow[F]{} p_2, \quad p_3 \xleftrightarrow[F]{} p_6, \quad p_4 \xleftrightarrow[F]{} p_5. \tag{3.42}$$

In NMRK the target-projectile map acts as

$$q_{1\perp} \xleftrightarrow[F]{} -q_{3\perp}, \quad p_{4\perp} \xleftrightarrow[F]{} p_{5\perp}, \quad p_4^\pm \xleftrightarrow[F]{} p_5^\mp. \tag{3.43}$$

In terms of the minimal set $\{w, z, X\}$ these flip relations can be expressed as

$$w \xleftrightarrow[F]{} z, \quad X \xleftrightarrow[F]{} \frac{|z|^2}{|w|^2} X. \tag{3.44}$$

⁷In the minimal coordinates, the limit $q_{2\perp}^* \rightarrow 0$ is equivalent to taking \bar{w} and \bar{z} to zero at the same rate. The ratio \bar{w}/\bar{z} is well defined in this limit.

Under these flips, the cross ratios for the σ_A ordering, eq. (3.19), change as

$$u_A \xleftrightarrow{F} u_A, \quad v_A \xleftrightarrow{F} w_A, \quad (3.45)$$

while the spurious poles change as

$$w + X|z|^2 \xrightarrow{F} z(1 + X\bar{z}), \quad w - z \xrightarrow{F} -(w - z), \quad 1 + X\bar{z} \xrightarrow{F} \frac{w + X|z|^2}{w}, \quad (3.46)$$

i.e. the first and third spurious-pole surfaces in eq. (3.21) are swapped. Furthermore, the rational coefficients (3.23) change as

$$\begin{aligned} R_{uv}^A &\xrightarrow{F} \frac{w\bar{z}}{\bar{w}z} R_{wu}^A, & R_{\bar{u}\bar{v}}^A &\xrightarrow{F} \frac{w\bar{z}}{\bar{w}z} R_{\bar{w}\bar{u}}^A, \\ R_{vw}^A &\xrightarrow{F} \frac{w\bar{z}}{\bar{w}z} R_{vw}^A, & R_{\bar{v}\bar{w}}^A &\xrightarrow{F} \frac{w\bar{z}}{\bar{w}z} R_{\bar{v}\bar{w}}^A, \\ R_{wu}^A &\xrightarrow{F} \frac{w\bar{z}}{\bar{w}z} R_{uv}^A, & R_{\bar{w}\bar{u}}^A &\xrightarrow{F} \frac{w\bar{z}}{\bar{w}z} R_{\bar{u}\bar{v}}^A, \end{aligned} \quad (3.47)$$

from which we see that both eqs. (3.22) and (3.24) are invariant under the target-projectile map F , up to an overall phase. By contrast, for the σ_B ordering we find that each cross ratio (eq. (3.33)) is invariant under this map,

$$u_B \xleftrightarrow{F} u_B, \quad v_B \xleftrightarrow{F} v_B, \quad w_B \xleftrightarrow{F} w_B, \quad (3.48)$$

the spurious singularity surfaces (3.39) are likewise invariant, while each rational term in eqs. (3.34) and (3.36) is invariant up to an overall phase,

$$R_{xy}^B \xrightarrow{F} \frac{w\bar{z}}{\bar{w}z} R_{xy}^B, \quad R_{\bar{x}\bar{y}}^B \xrightarrow{F} \frac{w\bar{z}}{\bar{w}z} R_{\bar{x}\bar{y}}^B, \quad x, y \in \{u, v, w\}, x \neq y.$$

Having investigated the tree-level CEV, and in particular the rational terms R_{xy}^I which comprise the BCFW representations of this CEV, we proceed to the study of this vertex at one loop.

4 The two-gluon central-emission vertex at one loop

In this section we will extract the two-gluon central-emission vertex at one loop in $\mathcal{N} = 4$ SYM. The plan is analogous to the extraction of the tree-level vertex in section 3. We will begin with the one-loop amplitude in general kinematics, and find the leading behaviour in the central NMRK limit defined in appendix A.3. We expect that in this limit, the amplitude will factorise into the known one-loop impact factors and Regge trajectories associated with the two large rapidity spans, and a new piece which depends only on the central degrees of freedom, i.e. the gluons 4 and 5 and the transverse t -channel momenta. We will identify this new central piece with the one-loop CEV.

The study of the two-gluon CEV in $\mathcal{N} = 4$ SYM is not only of interest in its own right; via the supersymmetric decomposition of QCD amplitudes at one loop [72–74], it is also an ingredient for the two-gluon CEV in QCD. As such, we will begin by clarifying the connection between the two.

The colour decomposition we use for the QCD one-loop six-gluon amplitude is [102],

$$\mathcal{M}_{\text{QCD}}^{(1)} = g_S^6 \sum_{\sigma \in S_5/\mathcal{R}} \left[\text{tr} (F^{a_{\sigma_1}} \dots F^{a_{\sigma_6}}) M_{\text{QCD}}^{(1)[\mathbf{8}]} (p_{\sigma_1}^{\nu_{\sigma_1}}, \dots, p_{\sigma_6}^{\nu_{\sigma_6}}) \right. \\ \left. + N_f \text{tr} (T^{a_{\sigma_1}} \dots T^{a_{\sigma_6}}) M_{\text{QCD}}^{(1)[\mathbf{3}]} (p_{\sigma_1}^{\nu_{\sigma_1}}, \dots, p_{\sigma_6}^{\nu_{\sigma_6}}) \right], \quad (4.1)$$

where $S_5 = S_6/\mathbb{Z}_6$ is the group of non-cyclic permutations and \mathcal{R} is the total reflection, e.g. $\mathcal{R}(1, 2, 3, 4, 5, 6) = (6, 5, 4, 3, 2, 1)$. The superscript $[\mathbf{R}]$ on colour-ordered amplitudes denotes the colour representation of the particle circulating in the loop. We remind the reader that F^{a_i} and T^{a_i} are generators in the adjoint and fundamental representations respectively. For convenience we define separate colour-dressed amplitudes for the gluon-loop and quark-loop contributions,

$$\mathcal{M}_{\text{QCD}}^{(1)[\mathbf{8}]} = g_S^6 \sum_{\sigma \in S_5/\mathcal{R}} \text{tr} (F^{a_{\sigma_1}} \dots F^{a_{\sigma_6}}) M_{\text{QCD}}^{(1)[\mathbf{8}]} (p_{\sigma_1}^{\nu_{\sigma_1}}, \dots, p_{\sigma_6}^{\nu_{\sigma_6}}), \quad (4.2)$$

$$\mathcal{M}_{\text{QCD}}^{(1)[\mathbf{3}]} = g_S^6 \sum_{\sigma \in S_5/\mathcal{R}} \text{tr} (T^{a_{\sigma_1}} \dots T^{a_{\sigma_6}}) M_{\text{QCD}}^{(1)[\mathbf{3}]} (p_{\sigma_1}^{\nu_{\sigma_1}}, \dots, p_{\sigma_6}^{\nu_{\sigma_6}}), \quad (4.3)$$

such that the QCD amplitude of eq. (4.1), with N_f Dirac fermions in the fundamental representation, is obtained by

$$\mathcal{M}_{\text{QCD}}^{(1)} = \mathcal{M}_{\text{QCD}}^{(1)[\mathbf{8}]} + N_f \mathcal{M}_{\text{QCD}}^{(1)[\mathbf{3}]} . \quad (4.4)$$

Colour-ordered gluon amplitudes in QCD at one loop may be further decomposed into supersymmetric multiplets circulating in the loop,

$$M_{\text{QCD}}^{(1)[\mathbf{8}]} = M_{\mathcal{N}=4}^{(1)} - 4M_{\mathcal{N}=1\chi}^{(1)} + M_{\text{scalar}}^{(1)}, \quad (4.5a)$$

$$M_{\text{QCD}}^{(1)[\mathbf{3}]} = M_{\mathcal{N}=1\chi}^{(1)} - M_{\text{scalar}}^{(1)}. \quad (4.5b)$$

To bring this supersymmetric decomposition to the level of colour-dressed QCD amplitudes we define the colour-dressed contribution from the $\mathcal{N} = 4$ multiplet,

$$\mathcal{M}_{\mathcal{N}=4}^{(1)} = g_S^6 \sum_{\sigma \in S_5/\mathcal{R}} \text{tr} (F^{a_{\sigma_1}} \dots F^{a_{\sigma_6}}) M_{\mathcal{N}=4}^{(1)} (p_{\sigma_1}^{\nu_{\sigma_1}}, \dots, p_{\sigma_6}^{\nu_{\sigma_6}}). \quad (4.6)$$

For the colour-dressed contributions from the $\mathcal{N} = 1$ multiplet and the scalar circulating in the loop, we separately consider the cases where these are in the adjoint or fundamental representations,

$$\mathcal{M}_{\mathcal{N}=1\chi}^{(1)[\mathbf{8}]} = g_S^6 \sum_{\sigma \in S_5/\mathcal{R}} \text{tr} (F^{a_{\sigma_1}} \dots F^{a_{\sigma_6}}) M_{\mathcal{N}=1\chi}^{(1)} (p_{\sigma_1}^{\nu_{\sigma_1}}, \dots, p_{\sigma_6}^{\nu_{\sigma_6}}), \quad (4.7a)$$

$$\mathcal{M}_{\mathcal{N}=1\chi}^{(1)[\mathbf{3}]} = g_S^6 \sum_{\sigma \in S_5/\mathcal{R}} \text{tr} (T^{a_{\sigma_1}} \dots T^{a_{\sigma_6}}) M_{\mathcal{N}=1\chi}^{(1)} (p_{\sigma_1}^{\nu_{\sigma_1}}, \dots, p_{\sigma_6}^{\nu_{\sigma_6}}), \quad (4.7b)$$

$$\mathcal{M}_{\text{scalar}}^{(1)[\mathbf{8}]} = g_S^6 \sum_{\sigma \in S_5/\mathcal{R}} \text{tr} (F^{a_{\sigma_1}} \dots F^{a_{\sigma_6}}) M_{\text{scalar}}^{(1)} (p_{\sigma_1}^{\nu_{\sigma_1}}, \dots, p_{\sigma_6}^{\nu_{\sigma_6}}), \quad (4.7c)$$

$$\mathcal{M}_{\text{scalar}}^{(1)[\mathbf{3}]} = g_S^6 \sum_{\sigma \in S_5/\mathcal{R}} \text{tr} (T^{a_{\sigma_1}} \dots T^{a_{\sigma_6}}) M_{\text{scalar}}^{(1)} (p_{\sigma_1}^{\nu_{\sigma_1}}, \dots, p_{\sigma_6}^{\nu_{\sigma_6}}), \quad (4.7d)$$

such that we can write the QCD one-loop colour-dressed amplitude as

$$\mathcal{M}_{\text{QCD}}^{(1)} = \left(\mathcal{M}_{\mathcal{N}=4}^{(1)} - 4\mathcal{M}_{\mathcal{N}=1\chi}^{(1)[8]} + \mathcal{M}_{\text{scalar}}^{(1)[8]} \right) + N_f \left(\mathcal{M}_{\mathcal{N}=1\chi}^{(1)[3]} - \mathcal{M}_{\text{scalar}}^{(1)[3]} \right). \quad (4.8)$$

At one loop, this decomposition holds also at the level of the Regge-factorised expressions. For example, we can write the one-loop coefficient of the impact factor in eq. (2.18) as

$$c_{\text{QCD}}^{g(1)} = \left(c_{\mathcal{N}=4}^{g(1)} - 4c_{\mathcal{N}=1\chi}^{g(1)[8]} + c_{\text{scalar}}^{g(1)[8]} \right) + N_f \left(c_{\mathcal{N}=1\chi}^{g(1)[3]} - c_{\text{scalar}}^{g(1)[3]} \right). \quad (4.9)$$

In this paper we focus on the $\mathcal{N} = 4$ component, $\mathcal{M}_{\mathcal{N}=4}^{(1)}$, of the one-loop amplitude. Let us begin by discussing the relevant helicity configurations. As at tree level, there are two distinct helicity configurations for the one-loop two-gluon central-emission vertex. In order to derive this CEV we take the central NMRK limit, as defined in eq. (A.23), of $\mathcal{M}_{\mathcal{N}=4}^{(1)}(p_1^{\nu_1}, p_2^{\nu_2}, p_3^{-\nu_2}, p_4^{\nu_4}, p_5^{\nu_5}, p_6^{-\nu_1})$. Thus, to obtain the same-helicity vertex, i.e. $\nu_4 = \nu_5$, the six-gluon amplitude we begin with must necessarily be an (anti-)MHV amplitude. In section 4.1 we take the central NMRK limit of (anti-)MHV one-loop six-gluon amplitudes in $\mathcal{N} = 4$ SYM to obtain the one-loop two-gluon CEV of this theory. In turn, in order to extract the one-loop opposite-helicity vertex we must instead take the NMRK limit of a helicity configuration with $\nu_4 \neq \nu_5$, which is necessarily an NMHV amplitude. This study is performed in section 4.2.

In both cases we can simplify the procedure by recalling some results from section 3. Although eq. (4.6) consists of a sum of 60 colour orderings, only 12 of these are not power suppressed by the rational terms in the central NMRK limit. This is straightforward for the MHV amplitudes, which are proportional to the tree-level result, up to logarithmically varying functions, as we will see in eq. (4.17). For the NMHV amplitudes, eqs. (D.9)–(D.11), this is not the case. However, each of the pairs of individual rational terms in these amplitudes are power suppressed in the NMRK limit for colour orderings that do not have both p_2 and p_3 adjacent, and p_6 and p_1 adjacent. This means we need only study the 12 colour orderings that are leading at tree-level also for the one-loop NMHV amplitudes. It will be useful to consider the representative colour orderings,

$$\sigma_A = \{1, 2, 3, 4, 5, 6\}, \quad \sigma_{A'} = \{1, 2, 3, 5, 4, 6\}, \quad \sigma_B = \{1, 4, 2, 3, 5, 6\}, \quad (4.10)$$

that we introduced in section 3. We further introduce the notation $\overset{\leftrightarrow}{\sigma}$ to indicate a kinematic (momentum and spin) interchange of $2 \leftrightarrow 3$, and $\overset{\leftrightarrow}{\sigma}$ to indicate a kinematic interchange of $1 \leftrightarrow 6$. As an example of this notation,

$$\overset{\leftrightarrow}{\sigma}_A^{\overset{\leftrightarrow}{\sigma}} = \{6, 3, 2, 4, 5, 1\}. \quad (4.11)$$

The amplitude can thus be written as a decomposition into symmetric (+) and antisymmetric (−) components, as done in eq. (2.19),

$$\mathcal{M}^{(1)} = \mathcal{M}^{(1)(+,+)} + \mathcal{M}^{(1)(+,-)} + \mathcal{M}^{(1)(-,+)} + \mathcal{M}^{(1)(-,-)}. \quad (4.12)$$

Owing to Bose symmetry for gluon amplitudes, these kinematic interchanges translate directly into interchanges of the corresponding colour indices, so for example $\mathcal{M}^{(1)(-,-)}$

corresponds to the component of the amplitude in which an antisymmetric colour representation is exchanged in both the t_1 and t_3 channels, $\mathcal{M}^{(1)(+,-)}$ corresponds to one in which a symmetric representation is exchanged in the t_1 channel, while an antisymmetric one in the t_3 channel, etc. In the central NMRK limit it will be useful to organise the colour-dressed amplitudes according to this symmetry. For example, when there is an adjoint representation circulating in the loop we obtain

$$\begin{aligned} \mathcal{M}^{(1)(-,-)} &= g_S^6 F^{a_3 a_2 c_1} F^{a_6 a_1 c_3} \\ &\times \frac{1}{4} \left\{ \text{tr} (F^{c_1} F^{a_4} F^{a_5} F^{c_3}) \times \left(M^{(1)}(\sigma_A) - M^{(1)}(\overset{\leftrightarrow}{\sigma}_A) - M^{(1)}(\overset{\leftrightarrow}{\sigma}_A) + M^{(1)}(\overset{\leftrightarrow}{\sigma}_A) \right) \right. \\ &\quad + \text{tr} (F^{c_1} F^{a_5} F^{a_4} F^{c_3}) \times \left(M^{(1)}(\sigma_{A'}) - M^{(1)}(\overset{\leftrightarrow}{\sigma}_{A'}) - M^{(1)}(\overset{\leftrightarrow}{\sigma}_{A'}) + M^{(1)}(\overset{\leftrightarrow}{\sigma}_{A'}) \right) \\ &\quad \left. + \text{tr} (F^{c_1} F^{a_4} F^{c_3} F^{a_5}) \times \left(M^{(1)}(\sigma_B) - M^{(1)}(\overset{\leftrightarrow}{\sigma}_B) - M^{(1)}(\overset{\leftrightarrow}{\sigma}_B) + M^{(1)}(\overset{\leftrightarrow}{\sigma}_B) \right) \right\}, \end{aligned} \quad (4.13)$$

which in particular is valid for one-loop gluon amplitudes in $\mathcal{N} = 4$ SYM, eq. (4.6). The analogous expressions for the other signatures are listed in eqs. (F.1)–(F.3).

Before extracting the same-helicity CEV in section 4.1 and the opposite-helicity CEV in section 4.2, we list here the known one-loop coefficients of the impact factor and Lipatov vertex in $\mathcal{N} = 4$ SYM, which will be of use in our extraction of both helicity configurations of the two-gluon CEV. The one-loop coefficient, eq. (2.18), of the impact factor in $\mathcal{N} = 4$ SYM is

$$c_{\mathcal{N}=4}^{g(1)}(t) = N_c \kappa_\Gamma \left(\frac{\mu^2}{-t} \right)^\epsilon \left(-\frac{2}{\epsilon^2} + \frac{1}{\epsilon} \log \left(\frac{\tau}{-t} \right) + \frac{\pi^2}{2} - \frac{\delta_R}{6} \right), \quad (4.14)$$

where $\delta_R = 1$ in conventional dimensional regularisation (CDR) and in 't-Hooft-Veltman (HV) schemes, while $\delta_R = 0$ in dimensional reduction. The QCD one-loop impact factor, from which eq. (4.14) may be understood through the decomposition of eq. (4.9), was computed for $\delta_R = 1$ in [45, 48, 49, 57], and for $\delta_R = 0$ in [48, 49]. Secondly, the single-gluon CEV to one-loop accuracy, eq. (2.23), in $\mathcal{N} = 4$ SYM is given by

$$\begin{aligned} v_{\mathcal{N}=4}^{g(1)}(t_1, |p_{4\perp}|^2, t_2) &= N_c \kappa_\Gamma \left(-\frac{1}{\epsilon^2} \left(\frac{\mu^2}{|p_{4\perp}|^2} \right)^\epsilon + \frac{\pi^2}{3} \right. \\ &\quad \left. + \frac{1}{\epsilon} \left[\left(\frac{\mu^2}{-t_1} \right)^\epsilon + \left(\frac{\mu^2}{-t_2} \right)^\epsilon \right] \log \left(\frac{\tau}{|p_{4\perp}|^2} \right) - \frac{1}{2} \log^2 \left(\frac{t_1}{t_2} \right) \right). \end{aligned} \quad (4.15)$$

Note that eq. (4.15) is independent of the helicity of the produced particle, and of the regularisation parameter δ_R . The one-loop coefficient was computed in QCD in [45–49], from which the $\mathcal{N} = 4$ part, eq. (4.15), may be extracted. We note that since in $\mathcal{N} = 4$ SYM the beta function vanishes, eqs. (4.14) and (4.15) do not need to be renormalised. In this paper we use the dimensional reduction choice with $\delta_R = 0$, preserving the uniform transcendentality property of the $\mathcal{N} = 4$ SYM amplitude.

4.1 Same-helicity vertex

In this section we take the NMRK limit of the MHV amplitude,

$$\mathcal{M}_{\mathcal{N}=4}^{(1)}(p_1^{\nu_1}, p_2^{\nu_2}, p_3^{-\nu_2}, p_4^\oplus, p_5^\oplus, p_6^{-\nu_1}). \quad (4.16)$$

After the CEV for $\nu_4 = \nu_5 = \oplus$ has been obtained, the CEV for $\nu_4 = \nu_5 = \ominus$ may be obtained by complex conjugation, just as for the tree-level vertex, eq. (3.7). The colour-ordered amplitudes for one-loop six-gluon MHV amplitudes in $\mathcal{N} = 4$ SYM are [73]

$$M_{\mathcal{N}=4}^{(1)}(p_{\sigma_1}^{\nu_{\sigma_1}}, \dots, p_{\sigma_6}^{\nu_{\sigma_6}}) = \frac{\kappa\Gamma}{(4\pi)^2} M^{(0)}(p_{\sigma_1}^{\nu_{\sigma_1}}, \dots, p_{\sigma_6}^{\nu_{\sigma_6}}) V_6(\sigma_1, \dots, \sigma_6), \quad (4.17)$$

where the transcendental terms are given by the function,

$$\begin{aligned} V_6(\sigma_1, \dots, \sigma_6) = & \sum_{i=1}^6 -\frac{1}{\epsilon^2} \left(\frac{\mu^2}{-t_i^{[2]}} \right)^\epsilon - \sum_{i=1}^6 \log \left(\frac{-t_i^{[2]}}{-t_i^{[3]}} \right) \log \left(\frac{-t_{i+1}^{[2]}}{-t_i^{[3]}} \right) \\ & + \frac{1}{2} \sum_{i=1}^3 \log^2 \left(\frac{-t_i^{[3]}}{-t_{i+1}^{[3]}} \right) - \sum_{i=1}^3 \text{Li}_2 \left[1 - \frac{(-t_i^{[2]})(-t_{i+3}^{[2]})}{(-t_i^{[3]})(-t_{i-1}^{[3]})} \right] + \pi^2, \end{aligned} \quad (4.18)$$

which does not depend on the helicities of the gluons. Here we have used the notation,

$$t_i^{[r]} = (p_{\sigma_i} + \dots + p_{\sigma_{i+r-1}})^2. \quad (4.19)$$

When analytically continuing to the physical region, as discussed in appendix A.1, we give all Mandelstam invariants a small positive imaginary part, $t_i^{[m]} \rightarrow t_i^{[m]} + i0$. For logarithms of ratios of invariants, this prescription yields

$$\log \left(\frac{-t_i^{[m]}}{-t_j^{[n]}} \right) = \log \left(\left| \frac{t_i^{[m]}}{t_j^{[n]}} \right| \right) - i\pi \left(\Theta(t_i^{[m]}) - \Theta(t_j^{[n]}) \right), \quad (4.20)$$

where the Heaviside function $\Theta(x)$ is defined as $\Theta(x) = 1$ for $x > 0$ and $\Theta(x) = 0$ otherwise. Care must be taken when performing the analytic continuation of the arguments of the dilogarithms in eq. (4.18) to the physical region, as discussed in appendix F.

From eq. (4.17) we see that the one-loop amplitudes in $\mathcal{N} = 4$ SYM in the same-helicity configuration are given by the tree-level gluon amplitude times the transcendental function V_6 . As a step towards taking the full NMRK limit of eq. (4.16), let us keep only the leading power terms of the rational functions. This means we neglect all but the 12 leading colour orderings in eq. (4.16), and for these 12 leading colour orderings, we take the NMRK limit of the tree-level colour-ordered amplitudes that appear in eq. (4.17). We recall that in the NMRK limit, an interchange of $p_2^{\nu_2} \leftrightarrow p_3^{\nu_3}$ or $p_6^{\nu_6} \leftrightarrow p_1^{\nu_1}$ leads only to a sign change of the leading tree-level amplitude. This lets us write, for example, the $(-, -)$ component of the

colour-dressed amplitude in the NMRK limit as

$$\begin{aligned}
\mathcal{M}_{\mathcal{N}=4}^{(1)(-, -)}(p_4^\nu, p_5^\nu) &\xrightarrow{\text{NMRK}} g_s^6 \frac{\kappa_\Gamma}{(4\pi)^2} F^{a_3 a_2 c_1} F^{a_6 a_1 c_3} \\
&\times \frac{1}{4} \left\{ \text{tr} (F^{c_1} F^{a_4} F^{a_5} F^{c_3}) M^{(0)}(\sigma_A) \Big|_{\text{NMRK}} \left(V_6(\sigma_A) + V_6(\vec{\sigma}_A) + V_6(\sigma_{\overleftrightarrow{A}}) + V_6(\vec{\sigma}_{\overleftrightarrow{A}}) \right) \right. \\
&\quad + \text{tr} (F^{c_1} F^{a_5} F^{a_4} F^{c_3}) M^{(0)}(\sigma_{A'}) \Big|_{\text{NMRK}} \left(V_6(\sigma_{A'}) + V_6(\vec{\sigma}_{A'}) + V_6(\sigma_{\overleftrightarrow{A'}}) + V_6(\vec{\sigma}_{\overleftrightarrow{A'}}) \right) \\
&\quad \left. + \text{tr} (F^{c_1} F^{a_4} F^{c_3} F^{a_5}) M^{(0)}(\sigma_B) \Big|_{\text{NMRK}} \left(V_6(\sigma_B) + V_6(\vec{\sigma}_B) + V_6(\sigma_{\overleftrightarrow{B}}) + V_6(\vec{\sigma}_{\overleftrightarrow{B}}) \right) \right\}, \tag{4.21}
\end{aligned}$$

where we factorised the tree amplitude for each colour ordering. The positive relative signs in this equation, in contrast to eq. (4.13), are due to the sign flips in the tree amplitude $M^{(0)}(\sigma)$. Here, and in the following, we suppress the momentum and helicity arguments of $\mathcal{M}_{\mathcal{N}=4}^{(1)}$, apart from the two central gluons 4 and 5. Next, we write the tree-level colour-ordered amplitudes in the central NMRK in a factorized form according to eq. (3.3), e.g. for the A colour ordering we use

$$M^{(0)}(\sigma_A) \Big|_{\text{NMRK}} = C^{g(0)}(p_2^{\nu_2}, p_3^{-\nu_2}) \frac{1}{t_1} A^{gg(0)}(q_1, p_4^\oplus, p_5^\oplus, q_3) \frac{1}{t_3} C^{g(0)}(p_1^{\nu_1}, p_6^{-\nu_1}) \tag{4.22}$$

and similarly for the A' and B orderings.

Turning our attention to the transcendental functions, we observe a major simplification in the central NMRK limit upon considering *the dispersive part of the amplitude*, defined by taking the real part of the transcendental functions. We find that the latter is given solely by the $(-, -)$ component, eq. (4.21), as the dispersive parts of the remaining components of eq. (4.12), quoted in eqs. (F.1)–(F.3), vanish. This simplification is due to the fact that, for the 12 leading configurations (shown in e.g. eq. (4.21)), the real part of the transcendental functions V_6 in the central NMRK limit is unchanged by an interchange of $p_2 \leftrightarrow p_3$ or $p_6 \leftrightarrow p_1$. In conclusion, the dispersive part of the colour-dressed amplitude in the central NMRK limit is given by

$$\begin{aligned}
\text{Disp} \left[\mathcal{M}_{\mathcal{N}=4}^{(1)}(p_4^\oplus, p_5^\oplus) \right] &\xrightarrow{\text{NMRK}} \\
&g_s^6 \frac{\kappa_\Gamma}{(4\pi)^2} s_{12} F^{a_3 a_2 c_1} C^{g(0)}(p_2^{\nu_2}, p_3^{-\nu_2}) \frac{1}{t_1} \frac{1}{t_3} F^{a_6 a_1 c_3} C^{g(0)}(p_1^{\nu_1}, p_6^{-\nu_1}) \times \\
&\left\{ \text{tr} (F^{c_1} F^{a_4} F^{a_5} F^{c_3}) A^{gg(0)}(q_1, p_4^\oplus, p_5^\oplus, q_3) \text{Re} [V_6(\sigma_A)|_{\text{NMRK}}] \right. \\
&\quad + \text{tr} (F^{c_1} F^{a_5} F^{a_4} F^{c_3}) A^{gg(0)}(q_1, p_5^\oplus, p_4^\oplus, q_3) \text{Re} [V_6(\sigma_{A'})|_{\text{NMRK}}] \\
&\quad \left. + \text{tr} (F^{c_1} F^{a_5} F^{c_3} F^{a_4}) B^{gg(0)}(q_1, p_4^\oplus, p_5^\oplus, q_3) \text{Re} [V_6(\sigma_B)|_{\text{NMRK}}] \right\}. \tag{4.23}
\end{aligned}$$

By contrast, the absorptive part of the amplitude, defined by taking the imaginary part of the transcendental functions, in NMRK receives contribution from all terms in the decomposition of eq. (4.12). The absorptive part of the amplitude is discussed further in appendix F, and the four signature components are listed in eqs. (F.8)–(F.11). In

section 4.3 we show that this absorptive part does not contribute to the colour-summed NLO $gg \rightarrow gggg$ squared matrix element in the central NMRK limit. This means that, in particular, only the dispersive part of the one-loop amplitude contributes to the dijet cross section at NNLL accuracy. We now move to the study of the real part of V_6 for the relevant colour orderings, leaving the analogous discussion of the imaginary parts of V_6 to appendix F.

As noted in ref. [16], the real part of V_6 can be written, *without any approximation*, as a combination of one-loop functions that describe amplitudes in MRK – the one-loop Regge trajectory of eq. (2.5), the impact factor of eq. (4.14) and the Lipatov vertex, eq. (4.15) – plus a remainder term that vanishes in the MRK limit. We will refer to this term as the NMRK remainder function (ΔV below). The arguments of the one-loop MRK functions can be chosen such that the remainder function is free from infrared (IR) divergences, and is a function of conformally-invariant cross ratios alone. For future convenience we choose to group these one-loop MRK functions into two components. One component is a function which collects the ‘central’ behaviour that will be relevant for our central NMRK limit,

$$U(\tilde{t}_1, \tilde{\eta}_{12}, \tilde{t}_2, \tilde{s}_2, \tilde{\eta}_{23}, \tilde{t}_3) = v_{\mathcal{N}=4}^{g(1)}(\tilde{t}_1, \tilde{\eta}_{12}, \tilde{t}_2) + \alpha^{(1)}(\tilde{t}_2) \log\left(\frac{\tilde{s}_2}{\tau}\right) + v_{\mathcal{N}=4}^{g(1)}(\tilde{t}_2, \tilde{\eta}_{23}, \tilde{t}_3) . \quad (4.24)$$

The other component collects the remaining ‘non-central’ behaviour,

$$E(\tilde{t}_1, \tilde{s}_1; \tilde{t}_3, \tilde{s}_3) = c_{\mathcal{N}=4}^{g(1)}(\tilde{t}_1; \tau) + \alpha^{(1)}(\tilde{t}_1) \log\left(\frac{\tilde{s}_1}{\tau}\right) + \alpha^{(1)}(\tilde{t}_3) \log\left(\frac{\tilde{s}_3}{\tau}\right) + c_{\mathcal{N}=4}^{g(1)}(\tilde{t}_3; \tau) . \quad (4.25)$$

The arguments decorated with tildes in eq. (4.24) and eq. (4.25) are placeholders: the arguments assigned will differ for each colour ordering in eq. (4.23). However, we will always make the natural choice of assigning $\tilde{t}_1 = t_1 = s_{23}$ and $\tilde{t}_3 = t_3 = s_{61}$, and we will assign $\tilde{t}_2 = t_2 = s_{234}$ when considering the MRK limit, and $\tilde{t}_2 = t'_2 = s_{235}$ when considering the MRK' limit. Based on the structure of V_6 in eq. (4.18), for a given colour ordering we will also choose the remaining arguments to be constructed from colour-ordered two- and three-particle Mandelstam invariants. This choice will be informed by our knowledge of the MRK and MRK' limit of this amplitude. However, these criteria do not lead to a unique assignment of the arguments of eqs. (4.24) and (4.25): the remaining freedom will be discussed separately for each colour ordering.

As a first example, let us see how this re-writing can be performed for the real part of $V_6(\sigma_A)$. We first separate the non-central function E , making the natural choice of Mandelstam variables for its arguments,

$$N_c \kappa_\Gamma \text{Re}[V_6(\sigma_A)] = E(s_{23}, s_{34}; s_{61}, s_{56}) + V_A . \quad (4.26)$$

This choice of arguments for E is the simplest choice which is compatible with the known MRK limit⁸,

$$E(s_{23}, s_{34}; s_{61}, s_{56}) \xrightarrow{(N)\text{MRK}} E(-|q_{1\perp}|^2, p_3^+ p_4^-; -|q_{3\perp}|^2, p_5^+ p_6^-) . \quad (4.27)$$

⁸As this function does not depend on the central degrees of freedom in the NMRK, no further simplification is obtained by taking the further MRK limit.

The function V_A in eq. (4.26) collects the remaining ‘central’ behaviour and it can be identified as the transcendental function associated with the two-gluon CEV for the A colour ordering. As anticipated, this function itself can be neatly written as

$$V_A = U_A + \Delta V_A(u_A, v_A, w_A), \quad (4.28)$$

where, again guided by the MRK limit, we fix U_A to equal the function U , eq. (4.24), with arguments assigned as follows

$$U_A = U \left(s_{23}, \frac{s_{34}s_{45}}{s_{345}\sqrt{u_A}}, s_{234}, s_{45}, \frac{s_{45}s_{56}}{s_{456}\sqrt{u_A}}, s_{61} \right). \quad (4.29)$$

This choice of kinematic arguments leads to a simple NMRK remainder function ΔV_A , which is IR-finite, vanishes in the MRK limit and depends only on the cross ratios, eq. (3.19),

$$\begin{aligned} \Delta V_A(u_A, v_A, w_A) = N_c \kappa_\Gamma \left(\frac{\pi^2}{3} - \frac{1}{4} \log^2(u_A) - \frac{1}{2} \log(u_A) \log(v_A w_A) \right. \\ \left. - \text{Li}_2(1 - u_A) - \text{Li}_2(1 - v_A) - \text{Li}_2(1 - w_A) \right). \end{aligned} \quad (4.30)$$

The MRK limit of the cross ratios is $u_A \rightarrow 1$, $v_A \rightarrow 0$, $w_A \rightarrow 0$ (see eq. (G.7)). It is easy to see that eq. (4.30) vanishes in this limit.

As mentioned above, eq. (4.29) is not the unique choice which leads to an IR-finite NMRK remainder. In eq. (4.29) we made the further choice of requiring U_A to be invariant under target-projectile exchange, eq. (3.42). Yet even this physically-motivated requirement does not uniquely specify arguments for U_A : a rescaling of the \tilde{t}_2 variable in eq. (4.29) by an arbitrary power of u_A , i.e. $s_{234} \rightarrow s_{234} \times (u_A)^p$ for real p , yields a NMRK remainder function which is an IR-finite function of cross ratios and is invariant under target-projectile exchange. Our ultimate choice of arguments in eq. (4.29) was guided by the intuition that the trajectory should be evaluated exactly at the t -channel invariant $t_2 = s_{234}$ also away from the strict MRK limit. It would be interesting to explore this same procedure at higher orders in ϵ , or at two loops, where, if such an organisation proves possible, there may be additional constraints on the kinematic arguments.

We stress that eq. (4.26) holds in general kinematics if no approximation is made to the kinematic invariants. However, we will proceed to make the kinematic approximations valid in the central NMRK limit, in order to exploit the invariance of the real part under the interchanges $p_2 \leftrightarrow p_3$ or $p_6 \leftrightarrow p_1$ in this limit, as in eq. (4.23). Thus, we specify eq. (4.28) to the NMRK limit, by making the approximation,

$$U_A \xrightarrow{\text{NMRK}} U \left(-|q_{1\perp}|^2, \frac{p_4^- s_{45}}{p_4^- + p_5^-}, -|q_{2\perp}|^2 - p_5^+ p_4^-, s_{45}, \frac{s_{45} p_5^+}{p_4^+ + p_5^+}, -|q_{3\perp}|^2 \right), \quad (4.31)$$

and also taking the NMRK approximation of the cross ratios, as listed in eq. (3.19), for the arguments of eq. (4.30). This NMRK approximation of V_A will later form one of the building blocks of the colour-dressed two-gluon CEV. The structure of the NMRK limit of the dispersive part of $M_{\mathcal{N}=4}^{(1)}$ is depicted in fig. 6.

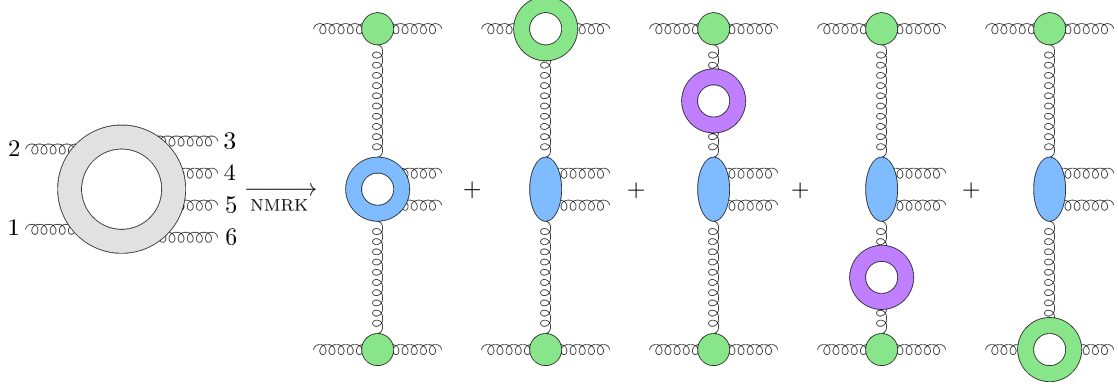


Figure 6. Schematic illustration of the behaviour of the dispersive part of the one-loop partial amplitude $M_{N=4}^{(1)}(\sigma_A)$ in the central NMRK limit. The first diagram on the right-hand side represents the transcendental functions that depend on the central degrees of freedom, V_A , which we identify as the one-loop correction to the two-gluon CEV for this colour ordering. The remaining four diagrams on the right-hand side are given by the known one-loop impact factors and gluon Regge trajectory contributions, and are collected in the function E of eq. (4.25).

The function $V_6(\sigma_{A'})$ is simply related to $V_6(\sigma_A)$ by an interchange of $p_4 \leftrightarrow p_5$. We now use the known MRK' limit of the amplitude as our guide, writing

$$N_c \kappa \Gamma \text{Re} [V_6(\sigma_{A'})|_{\text{NMRK}}] = E(s_{23}, s_{35}; s_{61}, s_{46}) + V_{A'}, \quad (4.32)$$

$$V_{A'} = U_{A'} + \Delta V_A(u_{A'}, w_{A'}, v_{A'}), \quad (4.33)$$

where $U_{A'}$ is related to eq. (4.29) by the interchange of $p_4 \leftrightarrow p_5$. As was true for the A ordering, in order to use the compact form of eq. (4.23), we will need to make the NMRK approximations to the arguments of ΔV_A in eq. (4.33), and similarly we make the approximation,

$$U_{A'} \xrightarrow{\text{NMRK}} U \left(-|q_{1\perp}|^2, \frac{p_5^- s_{45}}{p_4^+ + p_5^-}, -|q_{2\perp}|^2 - p_4^+ p_5^-, s_{45}, \frac{s_{45} p_4^+}{p_4^+ + p_5^+}, -|q_{3\perp}|^2 \right). \quad (4.34)$$

Note that the NMHV remainder function for the A' ordering is the same as for the A ordering, because $\Delta V_A(u, w, v) = \Delta V_A(u, v, w)$ based on eq. (4.30).

We now turn to study of the real part of $V_6(\sigma_B)$. The rational coefficient of this transcendental function, $M^{(0)}(\sigma_B)$, has a leading contribution in both the MRK and MRK' limits. It will be useful therefore to re-write this transcendental function in two ways: one guided by the known MRK limit of the amplitude, and the other by the known MRK' limit. As usual, we first separate the central and non-central functions,

$$N_c \kappa \Gamma \text{Re} [V_6(\sigma_B)] = E(s_{23}, -s_{42}; s_{61}, s_{56}) + V_B = E(s_{23}, s_{35}; s_{61}, -s_{14}) + V_{B'}. \quad (4.35)$$

The forms of the central functions V_B and $V_{B'}$ are guided, respectively, by the known MRK and MRK' limits of this function – note that both refer to the same colour ordering. These

central functions are given by

$$V_B = U_B + \Delta V_B(u_B, v_B, w_B), \quad V_{B'} = U_{B'} + \Delta V_B(v_B, u_B, w_B), \quad (4.36)$$

where we have chosen to use the kinematic arguments,

$$\begin{aligned} U_B &= U \left(s_{23}, \frac{s_{14}s_{42}}{s_{142}u_B}, s_{234}, -s_{235}, \frac{s_{35}s_{56}}{s_{356}u_B}, s_{61} \right), \\ U_{B'} &= U \left(s_{23}, \frac{s_{35}s_{56}}{s_{356}v_B}, s_{235}, -s_{234}, \frac{s_{14}s_{42}}{s_{142}v_B}, s_{61} \right), \end{aligned} \quad (4.37)$$

for the one-loop MRK functions.

Unlike the A colour ordering, target-projectile symmetry does not constrain the arguments of eq. (4.37): from eq. (3.48) we see that in NMRK, each cross ratio is invariant under target-projectile exchange. Our choice of kinematic arguments in eq. (4.37) were instead motivated by the requirement that U_B and $U_{B'}$ are related by the map which interchanges $\{p_2 \leftrightarrow p_3, p_4 \leftrightarrow p_5, p_1 \leftrightarrow p_6\}$, corresponding to a symmetry of the real part of $V_6(\sigma_B)$. We will refer to this map as G . For the natural assignment of variables in eq. (4.35), the real parts of E are related by this map.⁹ Choosing U_B and $U_{B'}$ to be related by G therefore means the respective NMRK remainder functions are also related by this map. For the cross ratios, eq. (3.33), the map G leads to $u_B \xleftrightarrow{G} v_B$, while w_B is invariant under G . The NMRK remainder function that follows from the choices made in eq. (4.37) is

$$\begin{aligned} \Delta V_B(u_B, v_B, w_B) &= \Delta V_B(v_B, u_B, w_B) \\ &= N_c \kappa_\Gamma \left(\frac{\pi^2}{3} - \log(u_B) \log(v_B) - \text{Li}_2(1 - u_B) - \text{Li}_2(1 - v_B) - \text{Li}_2(1 - w_B) \right), \end{aligned} \quad (4.38)$$

which is indeed invariant under G . We note, however, that by considering suitable rescaling of the arguments of U_B and $U_{B'}$ by powers of u_B or v_B respectively (the quantities which tend to unity in the MRK or MRK' limits respectively), there is one alternative set of kinematic assignments which lead to an NMRK remainder function that possesses the same desirable properties as eq. (4.38): as for the σ_A ordering, our final choice of arguments in eq. (4.37) was determined by requiring that \tilde{t}_2 is identified with the relevant t -channel momentum even in general kinematics, namely t_2 and t'_2 in the MRK and MRK' limits, respectively.

In order to use eq. (4.35) within the compact form of eq. (4.23), we must make the NMRK approximations

$$\begin{aligned} U_B &\xrightarrow{\text{NMRK}} U \left(-|q_{1\perp}|^2, -\frac{p_4^-}{p_5^-} t'_2, t_2, -t'_2, -\frac{p_5^+}{p_4^+} t'_2, -|q_{3\perp}|^2 \right), \\ U_{B'} &\xrightarrow{\text{NMRK}} U \left(-|q_{1\perp}|^2, -\frac{p_5^-}{p_4^-} t_2, t'_2, -t_2, -\frac{p_4^+}{p_5^+} t_2, -|q_{3\perp}|^2 \right), \end{aligned} \quad (4.39)$$

⁹Note that we always choose the signs of the arguments of E such that it is in fact a real function.

where it is understood that on the right hand side we use the NMRK limits of

$$t_2 = s_{234} \xrightarrow{\text{NMRK}} -(|q_{2\perp}|^2 + p_5^+ p_4^-), \quad t'_2 = s_{235} \xrightarrow{\text{NMRK}} -(|q'_{2\perp}|^2 + p_4^+ p_5^-). \quad (4.40)$$

Similarly, we apply the NMRK approximations listed in eq. (3.33) for the cross-ratio arguments of eq. (4.38). We see that in the NMRK limit, U_B and $U_{B'}$ (and therefore V_B and $V_{B'}$) are simply related by an interchange of $p_4 \leftrightarrow p_5$.

Having studied the three colour orderings of eq. (4.23), we will now move to a basis of colour structures that more closely resembles the colour structure of the tree-level amplitude, eq. (3.2). This basis will let us identify one-loop corrections associated with each of the tree-level colour structures, as well as highlight the new colour structure that starts contributing at one-loop level. Denoting the three traces by

$$T_A = \text{tr}(F^{c_1} F^{a_4} F^{a_5} F^{c_3}), \quad T_{A'} = \text{tr}(F^{c_1} F^{a_5} F^{a_4} F^{c_3}), \quad T_B = \text{tr}(F^{c_1} F^{a_5} F^{c_3} F^{a_4}), \quad (4.41)$$

we consider the following rotation of the sum inside the curly brackets in eq. (4.23)

$$\begin{aligned} T_A M_A + T_{A'} M_{A'} + T_B M_B &= (T_A - T_B) \times \frac{1}{3} (2M_A - M_{A'} - M_B) \\ &\quad + (T_{A'} - T_B) \times \frac{1}{3} (2M_{A'} - M_A - M_B) \\ &\quad + \frac{1}{3} (T_A + T_{A'} + T_B) \times (M_A + M_{A'} + M_B). \end{aligned} \quad (4.42)$$

Using the identities,

$$\text{tr}(F^a F^b F^c) = N_c F^{abc}, \quad \text{tr}(F^a F^b [F^c, F^d]) = N_c F^{abe} F^{ecd}, \quad (4.43)$$

we relate the first two combinations of colour structure on the right-hand side of eq. (4.42) to the tree-level structures $(F^{a\sigma_4} F^{a\sigma_5})_{c_1 c_3}$ of eq. (3.2), and define the third colour factor in terms of the fully-symmetric trace:

$$d_A^{a_1 a_2 a_3 a_4} = \frac{1}{4!} \sum_{\sigma \in S_4} \text{tr}(F^{a_{\sigma_1}} F^{a_{\sigma_2}} F^{a_{\sigma_3}} F^{a_{\sigma_4}}). \quad (4.44)$$

Making use of the additional relations that exist within NMRK, namely

$$\begin{aligned} E(t_1, -s_{42}; t_3, s_{56})|_{\text{NMRK}} &= E(t_1, s_{34}; t_3, s_{56})|_{\text{NMRK}}, \\ E(t_1, s_{35}; t_3, -s_{14})|_{\text{NMRK}} &= E(t_1, s_{35}; t_3, s_{46})|_{\text{NMRK}}, \end{aligned} \quad (4.45)$$

we now express eq. (4.23) as

$$\begin{aligned} \text{Disp} \left[\mathcal{M}_{\mathcal{N}=4}^{(1)}(p_4^\oplus, p_5^\oplus) \right] &\xrightarrow{\text{NMRK}} \frac{g_s^6}{(4\pi)^2} s_{12} F^{a_3 a_2 c_1} C^{g(0)}(p_2^{\nu_2}, p_3^{-\nu_2}) \frac{1}{t_1} \times \\ &\sum_{\sigma \in S_2} \left\{ (F^{a\sigma_4} F^{a\sigma_5})_{c_1 c_3} \left(A_{\text{F}}^{gg(1)}(q_1, p_{\sigma_4}^\oplus, p_{\sigma_5}^\oplus, q_3) + A^{gg(0)}(q_1, p_{\sigma_4}^\oplus, p_{\sigma_5}^\oplus, q_3) E(t_1, s_{3\sigma_4}; t_3, s_{\sigma_5 6}) \right) \right. \\ &\quad \left. + \frac{1}{N_c} d_A^{c_1 a\sigma_4 a\sigma_5 c_3} A_d^{gg(1)}(q_1, p_{\sigma_4}^\oplus, p_{\sigma_5}^\oplus, q_3) \right\} \times \frac{1}{t_3} F^{a_6 a_1 c_3} C^{g(0)}(p_1^{\nu_1}, p_6^{-\nu_1}), \end{aligned} \quad (4.46)$$

where the totally symmetric colour structure d_A starts contributing at one-loop level, with

$$A_d^{gg(1)}(q_1, p_4^\oplus, p_5^\oplus, q_3) = A^{gg(0)}(q_1, p_4^\oplus, p_5^\oplus, q_3) (V_A - V_B) . \quad (4.47)$$

The symmetry of the d_A colour structure under the permutation S_2 of eq. (4.46) means that after the sum over the σ_4, σ_5 permutations is performed, there are only three independent colour structures in this equation, as in eq. (4.23).

For the kinematic coefficient of the tree-level colour structures we find, using eqs. (3.31) and (4.42),

$$\begin{aligned} A_{\mathbb{F}}^{gg(1)}(q_1, p_4^\oplus, p_5^\oplus, q_3) \\ = \frac{1}{3} \left(A^{gg(0)}(q_1, p_4^\oplus, p_5^\oplus, q_3) (2V_A + V_B) - A^{gg(0)}(q_1, p_5^\oplus, p_4^\oplus, q_3) (V_{A'} - V_{B'}) \right) . \end{aligned} \quad (4.48)$$

We interpret this term as the one-loop coefficient of the all-orders expansion of this colour structure,

$$A_{\mathbb{F}}^{gg}(q_1, p_4^{\nu_4}, p_5^{\nu_5}, q_3) = A_{\mathbb{F}}^{gg(0)}(q_1, p_4^{\nu_4}, p_5^{\nu_5}, q_3) + \frac{\alpha_S}{4\pi} A_{\mathbb{F}}^{gg(1)}(q_1, p_4^{\nu_4}, p_5^{\nu_5}, q_3) + \mathcal{O}(\alpha_S^2), \quad (4.49)$$

with

$$A_{\mathbb{F}}^{gg(0)}(q_1, p_4^{\nu_4}, p_5^{\nu_5}, q_3) = A^{gg(0)}(q_1, p_4^{\nu_4}, p_5^{\nu_5}, q_3) . \quad (4.50)$$

As the structure d_A first appears at one-loop level we write

$$A_d^{gg}(q_1, p_4^{\nu_4}, p_5^{\nu_5}, q_3) = \frac{\alpha_S}{4\pi} A_d^{gg(1)}(q_1, p_4^{\nu_4}, p_5^{\nu_5}, q_3) + \mathcal{O}(\alpha_S^2), \quad (4.51)$$

in anticipation of higher-order corrections to this colour structure. We note that $A_d^{gg(1)}$ and $A_{\mathbb{F}}^{gg(1)}$ both depend on μ^2 and τ , but as for the one-loop coefficients of the impact factor and Lipatov vertex, we omit this dependence for brevity.

The notation introduced in this section makes it straightforward to verify that the eqs. (4.48) and (4.47) yield the expected MRK limit. We first note that by construction, eqs. (4.28) and (4.36) both tend to the same MRK limit,

$$U_A|_{\text{MRK}} = U_B|_{\text{MRK}} = U_{\text{MRK}} = U(-|q_{1\perp}|^2, |p_{4\perp}|^2, -|q_{2\perp}|^2, p_4^+ p_5^-, |p_{5\perp}|^2, -|q_{3\perp}|^2). \quad (4.52)$$

Using the MRK limits of the relevant cross ratios listed in eq. (G.7) together with the values of the dilogarithm,

$$\text{Li}_2(0) = 0, \quad \text{Li}_2(1) = \frac{\pi^2}{6}, \quad (4.53)$$

we see that both $\Delta V_A(u_A, v_A, w_A)$ and $\Delta V_B(u_B, v_B, w_B)$ vanish in the MRK limit as desired. This leads to the simple results,

$$A_{\mathbb{F}}^{gg(1)}(q_1, p_4^\oplus, p_5^\oplus, q_3) \xrightarrow{\text{MRK}} V^{g(0)}(q_1, p_4^\oplus, q_2) \frac{1}{t_2} V^{g(0)}(q_2, p_5^\oplus, q_3) U_{\text{MRK}}, \quad (4.54)$$

$$A_d^{gg(1)}(q_1, p_4^\oplus, p_5^\oplus, q_3) \xrightarrow{\text{MRK}} 0. \quad (4.55)$$

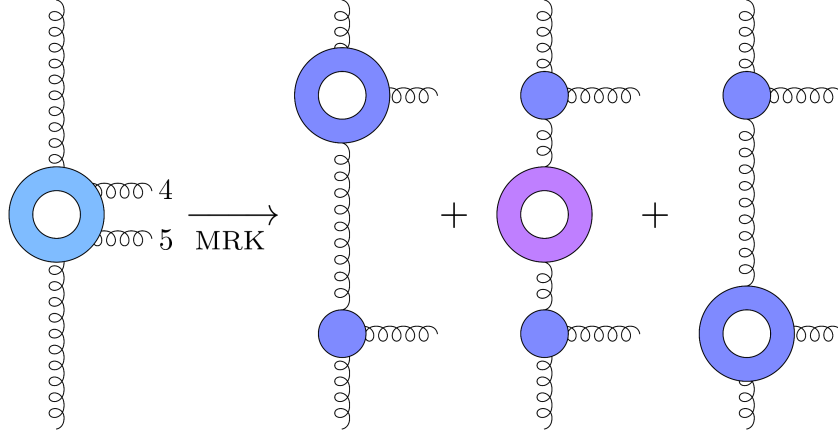


Figure 7. Schematic illustration of the further factorisation of the one-loop two-gluon CEV for the ordering σ_A in the MRK limit.

Equation (4.54) is depicted schematically in fig. 7. The function U_{MRK} generates all three of the loop corrections on the right-hand side of the figure, thanks to the definition (4.24). A similar analysis shows that

$$A_{\text{F}}^{gg(1)}(q_1, p_5^{\oplus}, p_4^{\oplus}, q_3) \xrightarrow{\text{MRK}'} V^{g(0)}(q_1, p_5^{\oplus}, q_2') \frac{1}{t_2'} V^{g(0)}(q_2', p_4^{\oplus}, q_3) U_{\text{MRK}'}, \quad (4.56)$$

$$A_d^{gg(1)}(q_1, p_5^{\oplus}, p_4^{\oplus}, q_3) \xrightarrow{\text{MRK}'} 0, \quad (4.57)$$

where

$$U_{A'}|_{\text{MRK}'} = U_{B'}|_{\text{MRK}'} = U_{\text{MRK}'} = U(-|q_{1\perp}|^2, |p_{5\perp}|^2, -|q_{2\perp}'|^2, p_5^+ p_4^-, |p_{4\perp}|^2, -|q_{3\perp}|^2). \quad (4.58)$$

In appendix G we investigate the soft and collinear limits of eq. (4.46). In section 5 we conjecture how the one-loop results of this section may be extended to all orders. In the next subsection we obtain expressions analogous to eqs. (4.48) and (4.47) but for the case where gluons 4 and 5 have opposite helicities.

4.2 Opposite-helicity vertex

We now perform an analogous study to section 4.1 for the opposite-helicity case, where we must start from an NMHV helicity configuration. We present the procedure for a configuration of the form $\mathcal{M}_{\mathcal{N}=4}^{(1)}(p_1^{\nu_1}, p_2^{\nu_2}, p_3^{-\nu_2}, p_4^{\oplus}, p_5^{\ominus}, p_6^{-\nu_1})$. As for the tree-level vertex, after the CEV for $\nu_4 = -\nu_5 = \oplus$ has been obtained, the CEV for $\nu_4 = -\nu_5 = \ominus$ may be obtained by complex conjugation. The colour-ordered one-loop six-gluon NMHV amplitudes in $\mathcal{N} = 4$ SYM are given in eqs. (D.9)–(D.11). Unlike eq. (4.17), these NMHV amplitudes are not proportional to the tree-level amplitude. Instead, the transcendental functions of the NMHV amplitude, W_i are multiplied by pairs of the rational functions that appear in the BCFW representations of the tree-level amplitude listed in appendix D.1. In the

NMRK, after dividing by the appropriate impact factors and t -channel propagators, these rational coefficients are simply given by sums of pairs of the rational functions which we have studied in sections 3.2 and 3.3,

$$S_{xy}^I = R_{xy}^I + R_{\bar{x}\bar{y}}^I \quad x, y \in \{u, v, w\}, \quad I \in \{A, A', B\}. \quad (4.59)$$

Like the tree-level amplitudes, these rational coefficients of the transcendental functions W_i change only by a sign under exchange of $p_2^{\nu_2} \leftrightarrow p_3^{\nu_3}$ or $p_6^{\nu_6} \leftrightarrow p_1^{\nu_1}$. For the 12 leading colour orderings, we further find that an exchange of $p_2 \leftrightarrow p_3$ or $p_6 \leftrightarrow p_1$ does not alter the real part of the functions W_i . These properties collectively allow the dispersive part of the amplitude to be written as

$$\begin{aligned} \text{Disp} \left[\mathcal{M}_{\mathcal{N}=4}^{(1)}(p_4^\oplus, p_5^\ominus) \right] &\xrightarrow{\text{NMRK}} \\ g_s^6 \frac{\kappa_\Gamma}{(4\pi)^2} s_{12} F^{a_3 a_2 c_1} C^{g(0)}(p_2^{\nu_2}, p_3^{-\nu_2}) \frac{1}{t_1} \frac{1}{t_3} F^{a_6 a_1 c_3} C^{g(0)}(p_1^{\nu_1}, p_6^{-\nu_1}) \\ &\times \left\{ \text{tr} (F^{c_1} F^{a_4} F^{a_5} F^{c_3}) \left[S_{uv}^A \text{Re} [W_1(\sigma_A)] + S_{vw}^A \text{Re} [W_2(\sigma_A)] + S_{wu}^A \text{Re} [W_3(\sigma_A)] \right] \right. \\ &\quad + \text{tr} (F^{c_1} F^{a_5} F^{a_4} F^{c_3}) \left[S_{uv}^{A'} \text{Re} [W_1(\sigma_{A'})] + S_{vw}^{A'} \text{Re} [W_2(\sigma_{A'})] + S_{wu}^{A'} \text{Re} [W_3(\sigma_{A'})] \right] \\ &\quad \left. + \text{tr} (F^{c_1} F^{a_5} F^{c_3} F^{a_4}) \left[S_{uv}^B \text{Re} [W_1(\sigma_B)] + S_{vw}^B \text{Re} [W_2(\sigma_B)] + S_{wu}^B \text{Re} [W_3(\sigma_B)] \right] \right\}, \end{aligned} \quad (4.60)$$

analogously to eq. (4.23). On the right-hand side of eq. (4.60), the transcendental functions are understood to be taken in the NMRK limit, but for brevity we do not indicate this explicitly. As in section 4.1, we find that the dispersive part of the amplitude is given solely by $(-, -)$ exchange. This is not true for the absorptive part, which is studied in appendix F. We will see in section 4.3 that the absorptive part does not contribute to the helicity- and colour-summed NLO squared matrix element for $gg \rightarrow gggg$, or to the dijet cross section at NNLL. The absorptive part will only contribute at N³LL. For the remainder of this section we focus on the dispersive part of the amplitude, eq. (4.60).

Unlike the tree-level expressions (e.g. eq. (3.22)), the sums of two rational terms, eq. (4.59), do contain genuine unphysical poles. To demonstrate that the dispersive part of the NMRK amplitude, eq. (4.60), is nonetheless free from unphysical singularities it is useful to use the fact that the sum of the three S_{xy}^I is twice the tree-level CEV to rewrite

eq. (4.60) as

$$\begin{aligned}
& \text{Disp} \left[\mathcal{M}_{\mathcal{N}=4}^{(1)}(p_4^\oplus, p_5^\ominus) \right] \xrightarrow{\text{NMRK}} g_s^6 \frac{\kappa_\Gamma}{(4\pi)^2} s_{12} F^{a_3 a_2 c_1} C^{g(0)}(p_2^{\nu_2}, p_3^{-\nu_2}) \frac{1}{t_1} \\
& \times \left\{ \text{tr} (F^{c_1} F^{a_4} F^{a_5} F^{c_3}) \left[2A^{gg(0)}(q_1, p_4^\oplus, p_5^\ominus, q_3) \text{Re} [W_2(\sigma_A)] \right. \right. \\
& \quad \left. \left. + S_{uv}^A \text{Re} [W_1(\sigma_A) - W_2(\sigma_A)] + S_{wu}^A \text{Re} [W_3(\sigma_A) - W_2(\sigma_A)] \right] \right. \\
& + \text{tr} (F^{c_1} F^{a_5} F^{a_4} F^{c_3}) \left[2A^{gg(0)}(q_1, p_5^\ominus, p_4^\oplus, q_3) \text{Re} [W_2(\sigma_{A'})] \right. \\
& \quad \left. \left. + S_{uv}^{A'} \text{Re} [W_1(\sigma_{A'}) - W_2(\sigma_{A'})] + S_{wu}^{A'} \text{Re} [W_3(\sigma_{A'}) - W_2(\sigma_{A'})] \right] \right. \\
& + \text{tr} (F^{c_1} F^{a_5} F^{c_3} F^{a_4}) \left[2B^{gg(0)}(q_1, p_4^\oplus, p_5^\ominus, q_3) \text{Re} [W_1(\sigma_B)] \right. \\
& \quad \left. \left. + S_{vv}^B \text{Re} [W_2(\sigma_B) - W_1(\sigma_B)] + S_{wu}^B \text{Re} [W_3(\sigma_B) - W_1(\sigma_B)] \right] \right\} \\
& \times \frac{1}{t_3} F^{a_6 a_1 c_3} C^{g(0)}(p_1^{\nu_1}, p_6^{-\nu_1}).
\end{aligned} \tag{4.61}$$

This rewriting simplifies our task for two reasons:

- From section 3 we know the functions $A^{gg(0)}$ and $B^{gg(0)}$ are free from unphysical singularities.
- The difference between two cyclic permutations of W is much simpler than a given permutation of W .

To expand on the second point, the difference between two cyclic permutations of W can be expressed as a single product of logarithms whose arguments are simple functions of the cross ratios. This property holds even in general kinematics, although in the following we implicitly consider the cross ratios to be taken in the NMRK limit. Let us first consider these terms in the σ_A ordering,

$$\begin{aligned}
W_1(\sigma_A) - W_2(\sigma_A) &= \log(v_A) \log\left(\frac{w_A}{u_A}\right), \\
W_3(\sigma_A) - W_2(\sigma_A) &= \log(w_A) \log\left(\frac{v_A}{u_A}\right).
\end{aligned} \tag{4.62}$$

We note in passing that these functions are related by the interchange of $u_A \leftrightarrow v_A$, which has the physical interpretation of target-projectile exchange, eq. (3.45). This provides our motivation for arranging eq. (4.61) as we have done, where $W_2(\sigma_A)$ multiplies the corresponding tree-level CEV, while the remaining terms are related by

$$S_{uv}^A \text{Re} [W_1(\sigma_A) - W_2(\sigma_A)] \xrightarrow{F} \frac{w\bar{z}}{\bar{w}z} S_{wu}^A \text{Re} [W_3(\sigma_A) - W_2(\sigma_A)]. \tag{4.63}$$

Table 1 lists the behaviour of the cross ratios at each unphysical-singularity surface. From this table we see that at $P_v^A = 0$ or $P_w^A = 0$, the transcendental terms which multiply

the divergent rational terms in eq. (4.61) vanish. For the remaining unphysical singularity at $P_u^A = 0$, we find

$$S_{uv}^A (W_1(\sigma_A) - W_2(\sigma_A)) + S_{wu}^A (W_3(\sigma_A) - W_2(\sigma_A)) \xrightarrow{P_u^A \rightarrow 0} (S_{uv}^A + S_{wu}^A) \log^2 \left(\frac{|z-1|^2 X}{(1+X)(1+|z|^2 X)} \right), \quad (4.64)$$

which is finite at $P_u^A = 0$, because in the sum $S_{uv}^A + S_{wu}^A = 2A^{gg(0)} - S_{vw}^A$, the apparent pole at $P_u^A = 0$ is a removable singularity.

	$P_u^A = 0$	$P_v^A = 0$	$P_w^A = 0$
u_A	1	$\frac{ w-1 ^2 X}{(1+X)(1+ w ^2 X)}$	$\frac{ z-1 ^2 X}{(1+X)(1+ z ^2 X)}$
v_A	$\frac{ z-1 ^2 X}{(1+X)(1+ z ^2 X)}$	1	$\frac{ z-1 ^2 X}{(1+X)(1+ z ^2 X)}$
w_A	$\frac{ z-1 ^2 X}{(1+X)(1+ z ^2 X)}$	$\frac{ w-1 ^2 X}{(1+X)(1+ w ^2 X)}$	1

Table 1. Behaviour of the cross ratios in the NMRK limit at the three unphysical-singularity surfaces of the rational terms of the ordering σ_A , listed in eq. (3.21).

The $\sigma_{A'}$ ordering is exactly analogous. For the σ_B ordering we have singled out in eq. (4.61) the transcendental function $W_1(\sigma_B)$ to multiply the tree-level amplitude. The other transcendental functions that appear in this colour structure are then

$$\begin{aligned} W_2(\sigma_B) - W_1(\sigma_B) &= \log(v_B) \log\left(\frac{u_B}{w_B}\right), \\ W_3(\sigma_B) - W_1(\sigma_B) &= \log(u_B) \log\left(\frac{v_B}{w_B}\right), \end{aligned} \quad (4.65)$$

which are related to each other by the map G introduced in section 4.1. For the NMHV tree-level rational functions in the NMRK limit, this map is equivalent to the composition of interchanging $p_4 \leftrightarrow p_5$ with complex conjugation, i.e. the remaining terms in eq. (4.61) have the property,

$$S_{vw}^B (W_2(\sigma_B) - W_1(\sigma_B)) \xleftrightarrow{p_4 \leftrightarrow p_5} (S_{wu}^B)^* (W_3(\sigma_B) - W_1(\sigma_B)), \quad (4.66)$$

where we have used eq. (3.41). Using the properties summarised in table 2, we see that this ordering is also free from unphysical singularities. At $P_u^B = 0$ or $P_v^B = 0$, the rational terms in eq. (4.61) which diverge are multiplied by transcendental terms (eq. (4.65)) that vanish. At $P_w^B = 0$ we see that the transcendental terms in eq. (4.65) become equal, allowing us to write

$$S_{vw}^B (W_2(\sigma_B) - W_1(\sigma_B)) + S_{wu}^B (W_3(\sigma_B) - W_1(\sigma_B)) \xrightarrow{P_w^B \rightarrow 0} (S_{vw}^B + S_{wu}^B) \log^2 \left(\frac{1}{1+|z|^2 X} \right). \quad (4.67)$$

	$P_u^B = 0$	$P_v^B = 0$	$P_w^B = 0$
u_B	1	$\frac{1}{1+ 1+\frac{w}{z} ^2 \frac{1}{X}}$	$\frac{1}{1+ z ^2 X}$
v_B	$\frac{1}{1+ z ^2 X}$	1	$\frac{1}{1+ z ^2 X}$
w_B	$\frac{1}{1+ z ^2 X}$	$\frac{1}{1+ 1+\frac{w}{z} ^2 \frac{1}{X}}$	1

Table 2. Behaviour of the cross ratios in the NMRK at the three unphysical-singularity surfaces of the rational terms of the ordering σ_B , listed in eq. (3.39).

The sum of rational terms $S_{vw}^B + S_{wu}^B$ is finite at $P_w^B = 0$, so we have shown that the dispersive part of the amplitude eq. (4.61) is free from unphysical singularities, as expected.

As in section 4.1, we can write the real part of the transcendental functions exactly in terms of the one-loop trajectory, impact factors and Lipatov vertex, plus a NMRK remainder term. We first separate the transcendental function into a ‘central’ and ‘non-central’ pieces,

$$2N_c \kappa_\Gamma \text{Re} [W_2(\sigma_A)] = E(t_1, s_{34}; t_3, s_{56}) + 2W_2^A, \quad (4.68)$$

with E given in eq. (4.25), and we further separate the central function into

$$2W_2^A = U_A + \Delta W_A(u_A, v_A, w_A). \quad (4.69)$$

The function U_A is given by eq. (4.29). In other words, this is a helicity-independent term. In contrast, for the opposite-helicity case the remainder function is given by

$$\Delta W_A(u_A, v_A, w_A) = N_c \kappa_\Gamma \left(-\frac{1}{4} \log^2(u_A) + \frac{1}{2} \log(u_A) \log(v_A w_A) - \log(v_A) \log(w_A) \right). \quad (4.70)$$

Note that, as for the same-helicity case, eq. (4.30), the variable assignment in eq. (4.29) leads to a NMRK remainder function which is IR-finite and symmetric under $v_A \leftrightarrow w_A$. However, we note that unlike eq. (4.30), eq. (4.70) does not vanish in the MRK limit. We will return to this point later. When working in NMRK, in order to exploit the equality of the real parts of the transcendental functions under an exchange of $p_1 \leftrightarrow p_6$ or $p_2 \leftrightarrow p_3$, we make the approximation eq. (4.31), and we make the NMRK approximation of the cross ratios in eq. (4.70). For the A' ordering we similarly write

$$\begin{aligned} 2N_c \kappa_\Gamma \text{Re} [W_2(\sigma_{A'})] &= E(t_1, s_{35}; t_3, s_{46}) + 2W_2^{A'}, \\ 2W_2^{A'} &= U_{A'} + \Delta W_A(u_{A'}, w_{A'}, v_{A'}). \end{aligned} \quad (4.71)$$

where $U_{A'}$ is related to U_A by exchange of $p_4 \leftrightarrow p_5$.

As in section 4.1, we can write the transcendental function of the σ_B ordering in terms of the one-loop factorised pieces in two different ways,

$$2N_c \kappa_\Gamma \text{Re} [W_1(\sigma_B)] = E(t_1, -s_{24}; t_3, s_{56}) + 2W_1^B = E(t_1, s_{35}; t_3, -s_{14}) + 2W_1^{B'}, \quad (4.72)$$

with

$$2W_1^B = U_B + \Delta W_B(u_B, v_B, w_B), \quad 2W_1^{B'} = U_{B'} + \Delta W_B(v_B, u_B, w_B). \quad (4.73)$$

The helicity-independent functions U_B and $U_{B'}$ are given in eq. (4.37), and the NMRK remainder is

$$\Delta W_B(u_B, v_B, w_B) = N_c \kappa_\Gamma \left(\log(v_B) \log\left(\frac{w_B}{u_B}\right) + \log(u_B) \log\left(\frac{w_B}{v_B}\right) \right). \quad (4.74)$$

We note that, similar to eq. (4.38), eq. (4.74) is IR finite, symmetric under $u_B \leftrightarrow v_B$, but does not vanish in either MRK or MRK' limits. We emphasise that eq. (4.72) is exact, but in the following we make the NMRK approximation (4.39) for U_B or $U_{B'}$, after which the functions U_B and $U_{B'}$ are related by $p_4 \leftrightarrow p_5$. We also make the NMRK approximation to the cross ratios in eq. (4.74), after which this function is symmetric under $p_4 \leftrightarrow p_5$.

Following the procedure of section 4.1, we now wish to express the opposite-helicity amplitude using the colour-structure basis of eq. (4.46). To this end, we apply the colour rotation of eq. (4.42) to the sum inside the curly brackets in eq. (4.61). We find that the structure of the kinematic coefficients is similar to the same-helicity case, motivating the following expression for general helicities, generalising eq. (4.46),

$$\begin{aligned} & \text{Disp} \left[\mathcal{M}_{\mathcal{N}=4}^{(1)}(p_4^{\nu_4}, p_5^{\nu_5}) \right] \xrightarrow{\text{NMRK}} \\ & \frac{g_s^6}{(4\pi)^2} s_{12} F^{a_3 a_2 c_1} C^{g(0)}(p_2^{\nu_2}, p_3^{-\nu_2}) \frac{1}{t_1} \times \\ & \sum_{\sigma \in S_2} \left\{ (F^{a_{\sigma_4}} F^{a_{\sigma_5}})_{c_1 c_3} \left(A_{\text{F}}^{gg(1)}(q_1, p_{\sigma_4}^{\nu_{\sigma_4}}, p_{\sigma_5}^{\nu_{\sigma_5}}, q_3) + A^{gg(0)}(q_1, p_{\sigma_4}^{\nu_{\sigma_4}}, p_{\sigma_5}^{\nu_{\sigma_5}}, q_3) E(t_1, s_{3\sigma_4}; t_3, s_{\sigma_5 6}) \right) \right. \\ & \quad \left. + \frac{1}{N_c} d_A^{c_1 a_{\sigma_4} a_{\sigma_5} c_3} A_d^{gg(1)}(q_1, p_{\sigma_4}^{\nu_{\sigma_4}}, p_{\sigma_5}^{\nu_{\sigma_5}}, q_3) \right\} \times \frac{1}{t_3} F^{a_6 a_1 c_3} C^{g(0)}(p_1^{\nu_1}, p_6^{-\nu_1}). \quad (4.75) \end{aligned}$$

For the opposite-helicity case we find that the kinematic coefficient of the tree-level colour structure is

$$\begin{aligned} & A_{\text{F}}^{gg(1)}(q_1, p_4^\oplus, p_5^\ominus, q_3) \\ & = \frac{1}{3} \left[2A^{gg(0)}(q_1, p_4^\oplus, p_5^\ominus, q_3) (2W_2^A + W_1^B) - 2A^{gg(0)}(q_1, p_5^\ominus, p_4^\oplus, q_3) (W_2^{A'} - W_1^{B'}) \right. \\ & \quad + 2 \left(S_{uv}^A (W_1^A - W_2^A) + S_{wu}^A (W_3^A - W_2^A) \right) - \left(S_{uv}^{A'} (W_1^{A'} - W_2^{A'}) + S_{wu}^{A'} (W_3^{A'} - W_2^{A'}) \right) \\ & \quad \left. - \left(S_{vw}^B (W_2^B - W_1^B) + S_{wu}^B (W_3^B - W_1^B) \right) \right]. \quad (4.76) \end{aligned}$$

There is some freedom in how to partition the kinematic coefficient of d_A as a sum over colour orderings. Before discussing our choice of how we organise this term, let us investigate the MRK limit of eq. (4.76). We first drop the rational terms that are power

suppressed in this limit,

$$\begin{aligned}
& A_{\mp}^{gg(1)}(q_1, p_4^{\oplus}, p_5^{\ominus}, q_3) \\
& \xrightarrow{\text{MRK}} \frac{1}{3} \left[A^{gg(0)}(q_1, p_4^{\oplus}, p_5^{\ominus}, q_3) \left(3U_{\text{MRK}} + 2\Delta W_A(u_A, v_A, w_A) + \Delta W_B(u_B, v_B, w_B) \right) \right. \\
& \quad \left. + 2 \left(S_{uv}^A(W_1^A - W_2^A) + S_{wu}^A(W_3^A - W_2^A) \right) - S_{vw}^B(W_2^B - W_1^B) \right], \quad (4.77)
\end{aligned}$$

where U_{MRK} is the helicity-independent MRK limit of the central transcendental functions, introduced in eq. (4.52). We now note that the nonvanishing terms of ΔW_A and ΔW_B cancel against the MRK limits of the terms proportional to S^A and S^B respectively, i.e.

$$\begin{aligned}
A^{gg(0)}(q_1, p_4^{\oplus}, p_5^{\ominus}, q_3) \Delta W_A(u_A, v_A, w_A) & \xrightarrow{\text{MRK}} -S_{uv}^A(W_1^A - W_2^A) - S_{wu}^A(W_3^A - W_2^A), \\
A^{gg(0)}(q_1, p_4^{\oplus}, p_5^{\ominus}, q_3) \Delta W_B(u_B, v_B, w_B) & \xrightarrow{\text{MRK}} S_{vw}^B(W_2^B - W_1^B). \quad (4.78)
\end{aligned}$$

With this we see that the MRK limit of eq. (4.77),

$$A_{\mp}^{gg(1)}(q_1, p_4^{\oplus}, p_5^{\ominus}, q_3) \xrightarrow{\text{MRK}} V^{g(0)}(q_1, p_4^{\oplus}, q_2) \frac{1}{t_2} V^{g(0)}(q_2, p_5^{\ominus}, q_3) U_{\text{MRK}}, \quad (4.79)$$

coincides with the MRK limit of the same-helicity amplitude, eq. (4.54), manifesting the helicity independence of the MRK limit. A similar analysis shows that the MRK' limit of eq. (4.77),

$$A_{\mp}^{gg(1)}(q_1, p_5^{\ominus}, p_4^{\oplus}, q_3) \xrightarrow{\text{MRK}'} V^{g(0)}(q_1, p_5^{\ominus}, q_2') \frac{1}{t_2'} V^{g(0)}(q_2', p_4^{\oplus}, q_3) U_{\text{MRK}'}, \quad (4.80)$$

coincides with the MRK' limit of the same-helicity vertex, eq. (4.56).

Equation (4.78) also provides our motivation for writing the kinematic coefficient of the totally symmetric colour structure as

$$\begin{aligned}
A_d^{gg(1)}(q_1, p_4^{\oplus}, p_5^{\ominus}, q_3) & = 2A^{gg(0)}(q_1, p_4^{\oplus}, p_5^{\ominus}, q_3) (W_2^A - W_1^B) \\
& \quad + S_{uv}^A(W_1^A - W_2^A) + S_{wu}^A(W_3^A - W_2^A) + S_{vw}^B(W_2^B - W_1^B), \quad (4.81)
\end{aligned}$$

with the aforementioned property eq. (4.66) leading to

$$\begin{aligned}
A_d^{gg(1)}(q_1, p_5^{\ominus}, p_4^{\oplus}, q_3) & = 2A^{gg(0)}(q_1, p_5^{\ominus}, p_4^{\oplus}, q_3) (W_2^{A'} - W_1^{B'}) \\
& \quad + S_{uv}^{A'}(W_1^{A'} - W_2^{A'}) + S_{wu}^{A'}(W_3^{A'} - W_2^{A'}) + S_{vw}^B(W_3^B - W_1^B). \quad (4.82)
\end{aligned}$$

This choice gives us the simple MRK and MRK' limits,

$$\begin{aligned}
A_d^{gg(1)}(q_1, p_4^{\oplus}, p_5^{\ominus}, q_3) & \xrightarrow{\text{MRK}} 0, \\
A_d^{gg(1)}(q_1, p_5^{\ominus}, p_4^{\oplus}, q_3) & \xrightarrow{\text{MRK}'} 0. \quad (4.83)
\end{aligned}$$

similar to eqs. (4.55) and (4.57).

4.3 NLO $gg \rightarrow gggg$ squared matrix element in the central NMRK limit

Having obtained the central NMRK limit of the six-gluon one-loop amplitude in $\mathcal{N} = 4$ SYM for all leading helicity configurations, we now consider the contribution of this amplitude to the squared matrix element for $gg \rightarrow gggg$ at NLO, i.e. the interference of this amplitude with the tree-level amplitude given in eqs. (3.2) and (3.3), summed over all colour indices:

$$2\text{Re} \left[\mathcal{M}_{6g}^{(0)*} \mathcal{M}_{6g}^{(1)} \right] = 2\text{Re} \left[\mathcal{M}_{6g}^{(0)*} \text{Disp} \left[\mathcal{M}_{6g}^{(1)} \right] \right] - 2\text{Im} \left[\mathcal{M}_{6g}^{(0)*} \text{Absorp} \left[\mathcal{M}_{6g}^{(1)} \right] \right]. \quad (4.84)$$

We consider these two contributions in turn.

Dispersive part

We first consider the contribution of the dispersive part of the one-loop amplitude, eq. (4.75), to eq. (4.84). The colour structures contributing to $\mathcal{M}_{6g}^{(0)*} \text{Disp}[\mathcal{M}_{6g}^{(1)}]$ are depicted as interference diagrams in figure 8. For each of them, after summing over the colour indices a_2, a_3 and a_1, a_6 , the factors associated with the impact factors are proportional to the identity in the adjoint representation, i.e.

$$\text{tr}(F^{c_1} F^{\tilde{c}_1}) = 2N_c \delta^{c_1 \tilde{c}_1}, \quad \text{tr}(F^{c_3} F^{\tilde{c}_3}) = 2N_c \delta^{c_3 \tilde{c}_3}. \quad (4.85)$$

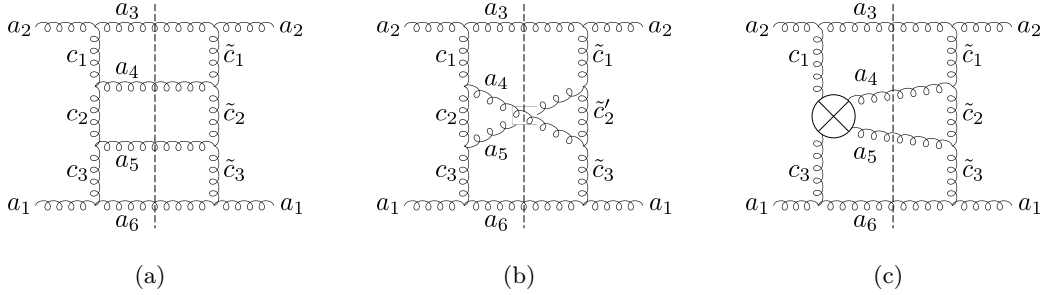


Figure 8. Three of the colour structures contributing to $\mathcal{M}_{6g}^{(0)*} \text{Disp}[\mathcal{M}_{6g}^{(1)}]$ using the basis of one-loop colour structures in eq. (4.75). The remaining three colour structures can be obtained by interchanging $a_4 \leftrightarrow a_5$. A three-gluon vertex represents the adjoint generator F , while the \otimes symbol represents the fully symmetric trace d_A of eq. (4.44).

We then see that the colour structures involving the totally symmetric tensor d_A vanish after contraction with the partially antisymmetric tree-level colour-structure:

$$4N_c^2 \delta^{c_1 \tilde{c}_1} \delta^{c_3 \tilde{c}_3} d_A^{c_1 a_4 a_5 c_3} (F^{a_4} F^{a_5})_{\tilde{c}_1 \tilde{c}_3} = -8N_c^2 d_A^{c_1 a_4 a_5 c_3} f^{c_1 a_4 \tilde{c}_2} f^{\tilde{c}_2 a_5 c_3} = 0. \quad (4.86)$$

The coefficient $A_d^{gg(1)}$ of the two-gluon CEV in eq. (4.75) therefore does not contribute to the NLO $gg \rightarrow 4\text{jet}$ cross section, or by extension, to the N³LO dijet cross section after phase-space integration. We emphasise that this conclusion applies to any helicity configuration of the one-loop two-gluon CEV.

By a similar argument, the symmetric colour structure of the two-gluon CEV does not contribute to the NNLL BFKL kernel. To see this we note that at this logarithmic

accuracy, the relevant interference, or ‘ladder’ diagrams describing an arbitrary number of real emissions along the ladder, including precisely one instance of the one-loop two-gluon CEV, have all other ‘rungs’ generated by the interference of tree-level impact factors and one-gluon CEVs (those appearing in fig. 1 (b)). The colour structure containing d_A of such a ladder diagram is depicted in figure 9. Given that the colour structure of the tree-level impact factors are either a fundamental generator or adjoint structure constant, and that the colour-structure of any one-gluon CEV is simply a structure constant, it follows that upon summing over the colour indices, the entire ladder of rungs above and below the one-loop two-gluon CEV collapse with the result proportional the identity in the adjoint representation (with each rung yielding an extra factor of $2N_c$). At the final stage, the contraction between d_A and the structure constant yields a vanishing result, just as in eq. (4.86).

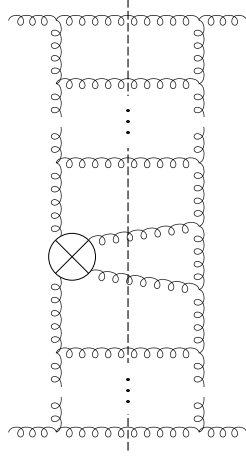


Figure 9. A colour structure of an interference, or ‘ladder’ diagram at NNLL accuracy, containing one instance of the one-loop two-gluon CEV, and all other real emissions given by tree-level one-gluon CEVs. The \otimes symbol represents the fully symmetric trace d_A of the two-gluon CEV. This colour structure vanishes upon summing over all colour indices, as discussed in the main text.

We further note that the symmetric colour structure of the two-gluon CEV is expected to contribute to the cross section and to the BFKL kernel at $N^3\text{LL}$ accuracy: at this order one must consider the square of the one-loop two-gluon CEV, where the interference involving two d_A terms survives, and yields a quartic Casimir invariant.

Having seen that the symmetric trace of four generators, d_A , which appears in the two-gluon CEV, does not contribute to the cross section or the BFKL kernel at NNLL, it is interesting to ask whether such symmetric colour structures contribute at this logarithmic accuracy to *any* of the interference diagrams making up the BFKL kernel in fig. 3. The answer is negative: upon summing over colour indices, the impact factors in any of these interference diagrams would be proportional to the identity in the adjoint representation. This argument holds for both gluon or quark impact factors. Having contracted the impact factors, the virtual loops and the central gluons only involve six colour vertices in total, which cannot form a quartic Casimir in any of the contributions in fig. 3. This may be

contrasted with contributions to the $2 \rightarrow 2$ amplitude from triple Reggeon exchange, which do involve quartic Casimirs at NNLL accuracy [26, 66, 68].

Absorptive part

We now consider the contribution of the absorptive part of the one-loop amplitude to eq. (4.84). As mentioned above, for the absorptive part of the one-loop amplitude, all signature components contribute at leading power in the NMRK limit, although they do not have logarithmic dependence on the large invariants s_{34} or s_{56} . The four signature components are listed in eqs. (F.8)–(F.11) for $\nu_4 = \nu_5$ and in eqs. (F.12)–(F.15) for $\nu_4 = -\nu_5$. However, the leading-power behaviour of the tree-level amplitude is given by the $(-, -)$ component alone, and this projects out the $(-, -)$ component of the absorptive one-loop amplitude in $\mathcal{M}_{6g}^{(0)*} \text{Absorp}[\mathcal{M}_{6g}^{(1)}]$ upon summing over the external colour indices. For the $(-, -)$ component of the absorptive part of the amplitude (eq. (F.8) for the $\nu_4 = \nu_5$ case and eq. (F.12) for the $\nu_4 = -\nu_5$ case), we can factor out an adjoint generator associated to the tree-level impact factors. Upon considering the interference between these absorptive parts and the tree-level amplitude, we therefore find that the colour factors associated with the impact factors are identical to the dispersive case above, eq. (4.85).

To proceed and evaluate the imaginary part of $\mathcal{M}_{6g}^{(0)*} \text{Absorp}[\mathcal{M}_{6g}^{(1)}]$ we now distinguish between the same-helicity case, where the relevant absorptive part is given in eq. (F.8), and the opposite-helicity case, where the relevant absorptive part is given in eq. (F.12). For the former case, the colour factors which contain $\text{tr}(F^{c_1} F^{a_4} F^{c_3} F^{a_5})$ or $\text{tr}(F^{c_1} F^{a_5} F^{a_4} F^{c_3})$ do not contribute to the absorptive interference term, due to either the vanishing of the colour factor or the reality of its kinematic coefficient. The remaining contribution is proportional to

$$\begin{aligned} & \text{tr}(F^{c_1} F^{a_5} F^{c_3} F^{a_4})(F^{a_4} F^{a_5})_{c_1 c_3} \text{Im} \left[B^{gg(0)}(q_1, p_4^\oplus, p_5^\oplus, q_3) A^{gg(0)*}(q_1, p_4^\oplus, p_5^\oplus, q_3) \right] \\ & + \text{tr}(F^{c_1} F^{a_5} F^{c_3} F^{a_4})(F^{a_5} F^{a_4})_{c_1 c_3} \text{Im} \left[B^{gg(0)}(q_1, p_4^\oplus, p_5^\oplus, q_3) A^{gg(0)*}(q_1, p_5^\oplus, p_4^\oplus, q_3) \right] = 0. \end{aligned} \quad (4.87)$$

To show that this quantity is zero we first note that the two colour factors are equal, which can be shown using the reversal-invariance property of the trace of four adjoint generators, along with a relabelling of the indices a_4 and a_5 . After factoring out the common colour factor one is left with the imaginary part of a kinematic factor which can be shown to be real using eq. (3.31). We conclude that the absorptive part of the amplitude does not contribute to the squared matrix element for $gg \rightarrow gggg$ at NLO in the central NMRK limit for the helicity configurations with $\nu_4 = \nu_5$.

Repeating the above analysis for the opposite-helicity case we find a non-vanishing

result. Specifically, for $\nu_4 = \oplus$ and $\nu_5 = \ominus$ we find that

$$\begin{aligned}
2\text{Im} \left[\mathcal{M}_{6g}^{(0)*}(p_4^\oplus, p_5^\ominus) \text{Absorp} \left[\mathcal{M}_{6g}^{(1)}(p_4^\oplus, p_5^\ominus) \right] \right] &\xrightarrow{\text{NMRK}} 2g_s^8 \frac{\alpha_s}{4\pi} \frac{\pi}{2} \frac{s^2}{t_1^2 t_3^2} \left| C^{g(0)}(p_2^{\nu_2}, p_3^{-\nu_2}) \right|^2 \\
&\times 8N_c^5(N_c^2 - 1) \left\{ \text{Im} \left[\left(S_{uv}^A \log(v_A) + S_{wu}^A \log(w_A) \right) A^{gg(0)*}(q_1, p_4^\oplus, p_5^\ominus, q_3) \right] \right. \\
&\quad + \text{Im} \left[\left(S_{uv}^{A'} \log(v_{A'}) + S_{wu}^{A'} \log(w_{A'}) \right) A^{gg(0)*}(q_1, p_5^\ominus, p_4^\oplus, q_3) \right] \\
&\quad \left. - \text{Im} \left[S_{uv}^B B^{gg(0)*}(q_1, p_4^\oplus, p_5^\ominus, q_3) \right] \log \left(\frac{w_B}{u_B v_B} \right) \right\} \times \left| C^{g(0)}(p_1^{\nu_1}, p_6^{-\nu_1}) \right|^2,
\end{aligned} \tag{4.88}$$

which is generically non-zero.

Next we observe that the absorptive interference term for $\nu_4 = \ominus$ and $\nu_5 = \oplus$ is equal to the complex conjugate of eq. (4.88). Therefore, the absorptive part of the one-loop amplitude in NMRK does not contribute to the helicity-summed squared matrix element for $gg \rightarrow gggg$ at NLO. Thus, the contribution of the one-loop six-gluon amplitude in the central NMRK limit to the cross section at this logarithmic accuracy is entirely driven by the dispersive part.

5 All-orders conjectures for amplitudes in a central NMRK limit

In section 4 we discussed the six-gluon $\mathcal{N} = 4$ SYM amplitude to one-loop accuracy. However, the results of section 4.1 and 4.2 are suggestive of the factorised form that amplitudes may take in the central NMRK limit at higher orders, and potentially at higher multiplicity. In this section we therefore make conjectures for the form that the dispersive part of amplitudes may take beyond one loop and beyond the six-gluon case.

The separation of the non-central E functions in eq. (4.75), multiplying the tree-level two-gluon CEV, strongly suggests a factorised picture, analogous to eq. (2.21), for the production of two gluons in the central NMRK limit. The one-loop two-gluon CEV extracted this way is a component of BFKL at NNLL accuracy. As noted in ref. [89], one can place limits on the pattern of Reggeization by requiring that the MRK limit of said CEV agrees with the known behaviour of amplitudes in MRK. The following Reggeization ansatz for the production of two gluons in the central NMRK limit is compatible with both the known MRK limit and with the structure of the dispersive part of the one-loop

amplitude eq. (4.75),

$$\begin{aligned}
& \text{Disp} \left[\mathcal{M}_{6g}^{(-,-)} \right] \xrightarrow{\text{NMRK}} s \left[g_S(F^{a_3})_{a_2 c_1} C^g(p_2^{\nu_2}, p_3^{\nu_3}) \right] \\
& \times \sum_{\sigma \in S_2} \left\{ \frac{1}{t_1} \frac{1}{2} \left[\left(\frac{s_{3\sigma_4}}{\tau} \right)^{\alpha(t_1)} + \left(\frac{-s_{3\sigma_4}}{\tau} \right)^{\alpha(t_1)} \right] \right. \\
& \times \left[g_S^2(F^{a_{\sigma_4}} F^{a_{\sigma_5}})_{c_1 c_3} A_{\mathbb{F}}^{gg}(q_1, p_{\sigma_4}^{\nu_{\sigma_4}}, p_{\sigma_5}^{\nu_{\sigma_5}}, q_3) + \frac{1}{N_c} d_A^{c_1 a_{\sigma_4} a_{\sigma_5} c_3} A_d^{gg}(q_1, p_{\sigma_4}^{\nu_{\sigma_4}}, p_{\sigma_5}^{\nu_{\sigma_5}}, q_3) \right] \\
& \times \left. \frac{1}{t_3} \frac{1}{2} \left[\left(\frac{s_{\sigma_5 6}}{\tau} \right)^{\alpha(t_3)} + \left(\frac{-s_{\sigma_5 6}}{\tau} \right)^{\alpha(t_3)} \right] \right\} \\
& \times \left[g_S(F^{a_6})_{a_1 c_3} C^g(p_1^{\nu_1}, p_6^{\nu_6}) \right] .
\end{aligned} \tag{5.1}$$

This factorization is illustrated schematically in figure 10 (a). The first thing to note is that, unlike amplitudes at LL, or signature-odd amplitudes at NLL, the amplitude is not fully factorised. Rather, eq. (5.1) is rather a sum over two colour orderings, each of which is factorised in the familiar form of impact factors, Reggeized gluons and a two-gluon CEV.

Further to this point are the assumptions we have made regarding the colour structure d_A beyond one-loop accuracy. In eq. (5.1) we have assumed that this totally-symmetric colour factor couples to Reggeized gluons at higher orders in α_S . Specifically, eq. (5.1) assumes a particular form for this Reggeization, based on the partitioning of the kinematic coefficient of d_A , sections 4.1 and 4.2. While this partitioning seems natural from the point of view of requiring compatibility with the known MRK limit, the nature of Reggeization of this term of course cannot be determined from the one-loop amplitude studied in this paper. It may be constrained by taking the central NMRK limit of the two-loop six-gluon amplitude. A similar structure is accessible through the non-central NMRK limit of the two-loop five-gluon amplitude.

With these assumptions in mind, we may consider how eq. (5.1) may be generalised to the case of $2 \rightarrow n$ scattering in any of the central NMRK limits where the rapidity separation between a pair of consecutive central gluons denoted by m and $m+1$ (with $4 \leq m \leq n-2$) is not necessarily large, while all other rapidity separations are large. We

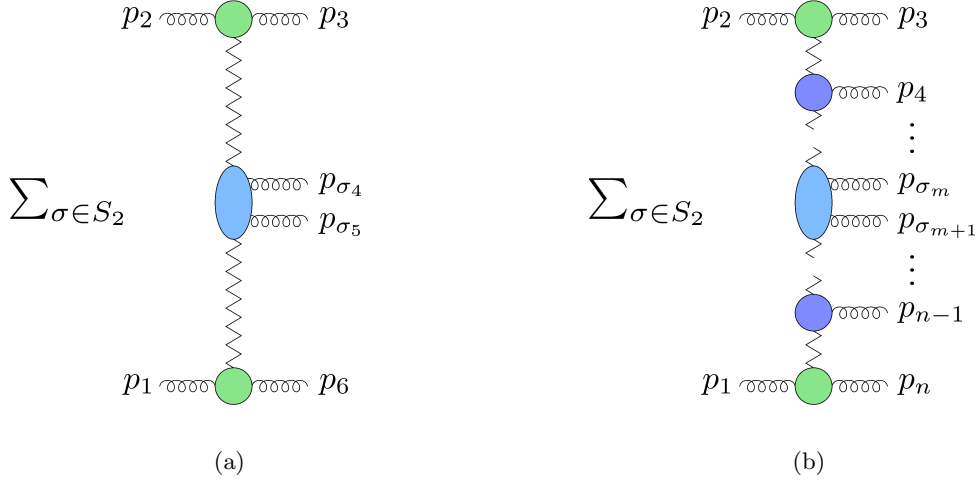


Figure 10. (a) The expected factorised picture of the dispersive part of a six-gluon amplitude in the central NMRK limit. (b) The expected factorization of an n -gluon amplitude in a central NMRK limit. The coloured blobs represent impact factors, and one- and two gluon CEVs, defined to all orders in perturbation theory, similarly to figure 4.

propose the following ansatz for an arbitrary number of legs:

$$\begin{aligned}
& \text{Disp} \left[\mathcal{M}_{ng}^{[8_a]} \right] \xrightarrow{\text{NMRK}} s \left[g_S(F^{a_3})_{a_2 c_1} C^g(p_2^{\nu_2}, p_3^{\nu_3}) \right] \\
& \times \prod_{i=4}^{m-1} \left(\frac{1}{t_{i-3}} \frac{1}{2} \left[\left(\frac{s_{i-1,i}}{\tau} \right)^{\alpha(t_{i-3})} + \left(\frac{-s_{i-1,i}}{\tau} \right)^{\alpha(t_{i-3})} \right] \left[g_S(F^{a_i})_{c_{i-3} c_{i-2}} V^g(q_{i-3}, p_i^{\nu_i}, q_{i-2}) \right] \right) \\
& \times \sum_{\sigma \in S_2} \left\{ \frac{1}{t_{m-3}} \frac{1}{2} \left[\left(\frac{s_{m-1,\sigma_m}}{\tau} \right)^{\alpha(t_{m-3})} + \left(\frac{-s_{m-1,\sigma_m}}{\tau} \right)^{\alpha(t_{m-3})} \right] \right. \\
& \times \left[g_S^2(F^{a_{\sigma_m}} F^{a_{\sigma_{m+1}}})_{c_{m-3} c_{m-1}} A_{\text{F}}^{gg}(q_{m-3}, p_{\sigma_m}^{\nu_{\sigma_m}}, p_{\sigma_{m+1}}^{\nu_{\sigma_{m+1}}}, q_{m-1}) \right. \\
& \quad \left. \left. + \frac{1}{N_c} d_A^{c_{m-3} a_{\sigma_m} a_{\sigma_{m+1}} c_{m-1}} A_d^{gg}(q_{m-3}, p_{\sigma_m}^{\nu_{\sigma_m}}, p_{\sigma_{m+1}}^{\nu_{\sigma_{m+1}}}, q_{m-1}) \right] \right\} \\
& \times \frac{1}{t_{m-1}} \frac{1}{2} \left[\left(\frac{s_{\sigma_{m+1},m+2}}{\tau} \right)^{\alpha(t_{m-1})} + \left(\frac{-s_{\sigma_{m+1},m+2}}{\tau} \right)^{\alpha(t_{m-1})} \right] \Bigg\} \\
& \times \prod_{i=m+2}^{n-1} \left(\left[g_S(F^{a_i})_{c_{i-3} c_{i-2}} V^g(q_{i-3}, p_i^{\nu_i}, q_{i-2}) \right] \frac{1}{t_{i-2}} \frac{1}{2} \left[\left(\frac{s_{i,i+1}}{\tau} \right)^{\alpha(t_{i-2})} + \left(\frac{-s_{i,i+1}}{\tau} \right)^{\alpha(t_{i-2})} \right] \right) \\
& \times \left[g_S(F^{a_n})_{a_1 c_{n-3}} C^g(p_1^{\nu_1}, p_n^{\nu_n}) \right], \tag{5.2}
\end{aligned}$$

which is written entirely in terms of the components extracted from $n \leq 6$ amplitudes. This factorised structure is depicted schematically in figure 10 (b), where real emissions that are strongly ordered in rapidity are described in a similar way to the MRK structure depicted in figure 4.

6 Conclusions

Taking the one-loop six-gluon amplitudes of $\mathcal{N} = 4$ SYM [73, 74] into the central NMRK limit, in this paper we have obtained the one-loop corrections to the two-gluon central-emission vertex (CEV) in this theory, in both the same-helicity and opposite-helicity configurations. This is a first step toward the determination of the same quantity in QCD.

In contrast with the one-gluon CEV, we find that the two-gluon CEV, eq. (4.13), receives one-loop corrections involving a new colour structure consisting of a fully symmetric trace of four adjoint generators, which is not present at tree level. We find, however, that this new structure does not contribute to the squared matrix element for $gg \rightarrow gggg$ at NLO, so it does not enter the NNLL BFKL kernel. We note, however that this symmetric colour structure does contribute to the squared matrix element at N^3 LL accuracy, where the interference between two one-loop two-gluon CEVs gives rise to a quartic Casimir invariant.

As discussed in section 4.3, none of the NNLL contributions to the BFKL kernel, which are described by the interference diagrams in fig. 3, gives rise to a quartic Casimir. This may be contrasted with contributions to the $2 \rightarrow 2$ amplitude from triple-Reggeon exchange, which do involve quartic Casimirs at NNLL accuracy [26, 66, 68].

In addition to the new colour structure, also the kinematic dependence of the two-gluon CEV is rather complex. In the same-helicity two-gluon CEV, which is extracted from an MHV amplitude, dilogarithms survive in the NMRK limit, eqs. (4.30) and (4.38). The dilogarithms depend on conformally-invariant cross ratios (3.19) and (3.33), the same variables which characterize six-gluon amplitudes in planar $\mathcal{N} = 4$ SYM [94].

Yet another layer of complexity arises in the case of the one-loop NMHV amplitude, from which the opposite-helicity two-gluon CEV is extracted. Considering this amplitude in central NMRK, eq. (4.75), eq. (4.76) and eq. (4.81), we find rational coefficients which are not proportional to the tree amplitude, accompanied by different transcendental functions, eq. (4.60). This structure involves an interplay between spurious poles of these rational coefficients and zeroes of the transcendental functions multiplying them, see eqs. (4.61)–(4.65) and tables 1 and 2. These features propagate into the one-loop opposite-helicity CEV.

Another consequence of the more complicated structure of the one-loop NMHV amplitude is that, in contrast with the MHV case, an absorptive part survives in the squared matrix element for $gg \rightarrow gggg$ at NLO, after summing over colour indices, as shown in section 4.3. However, upon summing over gluon helicities, this absorptive contribution vanishes, and thus only the dispersive part of the one-loop six-gluon amplitude contributes to unpolarised cross sections at NNLL.

In ref. [16], it was noted that the transcendental functions of the one-loop six-gluon MHV amplitude can be written exactly in terms of the known one-loop Regge components, eq. (4.26), consisting of impact factors, Reggeized gluons and Lipatov vertices, plus a remainder term (4.30) written in terms of the conformally-invariant cross ratios (3.19). In eqs. (4.68) and (4.70), we have shown that this holds also for the NMHV amplitude, and thus for the whole one-loop six-gluon amplitude in $\mathcal{N} = 4$ SYM. This parallels the

set-up of the two-loop six-gluon MHV amplitude in planar $\mathcal{N} = 4$ SYM, which can be expressed in terms of two-loop Regge components [103] and remainder functions depending on conformally-invariant cross ratios (3.19), and which can be evaluated in the central NMRK limit without any loss of generality [29, 30]. It would be interesting to extend this analysis to the two-loop six-gluon amplitude in full $\mathcal{N} = 4$ SYM.

It follows in particular that the transcendental functions making up the one-loop two-gluon CEV can be expressed in terms of one-loop MRK components, evaluated at NMRK kinematics, plus a remainder function. The former is independent of the helicity configuration, eq. (4.24), while the latter has a distinct functional form for each of the two helicity configurations.

Our one-loop analysis of the two-gluon CEV provides first hints with regards to the factorization and exponentiation properties of the six-gluon amplitude. In eq. (5.1) we have proposed an exponentiation pattern of the six-gluon amplitude in the central NMRK limit in which rapidity ordering is partially linked with colour ordering. The guiding principles have been the locality of the two-gluon CEV in rapidity, and its factorisation in the MRK limit into two one-gluon CEVs connected by a Regge trajectory. However, the link between rapidity and colour ordering in (5.1) is only partial, because of the presence of a fully-symmetric colour structure, which occurs first at the one-loop level, eq. (4.75): an evaluation of the two-loop amplitude in the NMRK limit is necessary to confirm or disprove this factorized structure. We leave the investigation of two-loop amplitudes in the NMRK limit to future work.

In the NLL corrections to the BFKL kernel (fig. 2 b), the one-loop one-gluon CEV is multiplied by the corresponding tree-level CEV, with the gluon p_4 emitted centrally along the ladder which is integrated over its phase space. No collinear divergences are allowed in MRK, eq. (2.7), however in the phase-space integration, the gluon p_4 may become soft and yield a pole of $\mathcal{O}(1/\epsilon)$. In order to generate all the finite terms of the squared amplitude, the one-loop one-gluon CEV must be evaluated to $\mathcal{O}(\epsilon)$ in the limit that the gluon p_4 is soft [47, 48], which requires the use of one-loop soft functions to $\mathcal{O}(\epsilon)$ [49]. In the NNLL corrections to the BFKL kernel, similar features are present: the one-loop two-gluon CEV is multiplied by the corresponding tree-level CEV with the gluons p_4 and p_5 emitted along the ladder, which are integrated over their phase space. In the phase-space integration, both gluons may become soft, as well as collinear to each other, yielding poles of up to $\mathcal{O}(1/\epsilon^3)$. Accordingly, the one-loop two-gluon CEV must be evaluated to $\mathcal{O}(\epsilon^3)$ in the limit that gluons p_4 and p_5 are soft, and/or collinear to each other. To higher order in ϵ , the one-loop splitting functions are known [104, 105], but the one-loop double-soft functions are yet to be determined. We leave the analysis of the higher-order terms of the one-loop two-gluon CEV to future work.

For generic gluon momenta, in order to obtain the two-gluon CEV in QCD using the supersymmetric decomposition of one-loop amplitudes, the next step is to perform a similar NMRK analysis of the contributions of a $\mathcal{N} = 1$ multiplet and of a scalar circulating in the loop. We also leave this analysis for the future.

Acknowledgements

We thank Claude Duhr for useful discussions. EG is supported by the STFC Consolidated Grant ‘Particle Physics at the Higgs Centre’. EB and JMS are supported by the ERC Starting Grant 715049 ‘QCDforfuture’. JMS is also supported by a Royal Society University Research Fellowship. This research was supported by the US Department of Energy under contract DE-AC02-76SF00515, and in part by the National Science Foundation under Grant No. NSF PHY-1748958. LD thanks the Kavli Institute for Theoretical Physics for hospitality during the completion of this work. For the purpose of open access, the authors have applied a Creative Commons Attribution (CC BY) licence to any Author Accepted Manuscript version arising from this submission.

A Kinematic regions

A.1 General multi-parton kinematics

We consider the production of four partons of momenta p_i , $i = 3, 4, 5, 6$, in the scattering between two partons of momenta p_1 and p_2 , as depicted in figure 11. By convention, we consider the scattering in the unphysical region where all momenta are taken as outgoing, and then we analytically continue to the physical region where $p_1^0 < 0$ and $p_2^0 < 0$. Thus partons are incoming or outgoing depending on the sign of their energy. Since the helicity of a positive-energy (negative-energy) massless spinor has the same (opposite) sign as its chirality, the helicities assigned to the partons depend on whether they are incoming or outgoing. We label outgoing (positive-energy) particles with their helicity; if they are incoming the actual helicity and charge are reversed, e.g. an incoming left-handed parton is labelled as an outgoing right-handed anti-parton.

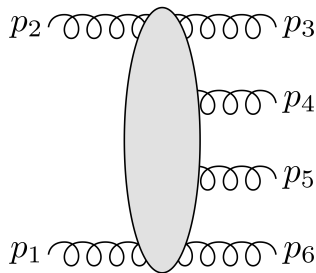


Figure 11. Depiction of the production of four gluons of momenta p_i , $i = 3, 4, 5, 6$, in the scattering between two partons of momenta p_1 and p_2 . We take all momenta to be outgoing.

Using light-cone coordinates $p^\pm = p^0 \pm p^z$, and complex transverse coordinates $p_\perp = p^x + ip^y$, with scalar product,

$$2p \cdot q = p^+ q^- + p^- q^+ - p_\perp q_\perp^* - p_\perp^* q_\perp, \quad (\text{A.1})$$

the four-momenta are,

$$\begin{aligned}
p_1 &= \left(\frac{p_1^-}{2}, 0, 0, \frac{-p_1^-}{2} \right) \equiv (0, p_1^-; 0, 0) , \\
p_2 &= \left(\frac{p_2^+}{2}, 0, 0, \frac{p_2^+}{2} \right) \equiv (p_2^+, 0; 0, 0) , \\
p_i &= \left(\frac{p_i^+ + p_i^-}{2}, \text{Re}[p_{i\perp}], \text{Im}[p_{i\perp}], \frac{p_i^+ - p_i^-}{2} \right) \equiv |p_{i\perp}| (e^{y_i}, e^{-y_i}; \cos \phi_i, \sin \phi_i) ,
\end{aligned} \tag{A.2}$$

where y is the rapidity, and $3 \leq i \leq 6$. The first notation in eq. (A.2) is the standard representation $p^\mu = (p^0, p^x, p^y, p^z)$, while in the second we have the $+$ and $-$ light-cone components on the left of the semicolon, and the transverse components on the right.

From momentum conservation,

$$\begin{aligned}
0 &= \sum_{i=3}^6 p_{i\perp} , \\
p_2^+ &= - \sum_{i=3}^6 p_i^+ , \\
p_1^- &= - \sum_{i=3}^6 p_i^- ,
\end{aligned} \tag{A.3}$$

and using the scalar product eq. (A.1), the Mandelstam invariants may be written as,

$$\begin{aligned}
s &= 2p_1 \cdot p_2 = \sum_{i,j=3}^6 p_i^+ p_j^- \\
s_{2i} &= 2p_2 \cdot p_i = - \sum_{j=3}^6 p_i^- p_j^+ \\
s_{1i} &= 2p_1 \cdot p_i = - \sum_{j=3}^6 p_i^+ p_j^- \\
s_{ik} &= 2p_i \cdot p_k = p_i^+ p_k^- + p_i^- p_k^+ - p_{i\perp} p_{k\perp}^* - p_{i\perp}^* p_{k\perp} ,
\end{aligned} \tag{A.4}$$

with $3 \leq i, k \leq 6$.

For the momenta in eq. (A.2), we find the following right-handed spinor products, $\langle k p \rangle = \bar{u}_-(k) u_+(p)$, in the notation of Ref. [70],

$$\begin{aligned}
\langle p_i p_j \rangle &= p_{i\perp} \sqrt{\frac{p_j^+}{p_i^+}} - p_{j\perp} \sqrt{\frac{p_i^+}{p_j^+}} , \\
\langle p_2 p_i \rangle &= -i \sqrt{\frac{-p_2^+}{p_i^+}} p_{i\perp} , \\
\langle p_i p_1 \rangle &= i \sqrt{-p_1^- p_i^+} , \\
\langle p_2 p_1 \rangle &= -\sqrt{p_2^+ p_1^-} ,
\end{aligned} \tag{A.5}$$

where we have used the mass-shell condition,

$$|p_{i\perp}|^2 = p_i^+ p_i^- . \quad (\text{A.6})$$

Left-handed spinor products, $[k p] = \bar{u}_+(k) u_-(p)$, are given by complex conjugation,

$$[k p] = \text{sign}(k^0 p^0) \langle p k \rangle^* . \quad (\text{A.7})$$

Spinor products are antisymmetric,

$$\langle k p \rangle = -\langle p k \rangle , \quad [k p] = -[p k] . \quad (\text{A.8})$$

We also use the currents, $[p|\gamma^\mu|k\rangle$ and $\langle p|\gamma^\mu|k]$, which are related by charge conjugation,

$$[p|\gamma^\mu|k\rangle = \langle k|\gamma^\mu|p] , \quad (\text{A.9})$$

and complex conjugation,

$$[p|\gamma^\mu|k\rangle^* = \text{sign}(k^0 p^0) [k|\gamma^\mu|p] . \quad (\text{A.10})$$

Through the Fierz rearrangement,

$$\langle k|\gamma^\mu|p\rangle \langle v|\gamma^\mu|q\rangle = 2\langle k v\rangle [q p] , \quad (\text{A.11})$$

and the Gordon identity,

$$[p|\gamma^\mu|p\rangle = \langle p|\gamma^\mu|p] = 2p^\mu , \quad (\text{A.12})$$

we obtain that

$$\begin{aligned} \langle k|\not{q}|p\rangle &= \langle k q\rangle [q p] , \\ [p|\not{q}|k\rangle &= [p q] \langle q k\rangle . \end{aligned} \quad (\text{A.13})$$

A.2 Multi-Regge kinematics

In multi-Regge kinematics, we require that the light-cone momenta of the gluons are strongly ordered and have comparable transverse momentum. In the six-gluon case, we take

$$\begin{aligned} p_3^+ \gg p_4^+ \gg p_5^+ \gg p_6^+ , \quad p_3^- \ll p_4^- \ll p_5^- \ll p_6^- , \\ |p_{3\perp}| \simeq |p_{4\perp}| \simeq |p_{5\perp}| \simeq |p_{6\perp}| . \end{aligned} \quad (\text{A.14})$$

The strong ordering of light-cone momenta in eq. (A.14) is equivalent to requiring a strong-ordering on the rapidities,

$$y_3 \gg y_4 \gg y_5 \gg y_6 . \quad (\text{A.15})$$

Momentum conservation in eq. (A.3) then becomes

$$\begin{aligned} 0 &= \sum_{i=3}^6 p_{i\perp} , \\ p_2^+ &\simeq -p_3^+ , \\ p_1^- &\simeq -p_6^- . \end{aligned} \quad (\text{A.16})$$

To leading accuracy, the Mandelstam invariants in eq. (A.4) are reduced to

$$\begin{aligned}
s &= 2p_1 \cdot p_2 \simeq p_3^+ p_6^- , \\
s_{2i} &= 2p_2 \cdot p_i \simeq -p_3^+ p_i^- , \\
s_{1i} &= 2p_1 \cdot p_i \simeq -p_i^+ p_6^- , \\
s_{ij} &= 2p_i \cdot p_j \simeq p_i^+ p_j^- ,
\end{aligned} \tag{A.17}$$

with $3 \leq i, j \leq 6$, and with $p_i^+ > p_j^+$, for $i < j$. Note that the mass-shell condition in eq. (A.6) implies that

$$s |p_{4\perp}|^2 |p_{5\perp}|^2 \simeq s_{34} s_{45} s_{56} , \tag{A.18}$$

which is an example of the general multi-Regge constraint,

$$s_{ij} \prod_{k=i+1}^{j-1} |p_{k\perp}|^2 = \prod_{k=i}^{j-1} s_{k,k+1} . \tag{A.19}$$

The spinor products in eq. (A.5) become,

$$\begin{aligned}
\langle p_i p_j \rangle &\simeq -\sqrt{\frac{p_i^+}{p_j^+}} p_{j\perp} \quad \text{for } y_i > y_j , \\
\langle p_2 p_i \rangle &\simeq -i \sqrt{\frac{p_3^+}{p_i^+}} p_{i\perp} , \\
\langle p_i p_1 \rangle &\simeq i \sqrt{p_i^+ p_6^-} , \\
\langle p_2 p_1 \rangle &\simeq -\sqrt{p_3^+ p_6^-} ,
\end{aligned} \tag{A.20}$$

with $3 \leq i \leq 6$. In eqs. (A.17) and (A.20) only the leading terms are displayed. Here and henceforth, it is understood that, if so required by the computation, sub-leading terms may need to be retained.

In the Euclidean region, where the Mandelstam invariants are taken as all negative, the ordering in eq. (A.14) becomes

$$-s_{12} \gg -s_{123}, -s_{345} \gg -s_{34}, -s_{45}, -s_{56} \gg -s_{23}, -s_{61}, -s_{234} . \tag{A.21}$$

Introducing a parameter $\lambda \ll 1$, the hierarchy in eq. (A.15) above is equivalent to the rescaling,

$$\{s_{123}, s_{345}\} = \mathcal{O}(\lambda) , \quad \{s_{34}, s_{45}, s_{56}\} = \mathcal{O}(\lambda^2) , \quad \{s_{23}, s_{61}, s_{234}\} = \mathcal{O}(\lambda^3) . \tag{A.22}$$

A.3 Central next-to-multi-Regge kinematics

We now consider the production of four partons of momenta p_i , with $3 \leq i \leq 6$, with the new constraint that partons 4 and 5 are in the central region along the gluon ladder,

$$\begin{aligned}
p_3^+ \gg p_4^+ \simeq p_5^+ \gg p_6^+ , \quad p_3^- \ll p_4^- \simeq p_5^- \ll p_6^- , \\
|p_{3\perp}| \simeq |p_{4\perp}| \simeq |p_{5\perp}| \simeq |p_{6\perp}| ,
\end{aligned} \tag{A.23}$$

and hence,

$$y_3 \gg y_4 \simeq y_5 \gg y_6. \quad (\text{A.24})$$

The leading contributions to momentum conservation are the same as in eq. (A.16). The Mandelstam invariants of eq. (A.4) become

$$\begin{aligned} s &\simeq p_3^+ p_6^-, \\ s_{2i} &\simeq -p_3^+ p_i^-, \\ s_{1i} &\simeq -p_i^+ p_6^-, \\ s_{jk} &\simeq p_j^+ p_k^-, \quad j \neq 4 \text{ and } k \neq 5, \\ s_{45} &= p_4^+ p_5^- + p_4^- p_5^+ - p_{4\perp}^* p_{5\perp} - p_{5\perp}^* p_{4\perp}, \end{aligned} \quad (\text{A.25})$$

with $3 \leq i, j, k \leq 6$, with $p_j^+ > p_k^+$ for $j < k$. Note that the mass-shell condition in eq. (A.6) and the Mandelstam invariants in eq. (A.25) imply that

$$\begin{aligned} s &\simeq \frac{s_{34} s_{56}}{p_4^- p_5^+} \\ &= \frac{s_{34} s_{56} p_4^+ p_5^-}{|p_{4\perp}|^2 |p_{5\perp}|^2}. \end{aligned} \quad (\text{A.26})$$

All three-particle Mandelstam invariants either simplify to a two-particle Mandelstam invariant, or are equal to one of the following, up to an overall sign,

$$\begin{aligned} s_{123} &\simeq (p_4^+ + p_5^+) p_6^-, \\ s_{234} &\simeq -|p_{3\perp} + p_{4\perp}|^2 - p_4^- p_5^+, \\ s_{235} &\simeq -|p_{3\perp} + p_{5\perp}|^2 - p_4^+ p_5^-, \\ s_{345} &\simeq p_3^+ (p_4^- + p_5^-). \end{aligned} \quad (\text{A.27})$$

In the Euclidean region, where the Mandelstam invariants are taken as all negative, the ordering in eq. (A.23) becomes

$$-s_{12} \gg -s_{34}, -s_{56}, -s_{123}, -s_{345} \gg -s_{23}, -s_{45}, -s_{61}, -s_{234}, -s_{235}. \quad (\text{A.28})$$

Introducing a parameter $\lambda \ll 1$, the hierarchy in eq. (A.23) above is equivalent to the rescaling,

$$\{s_{34}, s_{56}, s_{123}, s_{345}\} = \mathcal{O}(\lambda), \quad \{s_{23}, s_{45}, s_{61}, s_{234}, s_{235}\} = \mathcal{O}(\lambda^2). \quad (\text{A.29})$$

The spinor products in eq. (A.5) become

$$\begin{aligned} \langle p_2 p_1 \rangle &\simeq -\sqrt{p_3^+ p_6^-}, \\ \langle p_2 p_k \rangle &= -i \sqrt{\frac{-p_2^+}{p_k^+}} p_{k\perp} \simeq -i \sqrt{\frac{p_3^+}{p_k^+}} p_{k\perp}, \\ \langle p_k p_1 \rangle &= i \sqrt{-p_1^- p_k^+} \simeq i \sqrt{p_k^+ p_6^-}, \\ \langle p_j p_k \rangle &= p_{j\perp} \sqrt{\frac{p_k^+}{p_j^+}} - p_{k\perp} \sqrt{\frac{p_j^+}{p_k^+}} \simeq -p_{k\perp} \sqrt{\frac{p_j^+}{p_k^+}}, \quad j \neq 4 \text{ and } k \neq 5 \\ \langle p_4 p_5 \rangle &= p_{4\perp} \sqrt{\frac{p_5^+}{p_4^+}} - p_{5\perp} \sqrt{\frac{p_4^+}{p_5^+}}, \end{aligned} \quad (\text{A.30})$$

with $3 \leq j, k \leq 6$, with $p_j^+ > p_k^+$.

The following spinor strings occur in the BCFW representation of NMHV tree-level amplitudes. We list the spinor strings for two representative colour orderings. For the colour ordering $\{1, 2, 3, 4, 5, 6\}$ the relevant quantities are

$$\begin{aligned}\langle p_1 | \not{p}_2 + \not{p}_3 | p_4 \rangle &\simeq -i |q_{3\perp}| \sqrt{\frac{p_4^+}{p_6^+}} (q_{2\perp}^* + p_{4\perp}^* \frac{p_5^+}{p_4^+}), \\ \langle p_3 | \not{p}_4 + \not{p}_5 | p_6 \rangle &\simeq -q_{3\perp}^* \sqrt{\frac{p_3^+}{p_6^+}} (p_{4\perp} + p_{5\perp}), \\ \langle p_5 | \not{p}_6 + \not{p}_1 | p_2 \rangle &\simeq -ip_{5\perp} \sqrt{\frac{p_3^+}{p_5^+}} (q_{2\perp}^* + p_{5\perp}^* \frac{p_4^-}{p_5^+}),\end{aligned}\tag{A.31}$$

while for the colour ordering $\{1, 4, 2, 3, 5, 6\}$ the relevant quantities are

$$\begin{aligned}\langle p_1 | \not{p}_4 + \not{p}_2 | p_3 \rangle &\simeq -i |q_{3\perp}| \sqrt{\frac{p_3^+}{p_6^+}} (p_{5\perp}^* + q_{3\perp}^*), \\ \langle p_2 | \not{p}_3 + \not{p}_5 | p_6 \rangle &\simeq iq_{3\perp}^* \sqrt{\frac{p_3^+}{p_6^+}} (p_{4\perp} + q_{3\perp}), \\ \langle p_5 | \not{p}_6 + \not{p}_1 | p_4 \rangle &\simeq -p_{5\perp} q_{2\perp}^* \sqrt{\frac{p_4^+}{p_5^+}} - p_{4\perp}^* q_{2\perp}' \sqrt{\frac{p_5^+}{p_4^+}}.\end{aligned}\tag{A.32}$$

B Lorentz invariant quantities in minimal coordinates

In this section we collect useful expressions for Lorentz-invariant quantities, in the central NMRK region of appendix A.3, written in terms of the minimal set of coordinates, $\{w, z, X\}$, introduced in eqs. (3.10) and (3.11). We use the shorthand notation for spinors,

$$\langle i j \rangle = \langle p_i p_j \rangle, \quad [i j] = [p_i p_j], \quad \langle i | k + l | j \rangle = \langle p_i | \not{p}_l + \not{p}_k | p_j \rangle.\tag{B.1}$$

Of particular importance to the central NMRK limit is the spinor product,

$$\langle 4 5 \rangle = -q_{1\perp} \frac{w + Xz}{w\sqrt{X}(z-1)},\tag{B.2}$$

which is treated exactly in this limit. The three-particle invariants of eq. (A.27) become

$$\begin{aligned}s_{123} &= |q_{1\perp}|^2 \frac{p_4^+ (1+X) |w-1|^2 |z|^2}{p_6^+ X |z-1|^2 |w|^2}, \\ s_{234} &= -|q_{1\perp}|^2 \frac{(1+X|z|^2)}{X |z-1|^2}, \\ s_{235} &= -|q_{1\perp}|^2 \frac{(|w+z-wz|^2 + X|z|^2)}{|z-1|^2 |w|^2}, \\ s_{345} &= |q_{1\perp}|^2 \frac{p_3^+ (|w|^2 + X|z|^2)}{p_4^+ |z-1|^2 |w|^2}.\end{aligned}\tag{B.3}$$

The lightcone-momentum dependence cancels when considering physical quantities such as amplitudes. The spinor strings of eq. (A.31) become

$$\begin{aligned}
\langle 1|2+3|4\rangle &= -iq_{1\perp}^* |q_{1\perp}| \sqrt{\frac{p_4^+}{p_6^+}} \frac{|w-1||z|}{|z-1||w|} \frac{(1+X\bar{z})}{X(\bar{z}-1)}, \\
\langle 3|4+5|6\rangle &= |q_{1\perp}|^2 \sqrt{\frac{p_3^+}{p_6^+}} \frac{\bar{z}(\bar{w}-1)(w-z)}{|w|^2|z-1|^2}, \\
\langle 5|6+1|2\rangle &= -i|q_{1\perp}|^2 \sqrt{\frac{p_3^+}{p_5^+}} \frac{(w+X|z|^2)}{wX|z-1|^2},
\end{aligned} \tag{B.4}$$

while the spinor strings of eq. (A.32) become

$$\begin{aligned}
\langle 1|4+2|3\rangle &= -iq_{1\perp}^* |q_{1\perp}| \sqrt{\frac{p_3^+}{p_6^+}} \frac{|w-1||z|}{|z-1||w|} \frac{\bar{z}}{(\bar{z}-1)}, \\
\langle 2|3+5|6\rangle &= -i|q_{1\perp}|^2 \sqrt{\frac{p_3^+}{p_6^+}} \frac{\bar{z}(\bar{w}-1)(w+z-wz)}{|w|^2|z-1|^2}, \\
\langle 5|6+1|4\rangle &= -|q_{1\perp}|^2 \frac{(w+z-wz+X|z|^2)}{w\sqrt{X}|z-1|^2}.
\end{aligned} \tag{B.5}$$

The spurious surfaces listed in eqs. (3.21) and (3.39) can be recognised from eqs. (B.4) and (B.5) respectively.

B.1 Cross ratios in the NMRK limit

In general kinematics, the finite, dual conformally invariant part of the six-gluon amplitude in planar $\mathcal{N}=4$ SYM can be written in terms of multiple polylogarithms with the following 9-letter alphabet,

$$\{u, v, w, 1-u, 1-v, 1-w, y_u, y_v, y_w\}. \tag{B.6}$$

The cross ratios u, v and w for the canonical ordering are given in eq. (3.19), although we appended a further A subscript to distinguish this from the other colour orderings that are relevant away from the planar limit. The remaining letters can be constructed from the cross ratios. For $x \in \{u, v, w\}$, y_x is defined by

$$y_x \equiv \frac{x - z_+}{x - z_-}, \tag{B.7}$$

with

$$z_{\pm} \equiv \frac{1}{2}(u+v+w-1 \pm \sqrt{\Delta}), \quad \Delta \equiv (1-u-v-w)^2 - 4uvw. \tag{B.8}$$

In this section we investigate these quantities for the two representative colour orderings used throughout this paper, namely σ_A and σ_B of eq. (4.10). The corresponding quantities for $\sigma_{A'}$ can be obtained using the relations given in eq. (3.27).

Permutation σ_A

The cross ratios for this colour ordering, u_A , v_A and w_A , are given in eq. (3.19). In NMRK they lie in the range $[0, 1]$. In the central NMRK region we list the other six letters,

$$\begin{aligned} 1 - u_A &= \frac{X|w - z|^2}{(1 + X)(|w|^2 + X|z|^2)}, \\ 1 - v_A &= \frac{|1 + Xz|^2}{(1 + X|z|^2)(1 + X)}, \\ 1 - w_A &= \frac{|w + X|z|^2|^2}{(|w|^2 + X|z|^2)(1 + X|z|^2)}, \end{aligned} \tag{B.9}$$

$$\begin{aligned} y_{u_A} &= \frac{(w + Xz)(1 + X\bar{z})(\bar{w} + X|z|^2)}{(\bar{w} + X\bar{z})(1 + Xz)(w + X|z|^2)}, \\ y_{v_A} &= \frac{(\bar{w} - \bar{z})(z - 1)(w + X|z|^2)}{(w - z)(\bar{z} - 1)(\bar{w} + X|z|^2)}, \\ y_{w_A} &= \frac{\bar{z}(\bar{w} - 1)(w - z)(1 + Xz)}{z(w - 1)(\bar{w} - \bar{z})(1 + X\bar{z})}. \end{aligned} \tag{B.10}$$

We note that eq. (B.10) are complex phases, which results from the quantity,

$$\sqrt{\Delta_A} = \pm \frac{X \left((|w|^2 - X|z|^2)(z - \bar{z}) - |z|^2(1 - X)(w - \bar{w}) + (1 - X|z|^2)(w\bar{z} - \bar{w}z) \right)}{(1 + X)(1 + X|z|^2)(|w|^2 + X|z|^2)}, \tag{B.11}$$

being purely imaginary. Thus its square is negative, $\Delta_A < 0$. One can get from any $2 \rightarrow 4$ scattering kinematics to NMRK by a dual conformal transformation [29, 30]. Since Δ_A is dual conformally invariant, this means that $\Delta_A < 0$ for any nonsingular $2 \rightarrow 4$ scattering configuration. We further note that the minimal variables, introduced in section 3.1, rationalise $\sqrt{\Delta_A}$.

Permutation σ_B

The cross ratios for this colour ordering, u_B , v_B and w_B , are given in eq. (3.33), which in NMRK lie in the range $[0, 1]$. In the central NMRK region we list the other six letters,

$$\begin{aligned} 1 - u_B &= \frac{|w + z - wz|^2}{(|w + z - wz|^2 + X|z|^2)}, \\ 1 - v_B &= \frac{X|z|^2}{(1 + X|z|^2)}, \end{aligned} \tag{B.12}$$

$$\begin{aligned} 1 - w_B &= \frac{|w + z - wz + X|z|^2|^2}{(1 + X|z|^2)(|w + z - wz|^2 + X|z|^2)}, \\ y_{u_B} &= \frac{w + z - wz + X|z|^2}{\bar{w} + \bar{z} - \bar{w}\bar{z} + X|z|^2}, \\ y_{v_B} &= \frac{(w + z - wz)(\bar{w} + \bar{z} - \bar{w}\bar{z} + X|z|^2)}{(\bar{w} + \bar{z} - \bar{w}\bar{z})(w + z - wz + X|z|^2)}, \\ y_{w_B} &= \frac{(w - 1)(z - 1)(\bar{w} + \bar{z} - \bar{w}\bar{z})}{(\bar{w} - 1)(\bar{z} - 1)(w + z - wz)}. \end{aligned} \tag{B.13}$$

Again we find that eq. (B.13) are phases which is a result of

$$\sqrt{\Delta_B} = \pm \frac{X|z|^2 \left((\bar{w} + \bar{z} - \bar{w}\bar{z}) - (w + z - wz) \right)}{(1 + X|z|^2)(|w + z - wz|^2 + X|z|^2)}, \quad (\text{B.14})$$

being purely imaginary. We note that as in eq. (B.11), the minimal variables rationalise this quantity.

C The power-suppressed helicity configurations

The tree-level six gluon amplitude (3.2) describes a total of 50 helicity configurations. However, the helicity-flip impact factors $C^{g(0)}(p_2^\pm, p_3^\pm)$ and $C^{g(0)}(p_1^\pm, p_6^\pm)$ are power suppressed in t_1/s and t_3/s , respectively. Of the 20 NMHV configurations described by eq. (3.2), 12 are power suppressed in this manner, owing to one or two helicity-flip impact factors, as depicted in figure 12. Similarly, of the 30 MHV configurations described by eq. (3.2), 22 are power suppressed due to one or two helicity-flip impact factors and are depicted in figure 13.

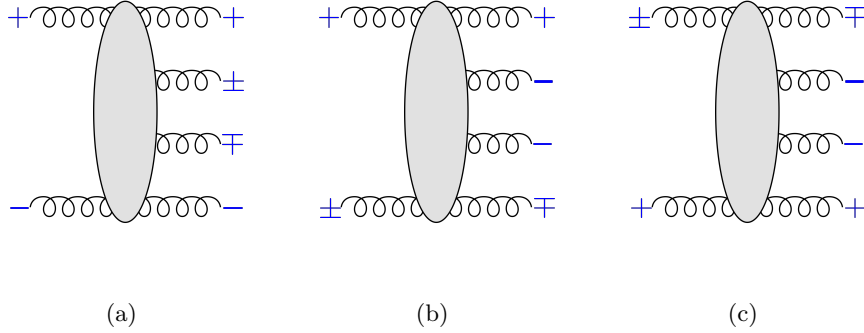


Figure 12. Six of the NMHV helicity configurations that are power suppressed in the central NMRK limit. The remaining six power-suppressed NMHV configurations can be obtained by flipping all helicities. The labelling of the gluons follows figure 11.

The remaining 16 helicity configurations of eq. (3.2) are all associated to amplitudes which do not have a helicity-flip impact factor, and these are the only configurations that we consider in this paper.

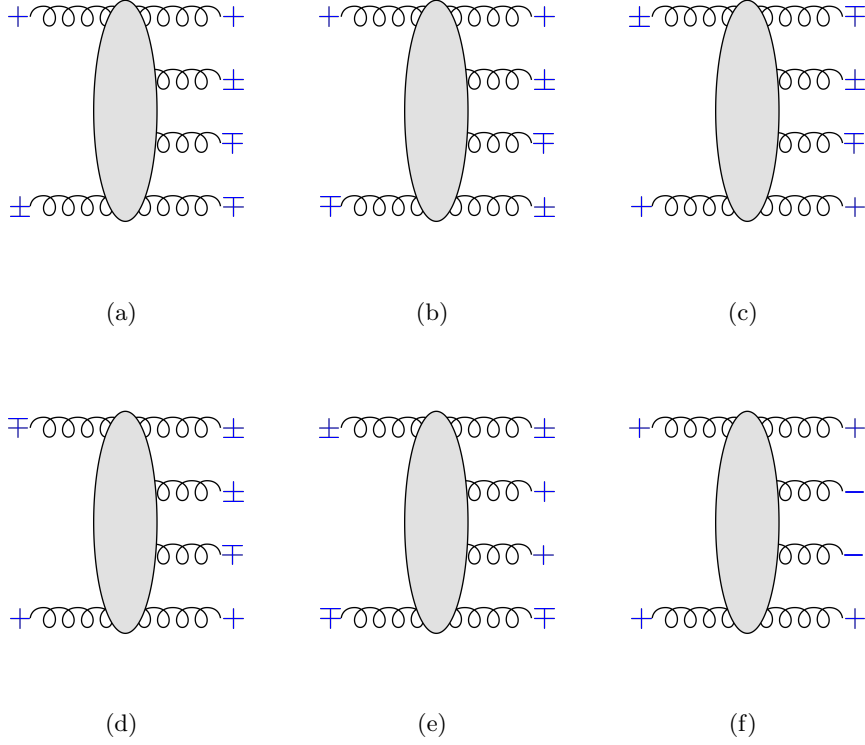


Figure 13. Eleven of the MHV helicity configurations that are power suppressed in the central NMRK limit. The remaining eleven power suppressed MHV configurations can be obtained by flipping all helicities. The labelling of the gluons follows figure 11.

D NMHV amplitudes in general kinematics

In this appendix we list the tree-level and one-loop six-gluon amplitudes in $\mathcal{N} = 4$ SYM which are used in the main text to obtain the two-gluon opposite-helicity CEV. For these amplitudes we use the shorthand notation for spinors listed in eq. (B.1).

D.1 Tree-level six-gluon NMHV amplitudes

Here we list a representation of the tree-level six-gluon NMHV colour-ordered amplitudes obtained through the BCFW on-shell recursion relations [90, 91],

$$M^{(0)}(p_1^\ominus, p_2^\ominus, p_3^\ominus, p_4^\oplus, p_5^\oplus, p_6^\oplus) = \frac{\langle 1|2+3|4\rangle^4}{D_2^*} + \frac{\langle 3|4+5|6\rangle^4}{D_3}, \quad (\text{D.1})$$

$$M^{(0)}(p_1^\ominus, p_2^\ominus, p_3^\oplus, p_4^\ominus, p_5^\oplus, p_6^\oplus) = \frac{\langle 4|1+2|3\rangle^4}{D_1^*} + \frac{\langle 2\,4\rangle^4[5\,6]^4}{D_2} + \frac{\langle 1\,2\rangle^4[3\,5]^4}{D_3^*}, \quad (\text{D.2})$$

$$M^{(0)}(p_1^\ominus, p_2^\oplus, p_3^\ominus, p_4^\oplus, p_5^\ominus, p_6^\oplus) = \frac{\langle 1\,3\rangle^4[4\,6]^4}{D_1} + \frac{[2\,4]^4\langle 1\,5\rangle^4}{D_2^*} + \frac{[2\,6]^4\langle 3\,5\rangle^4}{D_3}. \quad (\text{D.3})$$

The functions in the denominators are

$$D_1(1, 2, 3, 4, 5, 6) = -\langle 1\,2\rangle\langle 2\,3\rangle[4\,5][5\,6]s_{123}\langle 1|2+3|4\rangle\langle 3|4+5|6\rangle, \quad (\text{D.4})$$

and cyclic permutations thereof. We use the shorthand notation

$$D_i(\sigma) = D_i(\sigma_i, \sigma_{i+1}, \sigma_{i+2}, \sigma_{i+3}, \sigma_{i+4}, \sigma_{i+5}), \quad (\text{D.5})$$

where for the amplitudes in this section it is assumed – and left implicit – that the ordering σ is always taken to be that of the parent $M^{(0)}$, i.e. $\{1, 2, 3, 4, 5, 6\}$. $D_{i+1}(\sigma)$ is obtained from $D_i(\sigma)$ by replacing $\sigma_i \rightarrow \sigma_{i+1}$ in the latter, with all indices taken modulo 6. However, there are only three independent cyclic orderings due to the relation $D_{i+3}(\sigma) = D_i^*(\sigma)$.

We will see that the individual rational terms that occur in eqs. (D.1–D.3) will appear also in the one-loop amplitudes listed in the following subsection. The coefficient of the ϵ^{-2} pole of these one-loop amplitudes must be proportional to the tree-level amplitude, thus, using the one-loop amplitudes, we obtain an alternative set of representations for the tree-level amplitudes:

$$M^{(0)}(p_1^\ominus, p_2^\ominus, p_3^\ominus, p_4^\oplus, p_5^\oplus, p_6^\oplus) = \frac{(s_{123})^4}{D_1^*} + \frac{\langle 23 \rangle^4 [56]^4}{D_2} + \frac{\langle 12 \rangle^4 [45]^4}{D_3^*}, \quad (\text{D.6})$$

$$M^{(0)}(p_1^\ominus, p_2^\ominus, p_3^\oplus, p_4^\ominus, p_5^\oplus, p_6^\oplus) = \frac{\langle 12 \rangle^4 [56]^4}{D_1} + \frac{\langle 1|2+4|3|^4}{D_2^*} + \frac{\langle 4|1+2|6|^4}{D_3}, \quad (\text{D.7})$$

$$M^{(0)}(p_1^\ominus, p_2^\oplus, p_3^\ominus, p_4^\oplus, p_5^\ominus, p_6^\oplus) = \frac{\langle 5|1+3|2|^4}{D_1^*} + \frac{\langle 3|2+4|6|^4}{D_2} + \frac{\langle 1|2+6|4|^4}{D_3^*}. \quad (\text{D.8})$$

The representations eqs. (D.1–D.3) are complementary to the representations eqs. (D.6–D.8) in the sense that where the NMRK limit of the rational terms of the former give rise directly to R_{xy}^I (defined in eqs. (3.23) and (3.35)), the rational terms of the latter give rise to $R_{\bar{x}\bar{y}}^I$ (defined in eqs. (3.25) and (3.37)), and vice versa.

D.2 One-loop six-gluon NMHV amplitudes in $\mathcal{N} = 4$ SYM

We will need to study the NMRK limit of the colour-ordered amplitudes derived in ref. [74], namely:

$$\begin{aligned} \frac{(4\pi)^2}{\kappa_\Gamma} M_{\mathcal{N}=4}^{(1)}(p_1^\ominus, p_2^\ominus, p_3^\ominus, p_4^\oplus, p_5^\oplus, p_6^\oplus) &= \left(\frac{(s_{123})^4}{D_1^*} \right) W_1 \\ &+ \left(\frac{\langle 1|2+3|4|^4}{D_2^*} + \frac{\langle 23 \rangle^4 [56]^4}{D_2} \right) W_2 \\ &+ \left(\frac{\langle 3|4+5|6|^4}{D_3} + \frac{\langle 12 \rangle^4 [45]^4}{D_3^*} \right) W_3, \end{aligned} \quad (\text{D.9})$$

$$\begin{aligned} \frac{(4\pi)^2}{\kappa_\Gamma} M_{\mathcal{N}=4}^{(1)}(p_1^\ominus, p_2^\ominus, p_3^\oplus, p_4^\ominus, p_5^\oplus, p_6^\oplus) &= \left(\frac{\langle 4|1+2|3|^4}{D_1^*} + \frac{\langle 12 \rangle^4 [56]^4}{D_1} \right) W_1 \\ &+ \left(\frac{\langle 1|2+4|3|^4}{D_2^*} + \frac{\langle 24 \rangle^4 [56]^4}{D_2} \right) W_2 \\ &+ \left(\frac{\langle 4|1+2|6|^4}{D_3} + \frac{\langle 12 \rangle^4 [35]^4}{D_3^*} \right) W_3, \end{aligned} \quad (\text{D.10})$$

$$\begin{aligned}
\frac{(4\pi)^2}{\kappa_\Gamma} M_{\mathcal{N}=4}^{(1)}(p_1^\ominus, p_2^\oplus, p_3^\ominus, p_4^\oplus, p_5^\ominus, p_6^\oplus) &= \left(\frac{\langle 13 \rangle^4 [46]^4}{D_1} + \frac{\langle 5[1+3]2 \rangle^4}{D_1^*} \right) W_1 \\
&+ \left(\frac{[24]^4 \langle 15 \rangle^4}{D_2^*} + \frac{\langle 3[2+4]6 \rangle^4}{D_2} \right) W_2 \\
&+ \left(\frac{[26]^4 \langle 35 \rangle^4}{D_3} + \frac{\langle 1[2+6]4 \rangle^4}{D_3^*} \right) W_3.
\end{aligned} \tag{D.11}$$

The transcendental functions are given by

$$\begin{aligned}
W_i(\sigma) &= -\frac{1}{2\epsilon^2} \sum_{j=1}^6 \left(\frac{\mu^2}{-t_j^{[2]}} \right)^\epsilon - \log \left(\frac{-t_i^{[3]}}{-t_i^{[2]}} \right) \log \left(\frac{-t_i^{[3]}}{-t_{i+1}^{[2]}} \right) - \log \left(\frac{-t_i^{[3]}}{-t_{i+3}^{[2]}} \right) \log \left(\frac{-t_i^{[3]}}{-t_{i+4}^{[2]}} \right) \\
&+ \log \left(\frac{-t_i^{[3]}}{-t_{i+2}^{[2]}} \right) \log \left(\frac{-t_i^{[3]}}{-t_{i+5}^{[2]}} \right) + \frac{1}{2} \log \left(\frac{-t_i^{[2]}}{-t_{i+3}^{[2]}} \right) \log \left(\frac{-t_{i+1}^{[2]}}{-t_{i+4}^{[2]}} \right) \\
&+ \frac{1}{2} \log \left(\frac{-t_{i+5}^{[2]}}{-t_i^{[2]}} \right) \log \left(\frac{-t_{i+1}^{[2]}}{-t_{i+2}^{[2]}} \right) + \frac{1}{2} \log \left(\frac{-t_{i+2}^{[2]}}{-t_{i+3}^{[2]}} \right) \log \left(\frac{-t_{i+4}^{[2]}}{-t_{i+5}^{[2]}} \right) + \frac{\pi^2}{3},
\end{aligned} \tag{D.12}$$

where we use the same notation for the arguments and cyclic permutations as for the function D_i , discussed below eq. (D.4). While in eqs. (D.9–D.11) the ordering argument is left implicit, it is useful to display the ordering explicitly when the transcendental functions of different colour orderings appear in the same expression, e.g. in eq. (4.60). We note that the function W_i has cyclic symmetry in the form $W_{i+3} = W_i$ so there are only three independent cyclic permutations. In eq. (D.12) we use the compact notation for Mandelstam invariants introduced in eq. (4.19), and we use the prescription of eq. (4.20). We emphasise that the function W_i does not depend on the individual helicities of the particles.

E Additional forms of the opposite-helicity central-emission vertex

In ref. [60] an alternative form of the opposite-helicity two-gluon central-emission vertex was found by using the CSW rules [92],

$$\begin{aligned}
A^{gg(0)}(q_1, p_4^\oplus, p_5^\ominus, q_3) \Big|_4 &= \sqrt{\frac{x_4}{x_5}} \frac{|q_{1\perp}|^2 x_4 p_{5\perp}^3}{\langle 45 \rangle (x_5 |p_{4\perp}|^2 + x_4 |p_{5\perp}|^2)} p_{4\perp} (p_{4\perp} + p_{5\perp}) \\
&+ \sqrt{\frac{x_4}{x_5}} \frac{q_{1\perp}^* x_4 (q_{3\perp} + p_{5\perp})^3}{\left(q_{3\perp} \sqrt{\frac{x_4}{x_5}} - \langle 45 \rangle \right) (x_5 |p_{4\perp}|^2 + x_4 |q_{2\perp}|^2)} p_{4\perp} \\
&+ \frac{q_{1\perp} q_{3\perp} \sqrt{x_4 x_5 x_5}}{\langle 45 \rangle (x_5 p_{4\perp} - x_4 q_{2\perp})} - \sqrt{\frac{x_4}{x_5}} \frac{q_{1\perp}^* q_{3\perp} x_4}{(p_{4\perp} + p_{5\perp}) [45]}.
\end{aligned} \tag{E.1}$$

In the minimal variables of section 3.1 this is

$$\begin{aligned}
A^{gg(0)}(q_1, p_4^\oplus, p_5^\ominus, q_3) \Big|_4 &= -\frac{\bar{w} z^3 |1-z|^2 X^2}{(w-z)(w+Xz)(|w|^2 + X|z|^2)} + \frac{X^2 z^3 (1-\bar{z})}{(1+Xz)(1+X|z|^2)} \\
&+ \frac{(1-w)(1-z)zX}{(1+X)(1+Xz)(w+Xz)} + \frac{(1-w)(1-\bar{z})\bar{w}zX^2}{(1+X)(w-z)(\bar{w}+X\bar{z})},
\end{aligned} \tag{E.2}$$

which has the expected physical singularities of eqs. (3.14) and (3.15), and also spurious poles at $P_{u_A} = 0$ and $\bar{P}_{v_A} = 0$.

We also list a compact representation we have found

$$A^{gg(0)}(q_1, p_4^\oplus, p_5^\ominus, q_3) \Big|_5 = \frac{Xz(\bar{w}-1)(Xz+w+z-1)}{(X+1)(w+Xz)} - \frac{X\bar{w}(w-1)(\bar{w}+X)z}{(\bar{w}+X\bar{z})(w-z)(X+1)} \\ + \frac{X\bar{w}(z-1)z^2(Xz+|w|^2)}{(|w|^2+X|z|^2)(w-z)(w+Xz)} + \frac{Xz^2}{X|z|^2+1}, \quad (\text{E.3})$$

which has only a single spurious pole at $P_{u_A} = 0$. We finally list a representation which is compact when expressed in terms of light-cone coordinates, which was obtained by partial fractioning the third term of eq. (3.24),

$$A^{gg(0)}(q_1, p_4^\oplus, p_5^\ominus, q_3) \Big|_6 \\ = x_5 - y_5 \frac{|q_{1\perp}|^2}{p_{4\perp}p_{5\perp}^*} - \frac{q_{1\perp}^*(q_{1\perp} - p_{4\perp})^2}{p_{4\perp}s_{234}} - \frac{x_5p_{4\perp}^*(q_{1\perp} - p_{4\perp})}{x_4s_{234}} \\ + \frac{q_{1\perp}^*}{p_{4\perp}\langle 45 \rangle^*} x_4 \sqrt{\frac{x_4}{x_5}} (y_4 q_{1\perp} - p_{4\perp}) + \frac{q_{1\perp}}{p_{5\perp}^*\langle 45 \rangle} x_5 \sqrt{\frac{x_5}{x_4}} (y_5 q_{1\perp}^* - p_{5\perp}^*). \quad (\text{E.4})$$

E.1 BCFW representation for the ordering $\sigma_{A'}$

In this appendix we present the BCFW representations of the opposite-helicity vertex for the ordering $\sigma_{A'}$. These expressions can be obtained from the results for the ordering σ_A in section 3.3 by applying the rules listed in eq. (3.27).

For the $\sigma_{A'} = \{1, 2, 3, 5, 4, 6\}$ ordering we list the NMRK limits of the cross ratios,

$$u_{A'} = u_A, \\ v_{A'} = \frac{s_{23}s_{46}}{s_{235}s_{123}} \xrightarrow{\text{NMRK}} \frac{|w|^2|z-1|^2X}{(1+X)(|w+z-wz|^2+X|z|^2)}, \quad (\text{E.5}) \\ w_{A'} = \frac{s_{35}s_{61}}{s_{345}s_{235}} \xrightarrow{\text{NMRK}} \frac{|z|^4|w-1|^2X}{(|w|^2+X|z|^2)(|w+z-wz|^2+X|z|^2)}.$$

From the BCFW representations of the NMHV amplitudes of eqs. (D.1, D.3, D.7) we obtain the opposite-helicity central-emission vertex,

$$A^{gg(0)}(q_1, p_5^\ominus, p_4^\oplus, q_3) = R_{uv}^{A'} + R_{vw}^{A'} + R_{wu}^{A'}, \quad (\text{E.6})$$

with

$$R_{uv}^{A'} = \frac{|w-1|^2\bar{w}X^2|z|^2(\bar{z}-1)}{(\bar{w}+X\bar{z})(X+1)(w-z)(\bar{w}+\bar{z}-\bar{w}\bar{z}+X\bar{z})}, \\ R_{vw}^{A'} = \frac{wz(w-1)(z-1)(\bar{w}+\bar{z}-\bar{w}\bar{z})^4}{\bar{z}(|w+z-wz|^2+X|z|^2)(\bar{w}+\bar{z}-\bar{w}\bar{z}+X\bar{z})(w(\bar{w}+\bar{z}-\bar{w}\bar{z})+X|z|^2)}, \quad (\text{E.7}) \\ R_{wu}^{A'} = -\frac{(\bar{w}-1)|w|^2X^2|z-1|^2z^2|z|^2}{(w+Xz)(|w|^2+X|z|^2)(w(\bar{w}+\bar{z}-\bar{w}\bar{z})+X|z|^2)(w-z)}.$$

Instead starting from the BCFW representations of eqs. (D.2, D.6, D.8), we obtain the representation,

$$A^{gg(0)}(q_1, p_5^\ominus, p_4^\oplus, q_3) = R_{\bar{u}\bar{v}}^{A'} + R_{\bar{v}\bar{w}}^{A'} + R_{\bar{w}\bar{u}}^{A'}, \quad (\text{E.8})$$

with

$$\begin{aligned} R_{\bar{u}\bar{v}}^{A'} &= \frac{|w-1|^2 w(z-1)|z|^2}{(X+1)(\bar{w}-\bar{z})(w+Xz)(w+z-wz+Xz)}, \\ R_{\bar{v}\bar{w}}^{A'} &= \frac{\bar{w}(\bar{w}-1)(\bar{z}-1)z^2|z|^2 X^2}{(|w+z-wz|^2 + X|z|^2)(w+z-wz+Xz)(\bar{w}(w+z-wz) + X|z|^2)}, \\ R_{\bar{w}\bar{u}}^{A'} &= -\frac{(w-1)|w|^2 \bar{w}^4 |z-1|^2 z}{\bar{z}(|w|^2 + X|z|^2)(\bar{w}+X\bar{z})(\bar{w}(w+z-wz) + X|z|^2)(\bar{w}-\bar{z})}. \end{aligned} \quad (\text{E.9})$$

The physical-singularity surfaces of this ordering are

$$\begin{aligned} \langle 45 \rangle = 0 &\leftrightarrow p_{4\perp} \sqrt{\frac{p_4^+}{p_5^+}} - p_{5\perp} \sqrt{\frac{p_5^+}{p_4^+}} = 0 \leftrightarrow w + Xz = 0, \\ s_{123} = 0 &\leftrightarrow p_4^+ + p_5^+ = 0 \leftrightarrow 1 + X = 0, \\ s_{235} = 0 &\leftrightarrow |q'_{2\perp}|^2 + p_4^+ p_5^- = 0 \leftrightarrow |w+z-wz|^2 + X|z|^2 = 0, \\ s_{354} = 0 &\leftrightarrow p_4^- + p_5^- = 0 \leftrightarrow |w|^2 + X|z|^2 = 0, \end{aligned} \quad (\text{E.10})$$

while the unphysical-singularity surfaces are

$$\begin{aligned} \langle 1|2+3|5 \rangle = 0 &\leftrightarrow P_v^{A'} = 0 \leftrightarrow q_{2\perp}^* - p_{5\perp}^* \frac{p_4^+}{p_5^+} = 0 \leftrightarrow \bar{w} + \bar{z} - \bar{w}\bar{z} + X\bar{z} = 0, \\ \langle 3|5+4|6 \rangle = 0 &\leftrightarrow P_u^{A'} = 0 \leftrightarrow p_{4\perp} + p_{5\perp} = 0 \leftrightarrow w - z = 0, \\ \langle 4|6+1|2 \rangle = 0 &\leftrightarrow P_w^{A'} = 0 \leftrightarrow q_{2\perp}^* + p_{5\perp}^* \frac{p_{5\perp} p_4^+}{p_{4\perp} p_5^+} = 0 \leftrightarrow w(\bar{w} + \bar{z} - \bar{w}\bar{z}) + X|z|^2 = 0. \end{aligned} \quad (\text{E.11})$$

We note that

$$R_{xy}^A \xleftrightarrow{p_4 \leftrightarrow p_5} \left(R_{\bar{x}\bar{y}}^{A'} \right)^*. \quad (\text{E.12})$$

F Absorptive part of the one-loop six-gluon amplitude in NMRK

In eq. (4.12) we decomposed the $\mathcal{N} = 4$ SYM one-loop six-gluon amplitude in NMRK into a basis of symmetric (+) or antisymmetric (−) representations exchanged in the t_1 and t_3 channels. For one-loop amplitudes where an adjoint representation is circulating in the loop, the (−, −) component is given by eq. (4.13). We list here analogous expressions for

the remaining components:

$$\begin{aligned}
\mathcal{M}^{(1)(+,+)} &= \frac{g_S^6}{4} \\
&\times \left\{ \text{tr} \left(\{F^{a_2}, F^{a_3}\} F^{a_4} F^{a_5} \{F^{a_6}, F^{a_1}\} \right) \left(M^{(1)}(\sigma_A) + M^{(1)}(\overset{\leftrightarrow}{\sigma}_A) + M^{(1)}(\underset{\leftrightarrow}{\sigma}_A) + M^{(1)}(\overset{\leftrightarrow}{\sigma}_{A'}) \right) \right. \\
&+ \text{tr} \left(\{F^{a_2}, F^{a_3}\} F^{a_5} F^{a_4} \{F^{a_6}, F^{a_1}\} \right) \left(M^{(1)}(\sigma_{A'}) + M^{(1)}(\overset{\leftrightarrow}{\sigma}_{A'}) + M^{(1)}(\underset{\leftrightarrow}{\sigma}_{A'}) + M^{(1)}(\overset{\leftrightarrow}{\sigma}_B) \right) \\
&\left. + \text{tr} \left(\{F^{a_2}, F^{a_3}\} F^{a_4} \{F^{a_6}, F^{a_1}\} F^{a_5} \right) \left(M^{(1)}(\sigma_B) + M^{(1)}(\overset{\leftrightarrow}{\sigma}_B) + M^{(1)}(\underset{\leftrightarrow}{\sigma}_B) + M^{(1)}(\overset{\leftrightarrow}{\sigma}_{B'}) \right) \right\}. \tag{F.1}
\end{aligned}$$

$$\begin{aligned}
\mathcal{M}^{(1)(+,-)} &= \frac{g_S^6}{4} \\
&\times \left\{ \text{tr} \left(\{F^{a_2}, F^{a_3}\} F^{a_4} F^{a_5} [F^{a_6}, F^{a_1}] \right) \left(M^{(1)}(\sigma_A) + M^{(1)}(\overset{\leftrightarrow}{\sigma}_A) - M^{(1)}(\underset{\leftrightarrow}{\sigma}_A) - M^{(1)}(\overset{\leftrightarrow}{\sigma}_{A'}) \right) \right. \\
&+ \text{tr} \left(\{F^{a_2}, F^{a_3}\} F^{a_5} F^{a_4} [F^{a_6}, F^{a_1}] \right) \left(M^{(1)}(\sigma_{A'}) + M^{(1)}(\overset{\leftrightarrow}{\sigma}_{A'}) - M^{(1)}(\underset{\leftrightarrow}{\sigma}_{A'}) - M^{(1)}(\overset{\leftrightarrow}{\sigma}_B) \right) \\
&\left. + \text{tr} \left(\{F^{a_2}, F^{a_3}\} F^{a_4} [F^{a_6}, F^{a_1}] F^{a_5} \right) \left(M^{(1)}(\sigma_B) + M^{(1)}(\overset{\leftrightarrow}{\sigma}_B) - M^{(1)}(\underset{\leftrightarrow}{\sigma}_B) - M^{(1)}(\overset{\leftrightarrow}{\sigma}_{B'}) \right) \right\}. \tag{F.2}
\end{aligned}$$

$$\begin{aligned}
\mathcal{M}^{(1)(-,+)} &= \frac{g_S^6}{4} \\
&\times \left\{ \text{tr} \left([F^{a_2}, F^{a_3}] F^{a_4} F^{a_5} \{F^{a_6}, F^{a_1}\} \right) \left(M^{(1)}(\sigma_A) - M^{(1)}(\overset{\leftrightarrow}{\sigma}_A) + M^{(1)}(\underset{\leftrightarrow}{\sigma}_A) - M^{(1)}(\overset{\leftrightarrow}{\sigma}_{A'}) \right) \right. \\
&+ \text{tr} \left([F^{a_2}, F^{a_3}] F^{a_5} F^{a_4} \{F^{a_6}, F^{a_1}\} \right) \left(M^{(1)}(\sigma_{A'}) - M^{(1)}(\overset{\leftrightarrow}{\sigma}_{A'}) + M^{(1)}(\underset{\leftrightarrow}{\sigma}_{A'}) - M^{(1)}(\overset{\leftrightarrow}{\sigma}_B) \right) \\
&\left. + \text{tr} \left([F^{a_2}, F^{a_3}] F^{a_4} \{F^{a_6}, F^{a_1}\} F^{a_5} \right) \left(M^{(1)}(\sigma_B) - M^{(1)}(\overset{\leftrightarrow}{\sigma}_B) + M^{(1)}(\underset{\leftrightarrow}{\sigma}_B) - M^{(1)}(\overset{\leftrightarrow}{\sigma}_{B'}) \right) \right\}. \tag{F.3}
\end{aligned}$$

In section 4 we found that in the central NMRK, the dispersive amplitude received a contribution from the $(-, -)$ component alone. The same is not true for the absorptive part of the amplitude, which is the object of study of this appendix. To this end we list the NMRK limit of the imaginary parts of the transcendental functions eq. (4.18) and eq. (D.12), for the 12 colour orderings that appear in eqs. (F.1)–(F.3). We begin by giving

the results for the σ_A orderings:

$$\begin{aligned}
\text{Im}\left[V_6(\sigma_A)\right] &= 2\text{Im}\left[W_2(\sigma_A)\right] \xrightarrow{\text{NMRK}} -\frac{4\pi}{\epsilon} + \pi \log\left(\frac{t_1 p_4^- s_{45} p_5^+ t_3}{(\mu^2)^4}\right), \\
\text{Im}\left[V_6(\overset{\leftrightarrow}{\sigma}_A)\right] &= 2\text{Im}\left[W_2(\overset{\leftrightarrow}{\sigma}_A)\right] \xrightarrow{\text{NMRK}} -\frac{2\pi}{\epsilon} + \pi \log\left(\frac{p_4^- s_{45} p_5^+ t_3}{t_1 (\mu^2)^2}\right), \\
\text{Im}\left[V_6(\underset{\leftrightarrow}{\sigma}_A)\right] &= 2\text{Im}\left[W_2(\underset{\leftrightarrow}{\sigma}_A)\right] \xrightarrow{\text{NMRK}} -\frac{2\pi}{\epsilon} + \pi \log\left(\frac{t_1 p_4^- s_{45} p_5^+}{t_3 (\mu^2)^2}\right), \\
&\quad \text{Im}\left[V_6(\overset{\leftrightarrow}{\underset{\leftrightarrow}{\sigma}}_A)\right] \xrightarrow{\text{NMRK}} -\frac{2\pi}{\epsilon} + \pi \log\left(\frac{t_1 p_4^- p_5^+ t_3}{s_{45} (\mu^2)^2}\right) + 2\pi \log\left(\frac{u_A}{1-u_A}\right), \\
&\quad 2\text{Im}\left[W_2(\overset{\leftrightarrow}{\underset{\leftrightarrow}{\sigma}}_A)\right] \xrightarrow{\text{NMRK}} -\frac{2\pi}{\epsilon} + \pi \log\left(\frac{t_1 p_4^- p_5^+ t_3}{s_{45} (\mu^2)^2}\right) - 2\pi \log\left(\frac{v_A w_A}{u_A}\right).
\end{aligned} \tag{F.4}$$

We provide the results for W_1 and W_3 as differences from those for W_2 . Interestingly, $\overset{\leftrightarrow}{\underset{\leftrightarrow}{\sigma}}_A$ is the only ordering which leads to differing imaginary parts for different cyclic permutations of W_i :

$$\begin{aligned}
\text{Im}\left[W_1(\sigma_A) - W_2(\sigma_A)\right] &= 0, & \text{Im}\left[W_3(\sigma_A) - W_2(\sigma_A)\right] &= 0, \\
\text{Im}\left[W_1(\overset{\leftrightarrow}{\sigma}_A) - W_2(\overset{\leftrightarrow}{\sigma}_A)\right] &= 0, & \text{Im}\left[W_3(\overset{\leftrightarrow}{\sigma}_A) - W_2(\overset{\leftrightarrow}{\sigma}_A)\right] &= 0, \\
\text{Im}\left[W_1(\underset{\leftrightarrow}{\sigma}_A) - W_2(\underset{\leftrightarrow}{\sigma}_A)\right] &= 0, & \text{Im}\left[W_3(\underset{\leftrightarrow}{\sigma}_A) - W_2(\underset{\leftrightarrow}{\sigma}_A)\right] &= 0, \\
\text{Im}\left[W_1(\overset{\leftrightarrow}{\underset{\leftrightarrow}{\sigma}}_A) - W_2(\overset{\leftrightarrow}{\underset{\leftrightarrow}{\sigma}}_A)\right] &= 2\pi \log(v_A), & \text{Im}\left[W_3(\overset{\leftrightarrow}{\underset{\leftrightarrow}{\sigma}}_A) - W_2(\overset{\leftrightarrow}{\underset{\leftrightarrow}{\sigma}}_A)\right] &= 2\pi \log(w_A).
\end{aligned} \tag{F.5}$$

We further note that only for the ordering $\overset{\leftrightarrow}{\underset{\leftrightarrow}{\sigma}}_A$ does the analytic continuation of the dilogarithms in eq. (4.18) to our physical region produce an imaginary part. For this colour ordering, the cross ratio

$$\frac{s_{63}s_{45}}{s_{632}s_{245}},$$

which is related to u_A by interchange of $p_1 \leftrightarrow p_6$ and $p_2 \leftrightarrow p_3$, has two positive invariants in the numerator and two negative invariants in the denominator. The analytic continuation of the dilogarithm that depends on this cross ratio leads to factor of $i\pi \log(1-u_A)$ which is related to the factorisation breaking term discovered in ref. [16]. The interpretation of this quantity is different in our paper; ref. [16] considers the single planar colour ordering of the amplitude, analytically continued to the physical region where $s_{12}, s_{45} > 0$, $s_{23}, s_{34}, s_{56}, s_{61}, s_{234}, s_{345} < 0$, while we consider a certain colour-ordered amplitude in the physical region where $s_{12}, s_{34}, s_{45}, s_{56}, s_{345} > 0$, $s_{23}, s_{61}, s_{234} < 0$. However, the consequence is the same, namely that this term is not compatible with Regge-pole factorisation of the amplitude, which only applies to its dispersive part. Instead it contributes to a Regge cut.

Expressions for the $\sigma_{A'}$ orderings are related by an interchange of $p_4 \leftrightarrow p_5$.

For the σ_B orderings we obtain

$$\begin{aligned}
\text{Im}\left[V_6(\sigma_B)\right] &= 2\text{Im}\left[W_1(\sigma_B)\right] \xrightarrow{\text{NMRK}} -\frac{2\pi}{\epsilon} + \pi \log\left(\frac{t_1 p_5^+ p_5^- t_3}{p_4^+ p_4^- (\mu^2)^2}\right), \\
\text{Im}\left[V_6(\overset{\leftrightarrow}{\sigma}_B)\right] &\xrightarrow{\text{NMRK}} -\frac{2\pi}{\epsilon} + \pi \log\left(\frac{t_1 p_4^+ p_5^- t_3}{p_4^- p_5^+ (\mu^2)^2}\right) + 2\pi \log\left(\frac{v_B}{1-v_B}\right), \\
2\text{Im}\left[W_1(\overset{\leftrightarrow}{\sigma}_B)\right] &\xrightarrow{\text{NMRK}} -\frac{2\pi}{\epsilon} + \pi \log\left(\frac{t_1 p_4^+ p_5^- t_3}{p_4^- p_5^+ (\mu^2)^2}\right) + 2\pi \log\left(\frac{u_B v_B}{w_B}\right), \\
\text{Im}\left[V_6(\underset{\leftrightarrow}{\sigma}_B)\right] &\xrightarrow{\text{NMRK}} -\frac{2\pi}{\epsilon} + \pi \log\left(\frac{t_1 p_4^- p_5^+ t_3}{p_4^+ p_5^- (\mu^2)^2}\right) + 2\pi \log\left(\frac{u_B}{1-u_B}\right), \\
2\text{Im}\left[W_1(\underset{\leftrightarrow}{\sigma}_B)\right] &\xrightarrow{\text{NMRK}} -\frac{2\pi}{\epsilon} + \pi \log\left(\frac{t_1 p_4^- p_5^+ t_3}{p_4^+ p_5^- (\mu^2)^2}\right) + 2\pi \log\left(\frac{u_B v_B}{w_B}\right), \\
\text{Im}\left[V_6(\overset{\leftrightarrow}{\underset{\leftrightarrow}{\sigma}}_B)\right] &= 2\text{Im}\left[W_1(\overset{\leftrightarrow}{\underset{\leftrightarrow}{\sigma}}_B)\right] \xrightarrow{\text{NMRK}} -\frac{2\pi}{\epsilon} + \pi \log\left(\frac{t_1 p_4^+ p_4^- t_3}{p_5^+ p_5^- (\mu^2)^2}\right).
\end{aligned} \tag{F.6}$$

Again the orderings that lead to imaginary contributions from the dilogarithms (namely $\overset{\leftrightarrow}{\sigma}_B$, σ_B) are the same orderings for which the imaginary parts of the distinct cyclic permutations of W_i differ:

$$\begin{aligned}
\text{Im}\left[W_2(\sigma_B) - W_1(\sigma_B)\right] &= 0, & \text{Im}\left[W_3(\sigma_B) - W_1(\sigma_B)\right] &= 0, \\
\text{Im}\left[W_2(\overset{\leftrightarrow}{\sigma}_B) - W_1(\overset{\leftrightarrow}{\sigma}_B)\right] &= 2\pi \log\left(\frac{w_B}{u_B}\right), & \text{Im}\left[W_3(\overset{\leftrightarrow}{\sigma}_B) - W_1(\overset{\leftrightarrow}{\sigma}_B)\right] &= -2\pi \log(u_B), \\
\text{Im}\left[W_2(\underset{\leftrightarrow}{\sigma}_B) - W_1(\underset{\leftrightarrow}{\sigma}_B)\right] &= -2\pi \log(v_B), & \text{Im}\left[W_3(\underset{\leftrightarrow}{\sigma}_B) - W_1(\underset{\leftrightarrow}{\sigma}_B)\right] &= 2\pi \log\left(\frac{w_B}{v_B}\right), \\
\text{Im}\left[W_2(\overset{\leftrightarrow}{\underset{\leftrightarrow}{\sigma}}_B) - W_1(\overset{\leftrightarrow}{\underset{\leftrightarrow}{\sigma}}_B)\right] &= 0, & \text{Im}\left[W_3(\overset{\leftrightarrow}{\underset{\leftrightarrow}{\sigma}}_B) - W_1(\overset{\leftrightarrow}{\underset{\leftrightarrow}{\sigma}}_B)\right] &= 0.
\end{aligned} \tag{F.7}$$

Absorptive part of the same-helicity amplitude

From the above lists of imaginary parts we can now assemble the absorptive parts of the colour-dressed amplitude for the case where $\nu_4 = \nu_5 = \oplus$:

$$\begin{aligned}
&\text{Absorp}\left[\mathcal{M}_{\mathcal{N}=4}^{(1)(-,-)}(p_4^\oplus, p_5^\oplus)\right] \xrightarrow{\text{NMRK}} g_s^6 \frac{\kappa_\Gamma}{(4\pi)^2} s_{12} F^{a_3 a_2 c_1} C^{g(0)}(p_2^{\nu_2}, p_3^{-\nu_2}) \frac{1}{t_1} \\
&\times \frac{\pi}{2} \left\{ \text{tr}(F^{c_1} F^{a_4} F^{a_5} F^{c_3}) A^{gg(0)}(q_1, p_4^\oplus, p_5^\oplus, q_3) \left(\frac{-5}{\epsilon} + \log\left(\frac{t_1 s_{45} (p_4^- p_5^+)^2 t_3}{(\mu^2)^5} \frac{u_A}{1-u_A}\right) \right) \right. \\
&\quad + \text{tr}(F^{c_1} F^{a_5} F^{a_4} F^{c_3}) A^{gg(0)}(q_1, p_5^\oplus, p_4^\oplus, q_3) \left(\frac{-5}{\epsilon} + \log\left(\frac{t_1 s_{45} (p_4^+ p_5^-)^2 t_3}{(\mu^2)^5} \frac{u_{A'}}{1-u_{A'}}\right) \right) \\
&\quad \left. + \text{tr}(F^{c_1} F^{a_5} F^{c_3} F^{a_4}) B^{gg(0)}(q_1, p_4^\oplus, p_5^\oplus, q_3) \left(\frac{-4}{\epsilon} + \log\left(\frac{t_1^2 t_3^2}{(\mu^2)^4} \frac{v_B}{1-v_B} \frac{u_B}{1-u_B}\right) \right) \right\} \\
&\times \frac{1}{t_3} F^{a_6 a_1 c_3} C^{g(0)}(p_1^{\nu_1}, p_6^{-\nu_1}),
\end{aligned} \tag{F.8}$$

$$\begin{aligned}
& \text{Absorp} \left[\mathcal{M}_{\mathcal{N}=4}^{(1)(+,-)}(p_4^\oplus, p_5^\oplus) \right] \xrightarrow{\text{NMRK}} \frac{\pi}{2} g_s^6 \frac{\kappa_\Gamma}{(4\pi)^2} s_{12} C^{g(0)}(p_2^{\nu_2}, p_3^{-\nu_2}) \frac{1}{t_1} \frac{1}{t_3} C^{g(0)}(p_1^{\nu_1}, p_6^{-\nu_1}) \\
& \times \left\{ \text{tr} \left(\{F^{a_2}, F^{a_3}\} F^{a_4} F^{a_5} [F^{a_6}, F^{a_1}] \right) A^{gg(0)}(q_1, p_4^\oplus, p_5^\oplus, q_3) \left(\frac{-1}{\epsilon} + \log \left(\frac{t_3 s_{45}}{t_1 \mu^2} \frac{1-u_A}{u_A} \right) \right) \right. \\
& + \text{tr} \left(\{F^{a_2}, F^{a_3}\} F^{a_5} F^{a_4} [F^{a_6}, F^{a_1}] \right) A^{gg(0)}(q_1, p_5^\oplus, p_4^\oplus, q_3) \left(\frac{-1}{\epsilon} + \log \left(\frac{t_3 s_{45}}{t_1 \mu^2} \frac{1-u_{A'}}{u_{A'}} \right) \right) \\
& \left. + \text{tr} \left(\{F^{a_2}, F^{a_3}\} F^{a_4} [F^{a_6}, F^{a_1}] F^{a_5} \right) B^{gg(0)}(q_1, p_4^\oplus, p_5^\oplus, q_3) \log \left(\left(\frac{p_5^-}{p_4^+} \right)^2 \frac{1-u_B}{u_B} \frac{v_B}{1-v_B} \right) \right\}, \tag{F.9}
\end{aligned}$$

$$\begin{aligned}
& \text{Absorp} \left[\mathcal{M}_{\mathcal{N}=4}^{(1)(-,+)}(p_4^\oplus, p_5^\oplus) \right] \xrightarrow{\text{NMRK}} \frac{\pi}{2} g_s^6 \frac{\kappa_\Gamma}{(4\pi)^2} s_{12} C^{g(0)}(p_2^{\nu_2}, p_3^{-\nu_2}) \frac{1}{t_1} \frac{1}{t_3} C^{g(0)}(p_1^{\nu_1}, p_6^{-\nu_1}) \\
& \times \left\{ \text{tr} \left([F^{a_2}, F^{a_3}] F^{a_4} F^{a_5} \{F^{a_6}, F^{a_1}\} \right) A^{gg(0)}(q_1, p_4^\oplus, p_5^\oplus, q_3) \left(\frac{-1}{\epsilon} + \log \left(\frac{t_1 s_{45}}{t_3 \mu^2} \frac{1-u_A}{u_A} \right) \right) \right. \\
& + \text{tr} \left([F^{a_2}, F^{a_3}] F^{a_5} F^{a_4} \{F^{a_6}, F^{a_1}\} \right) A^{gg(0)}(q_1, p_5^\oplus, p_4^\oplus, q_3) \left(\frac{-1}{\epsilon} + \log \left(\frac{t_1 s_{45}}{t_3 \mu^2} \frac{1-u_{A'}}{u_{A'}} \right) \right) \\
& \left. + \text{tr} \left([F^{a_2}, F^{a_3}] F^{a_4} \{F^{a_6}, F^{a_1}\} F^{a_5} \right) B^{gg(0)}(q_1, p_4^\oplus, p_5^\oplus, q_3) \log \left(\left(\frac{p_5^+}{p_4^-} \right)^2 \frac{u_B}{1-u_B} \frac{1-v_B}{v_B} \right) \right\}, \tag{F.10}
\end{aligned}$$

$$\begin{aligned}
& \text{Absorp} \left[\mathcal{M}_{\mathcal{N}=4}^{(1)(+,+)}(p_4^\oplus, p_5^\oplus) \right] \xrightarrow{\text{NMRK}} \frac{\pi}{2} g_s^6 \frac{\kappa_\Gamma}{(4\pi)^2} s_{12} C^{g(0)}(p_2^{\nu_2}, p_3^{-\nu_2}) \frac{1}{t_1} \frac{1}{t_3} C^{g(0)}(p_1^{\nu_1}, p_6^{-\nu_1}) \\
& \times \left\{ \text{tr} \left(\{F^{a_2}, F^{a_3}\} F^{a_4} F^{a_5} \{F^{a_6}, F^{a_1}\} \right) A^{gg(0)}(q_1, p_4^\oplus, p_5^\oplus, q_3) \left(\frac{-1}{\epsilon} + \log \left(\frac{t_1 t_3}{s_{45} \mu^2} \frac{u_A}{1-u_A} \right) \right) \right. \\
& + \text{tr} \left(\{F^{a_2}, F^{a_3}\} F^{a_5} F^{a_4} \{F^{a_6}, F^{a_1}\} \right) A^{gg(0)}(q_1, p_5^\oplus, p_4^\oplus, q_3) \left(\frac{-1}{\epsilon} + \log \left(\frac{t_1 t_3}{s_{45} \mu^2} \frac{u_{A'}}{1-u_{A'}} \right) \right) \\
& \left. + \text{tr} \left(\{F^{a_2}, F^{a_3}\} F^{a_4} \{F^{a_6}, F^{a_1}\} F^{a_5} \right) B^{gg(0)}(q_1, p_4^\oplus, p_5^\oplus, q_3) \log \left(\frac{1-u_B}{u_B} \frac{1-v_B}{v_B} \right) \right\}. \tag{F.11}
\end{aligned}$$

In section 4.3 we show that the absorptive parts listed in eqs. (F.8–F.11) do not contribute to the NLO $gg \rightarrow gggg$ squared matrix element. These terms will only contribute to the squared matrix element at higher orders in the coupling.

Absorptive part of the opposite-helicity amplitude

Here we similarly list the absorptive parts of the colour-dressed amplitude for the case where $\nu_4 = -\nu_5 = \oplus$:

$$\begin{aligned}
& \text{Absorp} \left[\mathcal{M}_{\mathcal{N}=4}^{(1)(-, -)}(p_4^\oplus, p_5^\ominus) \right] \xrightarrow{\text{NMRK}} g_s^6 \frac{\kappa_\Gamma}{(4\pi)^2} s_{12} F^{a_3 a_2 c_1} C^{g(0)}(p_2^\ominus, p_3^\oplus) \frac{1}{t_1} \\
& \times \frac{\pi}{2} \left\{ \text{tr} (F^{c_1} F^{a_4} F^{a_5} F^{c_3}) \left[A^{gg(0)}(q_1, p_4^\oplus, p_5^\ominus, q_3) \left(\frac{-5}{\epsilon} + \log \left(\frac{t_1 s_{45} (p_4^- p_5^+)^2 t_3}{(\mu^2)^5} \frac{u_A}{v_A w_A} \right) \right) \right. \right. \\
& \qquad \qquad \qquad \left. \left. + S_{uv}^A \log(v_A) + S_{wu}^A \log(w_A) \right] \right. \\
& + \text{tr} (F^{c_1} F^{a_5} F^{a_4} F^{c_3}) \left[A^{gg(0)}(q_1, p_5^\ominus, p_4^\oplus, q_3) \left(\frac{-5}{\epsilon} + \log \left(\frac{t_1 s_{45} (p_4^+ p_5^-)^2 t_3}{(\mu^2)^5} \frac{u_{A'}}{v_{A'} w_{A'}} \right) \right) \right. \\
& \qquad \qquad \qquad \left. \left. + S_{uv}^{A'} \log(v_{A'}) + S_{wu}^{A'} \log(w_{A'}) \right] \right. \\
& + \text{tr} (F^{c_1} F^{a_5} F^{c_3} F^{a_4}) \left[B^{gg(0)}(q_1, p_4^\oplus, p_5^\ominus, q_3) \left(\frac{-4}{\epsilon} + \log \left(\frac{t_1^2 t_3^2}{(\mu^2)^4} \right) \right) \right. \\
& \qquad \qquad \qquad \left. \left. - S_{uv}^B \log \left(\frac{w_B}{u_B v_B} \right) \right] \right\} \times \frac{1}{t_3} F^{a_6 a_1 c_3} C^{g(0)}(p_6^\oplus, p_1^\ominus), \tag{F.12}
\end{aligned}$$

$$\begin{aligned}
& \text{Absorp} \left[\mathcal{M}_{\mathcal{N}=4}^{(1)(+, -)}(p_4^\oplus, p_5^\ominus) \right] \xrightarrow{\text{NMRK}} \frac{\pi}{2} g_s^6 \frac{\kappa_\Gamma}{(4\pi)^2} s_{12} C^{g(0)}(p_2^{\nu_2}, p_3^{-\nu_2}) \frac{1}{t_1} \frac{1}{t_3} C^{g(0)}(p_1^{\nu_1}, p_6^{-\nu_1}) \\
& \times \left\{ \text{tr} (\{F^{a_2}, F^{a_3}\} F^{a_4} F^{a_5} [F^{a_6}, F^{a_1}]) \right. \\
& \quad \times \left[A^{gg(0)}(q_1, p_4^\oplus, p_5^\ominus, q_3) \left(\frac{-1}{\epsilon} + \log \left(\frac{t_3 s_{45}}{t_1 \mu^2} \frac{v_A w_A}{u_A} \right) \right) - S_{uv}^A \log(v_A) - S_{wu}^A \log(w_A) \right] \\
& + \text{tr} (\{F^{a_2}, F^{a_3}\} F^{a_5} F^{a_4} [F^{a_6}, F^{a_1}]) \\
& \quad \times \left[A^{gg(0)}(q_1, p_5^\ominus, p_4^\oplus, q_3) \left(\frac{-1}{\epsilon} + \log \left(\frac{t_3 s_{45}}{t_1 \mu^2} \frac{v_{A'} w_{A'}}{u_{A'}} \right) \right) - S_{uv}^{A'} \log(v_{A'}) - S_{wu}^{A'} \log(w_{A'}) \right] \\
& + \text{tr} (\{F^{a_2}, F^{a_3}\} F^{a_4} [F^{a_6}, F^{a_1}] F^{a_5}) \\
& \quad \times \left[2B^{gg(0)}(q_1, p_4^\oplus, p_5^\ominus, q_3) \log \left(\frac{p_5^-}{p_4^+} \right) + S_{vw}^B \log \left(\frac{u_B}{v_B w_B} \right) - S_{wu}^B \log \left(\frac{v_B}{w_B u_B} \right) \right] \Big\}, \tag{F.13}
\end{aligned}$$

$$\begin{aligned}
& \text{Absorp} \left[\mathcal{M}_{\mathcal{N}=4}^{(1)(-,+)}(p_4^\oplus, p_5^\ominus) \right] \xrightarrow{\text{NMRK}} \frac{\pi}{2} g_s^6 \frac{\kappa_\Gamma}{(4\pi)^2} s_{12} C^{g(0)}(p_2^{\nu_2}, p_3^{-\nu_2}) \frac{1}{t_1} \frac{1}{t_3} C^{g(0)}(p_1^{\nu_1}, p_6^{-\nu_1}) \\
& \times \left\{ \text{tr} ([F^{a_2}, F^{a_3}] F^{a_4} F^{a_5} \{F^{a_6}, F^{a_1}\}) \right. \\
& \quad \times \left[A^{gg(0)}(q_1, p_4^\oplus, p_5^\ominus, q_3) \left(\frac{-1}{\epsilon} + \log \left(\frac{t_1 s_{45}}{t_3 \mu^2} \frac{v_A w_A}{u_A} \right) \right) - S_{uv}^A \log(v_A) - S_{wu}^A \log(w_A) \right] \\
& \quad + \text{tr} ([F^{a_2}, F^{a_3}] F^{a_5} F^{a_4} \{F^{a_6}, F^{a_1}\}) \\
& \quad \times \left[A^{gg(0)}(q_1, p_5^\ominus, p_4^\oplus, q_3) \left(\frac{-1}{\epsilon} + \log \left(\frac{t_1 s_{45}}{t_3 \mu^2} \frac{v_{A'} w_{A'}}{u_{A'}} \right) \right) - S_{uv}^{A'} \log(v_{A'}) - S_{wu}^{A'} \log(w_{A'}) \right] \\
& \quad + \text{tr} ([F^{a_2}, F^{a_3}] F^{a_4} \{F^{a_6}, F^{a_1}\} F^{a_5}) \\
& \quad \times \left[2B^{gg(0)}(q_1, p_4^\oplus, p_5^\ominus, q_3) \log \left(\frac{p_5^-}{p_4^+} \right) - S_{vw}^B \log \left(\frac{u_B}{v_B w_B} \right) + S_{wu}^B \log \left(\frac{v_B}{w_B u_B} \right) \right] \Bigg\}, \tag{F.14}
\end{aligned}$$

$$\begin{aligned}
& \text{Absorp} \left[\mathcal{M}_{\mathcal{N}=4}^{(1)(+,+)}(p_4^\oplus, p_5^\ominus) \right] \xrightarrow{\text{NMRK}} \frac{\pi}{2} g_s^6 \frac{\kappa_\Gamma}{(4\pi)^2} s_{12} C^{g(0)}(p_2^{\nu_2}, p_3^{-\nu_2}) \frac{1}{t_1} \frac{1}{t_3} C^{g(0)}(p_1^{\nu_1}, p_6^{-\nu_1}) \\
& \times \left\{ \text{tr} (\{F^{a_2}, F^{a_3}\} F^{a_4} F^{a_5} \{F^{a_6}, F^{a_1}\}) \right. \\
& \quad \times \left[A^{gg(0)}(q_1, p_4^\oplus, p_5^\ominus, q_3) \left(\frac{-1}{\epsilon} + \log \left(\frac{t_1 t_3}{s_{45} \mu^2} \frac{u_A}{v_A w_A} \right) \right) + S_{uv}^A \log(v_A) + S_{wu}^A \log(w_A) \right] \\
& \quad + \text{tr} (\{F^{a_2}, F^{a_3}\} F^{a_5} F^{a_4} \{F^{a_6}, F^{a_1}\}) \\
& \quad \times \left[A^{gg(0)}(q_1, p_5^\ominus, p_4^\oplus, q_3) \left(\frac{-1}{\epsilon} + \log \left(\frac{t_1 t_3}{s_{45} \mu^2} \frac{u_{A'}}{v_{A'} w_{A'}} \right) \right) + S_{uv}^{A'} \log(v_{A'}) + S_{wu}^{A'} \log(w_{A'}) \right] \\
& \quad + \text{tr} (\{F^{a_2}, F^{a_3}\} F^{a_4} \{F^{a_6}, F^{a_1}\} F^{a_5}) \times \left[S_{uv}^B \log \left(\frac{w_B}{u_B v_B} \right) \right] \Bigg\}. \tag{F.15}
\end{aligned}$$

In section 4.3 we show that at the level of the NLO $gg \rightarrow gggg$ squared matrix element, eq. (F.12) is the only absorptive component of the amplitude which can contribute for a specific helicity configuration. This contribution vanishes in the sum over helicities ν_4 and ν_5 . All components eq. (F.8)–(F.15) will contribute at higher orders in the coupling.

G Kinematic limits of the two-gluon central-emission vertex

Starting from the central NMRK region, it is possible to take further kinematic limits to regions which are contained within NMRK. In these more restricted kinematic regions further simplifications occur. A key example are the regions where we additionally require $p_4^+ \gg p_5^+$ or $p_5^+ \gg p_4^+$ which we refer to as the MRK and MRK' limits respectively. These limits of the two-gluon CEV are studied in appendix G.1. From the central NMRK region we may alternatively take the limit where one of the central gluons becomes soft, which is the subject of appendix G.2, or the limit where the two central gluons become collinear to

each other, which is the subject of appendix G.3. These further limits act as checks on the results presented in this paper, and also provide intuition for the kinematic dependence of the cross ratios and the two-gluon CEV. One may also investigate the limits where both of the central gluons become soft, but this is not pursued in this appendix.

G.1 MRK limit

Recall that the MRK (MRK') limit is obtained by taking $X \rightarrow \infty$ ($X \rightarrow 0$). In the MRK or MRK' limit, the tree-level two-gluon CEV factorises into a product of Lipatov vertices times a t -channel pole. This factorization property applies for any helicity configuration, for example, for opposite helicities

$$\begin{aligned} A^{gg(0)}(q_1, p_4^\oplus, p_5^\ominus, q_3) \Big|_{\text{MRK}} &= V^{g(0)}(q_1, p_4^\oplus, q_2) \frac{1}{t_2} V^{g(0)}(q_2, p_5^\ominus, q_3) \\ &= \frac{z}{\bar{z}} (\bar{w} - 1)(\bar{z} - 1), \end{aligned} \quad (\text{G.1})$$

$$\begin{aligned} A^{gg(0)}(q_1, p_5^\ominus, p_4^\oplus, q_3) \Big|_{\text{MRK}'} &= V^{g(0)}(q_1, p_5^\ominus, q'_2) \frac{1}{t'_2} V^{g(0)}(q'_2, p_4^\oplus, q_3) \\ &= \frac{z}{\bar{z}} \frac{(\bar{w}(\bar{z} - 1) - \bar{z})}{(w(z - 1) - z)} (w - 1)(z - 1), \end{aligned} \quad (\text{G.2})$$

with Lipatov vertex $V^{g(0)}$ in eq. (2.9). Considering the opposite helicity configuration at one loop, we saw in section 4.2 that different transcendental terms multiply rational terms which are not simply the tree amplitudes. This prompts an analysis of these individual rational terms in the MRK and MRK' limits. As a consistency check on the MRK and MRK' limits of these individual rational terms, the relevant sums of these rational terms given in eq. (3.22), eq. (3.24), eq. (E.6) and eq. (E.8) should reproduce the limits eq. (G.1) and eq. (G.2).

For the σ_A ordering in the MRK, from eqs. (3.23) and (3.25) we obtain

$$\begin{aligned} R_{uv}^A &\xrightarrow{\text{MRK}} \frac{w - 1}{w - z} A^{gg(0)}(q_1, p_4^\oplus, p_5^\ominus, q_3) \Big|_{\text{MRK}} \\ R_{v\bar{w}}^A &\xrightarrow{\text{MRK}} A^{gg(0)}(q_1, p_4^\oplus, p_5^\ominus, q_3) \Big|_{\text{MRK}} \\ R_{wu}^A &\xrightarrow{\text{MRK}} -\frac{z - 1}{w - z} A^{gg(0)}(q_1, p_4^\oplus, p_5^\ominus, q_3) \Big|_{\text{MRK}} \end{aligned} \quad (\text{G.3})$$

while $R_{u\bar{v}}^A$, R_{vw}^A and $R_{w\bar{u}}^A$ vanish in this limit. All six of these rational terms vanish in the MRK' limit. The limits listed in eq. (G.3) can be used to show eq. (G.1), starting from either of the representations eq. (3.22) or eq. (3.24). On the other hand, for the $\sigma_{A'}$ permutation, all rational terms vanish in MRK. In MRK', $R_{uv}^{A'}$, $R_{v\bar{w}}^{A'}$ and $R_{wu}^{A'}$ vanish, while the remaining terms tend to

$$\begin{aligned} R_{u\bar{v}}^{A'} &\xrightarrow{\text{MRK}'} -\frac{(\bar{w} - 1)\bar{z}^2}{(\bar{w} - \bar{z})(\bar{w}(\bar{z} - 1) - \bar{z})} A^{gg(0)}(q_1, p_5^\ominus, p_4^\oplus, q_3) \Big|_{\text{MRK}'} \\ R_{v\bar{w}}^{A'} &\xrightarrow{\text{MRK}'} A^{gg(0)}(q_1, p_5^\ominus, p_4^\oplus, q_3) \Big|_{\text{MRK}'} \\ R_{w\bar{u}}^{A'} &\xrightarrow{\text{MRK}'} \frac{\bar{w}^2(\bar{z} - 1)}{(\bar{w} - \bar{z})(\bar{w}(\bar{z} - 1) - \bar{z})} A^{gg(0)}(q_1, p_5^\ominus, p_4^\oplus, q_3) \Big|_{\text{MRK}'} . \end{aligned} \quad (\text{G.4})$$

Using the representation eq. (E.6) or eq. (E.8) we see that these limits are consistent with the limit of the tree-level amplitude eq. (G.2). Finally for the B configurations, we get terms that survive in the MRK limit,

$$\begin{aligned}
R_{uv}^B &\xrightarrow{\text{MRK}} -\frac{(w-1)(z-1)}{w(z-1)-z} A^{gg(0)}(q_1, p_4^\oplus, p_5^\ominus, q_3) \Big|_{\text{MRK}} \\
R_{\bar{u}\bar{v}}^B &\xrightarrow{\text{MRK}} 0 \\
R_{vw}^B &\xrightarrow{\text{MRK}} 0 \\
R_{\bar{v}\bar{w}}^B &\xrightarrow{\text{MRK}} -A^{gg(0)}(q_1, p_4^\oplus, p_5^\ominus, q_3) \Big|_{\text{MRK}} \\
R_{wu}^B &\xrightarrow{\text{MRK}} \frac{1}{w(z-1)-z} A^{gg(0)}(q_1, p_4^\oplus, p_5^\ominus, q_3) \Big|_{\text{MRK}} \\
R_{\bar{w}\bar{u}}^B &\xrightarrow{\text{MRK}} 0,
\end{aligned} \tag{G.5}$$

and also terms that survive in the MRK' limit,

$$\begin{aligned}
R_{uv}^B &\xrightarrow{\text{MRK}'} -\frac{(\bar{w}-1)(\bar{z}-1)}{\bar{w}(\bar{z}-1)-\bar{z}} A^{gg(0)}(q_1, p_5^\ominus, p_4^\oplus, q_3) \Big|_{\text{MRK}'} \\
R_{\bar{u}\bar{v}}^B &\xrightarrow{\text{MRK}'} 0 \\
R_{vw}^B &\xrightarrow{\text{MRK}'} \frac{1}{\bar{w}(\bar{z}-1)-\bar{z}} A^{gg(0)}(q_1, p_5^\ominus, p_4^\oplus, q_3) \Big|_{\text{MRK}'} \\
R_{\bar{v}\bar{w}}^B &\xrightarrow{\text{MRK}'} 0 \\
R_{wu}^B &\xrightarrow{\text{MRK}'} 0 \\
R_{\bar{w}\bar{u}}^B &\xrightarrow{\text{MRK}'} -A^{gg(0)}(q_1, p_5^\ominus, p_4^\oplus, q_3) \Big|_{\text{MRK}'}.
\end{aligned} \tag{G.6}$$

The MRK and MRK' limits of the one-loop two gluon CEV in $\mathcal{N} = 4$ SYM are discussed in section 4. The notation introduced in that section makes it trivial to obtain the MRK and MRK' limits of the transcendental terms, with the exception of terms that can be compactly described in terms of the cross ratios of eqs. (3.19), (E.5) and (3.33). To facilitate the investigation of these latter transcendental functions, we list the cross ratios in the MRK and MRK' limits:

$$\begin{aligned}
u_A &\xrightarrow{\text{MRK}} 1, & v_A &\xrightarrow{\text{MRK}} \frac{(-t_1)p_5^+}{(-t_2)p_4^+}, & w_A &\xrightarrow{\text{MRK}} \frac{(-t_3)p_4^-}{(-t_2)p_5^-}, \\
u_{A'} &\xrightarrow{\text{MRK}'} 1, & v_{A'} &\xrightarrow{\text{MRK}'} \frac{(-t_1)p_4^+}{(-t_2')p_5^+}, & w_{A'} &\xrightarrow{\text{MRK}'} \frac{(-t_1)p_5^-}{(-t_2')p_4^-}, \\
u_B &\xrightarrow{\text{MRK}} 1, & v_B &\xrightarrow{\text{MRK}} \frac{p_4^+ p_5^+}{(-t_2)}, & w_B &\xrightarrow{\text{MRK}} \frac{(-t_1)(-t_3)}{(-t_2)p_4^+ p_5^-}, \\
u_B &\xrightarrow{\text{MRK}'} \frac{p_4^+ p_5^-}{(-t_2')}, & v_B &\xrightarrow{\text{MRK}'} 1, & w_B &\xrightarrow{\text{MRK}'} \frac{(-t_1)(-t_3)}{(-t_2')p_4^- p_5^+}.
\end{aligned} \tag{G.7}$$

G.2 Soft limits

In the limit that either of the gluons of the tree two-gluon CEV become soft, $p_4 \rightarrow 0$ or $p_5 \rightarrow 0$, the amplitude given in eq. (3.3) is singular. It factorises into an eikonal factor,

which behaves like $1/p_4$ or $1/p_5$, and a five-gluon amplitude in MRK. For example, taking the limit where all components of p_4 tend to zero at the same rate, eq. (3.3) factorises as

$$M_{6g}^{(0)}(p_1^{\nu_1}, p_2^{\nu_2}, p_3^{\nu_3}, p_4^{\nu_4}, p_5^{\nu_5}, p_6^{\nu_6}) \Big|_{\text{NMRK}} \xrightarrow{p_4 \rightarrow 0} \left[\text{Soft}^{(0)}(p_3, p_4^{\nu_4}, p_5) \right]_{\text{NMRK}} \left[M_{5g}^{(0)}(p_1^{\nu_1}, p_2^{\nu_2}, p_3^{\nu_3}, p_5^{\nu_5}, p_6^{\nu_6}) \right]_{\text{MRK}}, \quad (\text{G.8})$$

where the five-gluon amplitude in MRK is

$$M_{5g}^{(0)}(p_1^{\nu_1}, p_2^{\nu_2}, p_3^{\nu_3}, p_5^{\nu_5}, p_6^{\nu_6}) \Big|_{\text{MRK}} = s C^{g(0)}(p_2^{\nu_2}, p_3^{\nu_3}) \frac{1}{t_1} V^{g(0)}(q_1, p_5^{\nu_5}, q_3) \frac{1}{t_3} C^{g(0)}(p_1^{\nu_1}, p_6^{\nu_6}), \quad (\text{G.9})$$

with $q_3 = q_1 - p_5$ and $V^{g(0)}$ given in eq. (2.9). In eq. (G.8), the positive-helicity soft factor, or eikonal factor is

$$\text{Soft}^{(0)}(p_3, p_4^{\oplus}, p_5) = \frac{\langle 35 \rangle}{\langle 34 \rangle \langle 45 \rangle}. \quad (\text{G.10})$$

Note that this eikonal factor does not depend on the helicities of particles 3 and 5, and in fact not even on their parton flavour. The negative-helicity eikonal factor is obtained by complex conjugation. In the NMRK limit the positive-helicity eikonal factor becomes

$$\text{Soft}^{(0)}(p_3, p_4^{\oplus}, p_5) \Big|_{\text{NMRK}} = \text{Soft}_A^{(0)}(p_4^{\oplus}, p_5) = \frac{p_{5\perp}}{p_{4\perp}} \sqrt{\frac{p_4^+}{p_5^+}} \frac{1}{\langle 45 \rangle}, \quad (\text{G.11})$$

where in the first equality we have introduced a notation which makes it clear that this function no longer depends on p_3 once we have taken the NMRK limit. Using this notation, eq. (G.8) implies that the two-gluon CEV factorises as

$$A^{gg(0)}(q_1, p_4^{\nu_4}, p_5^{\nu_5}, q_3) \xrightarrow{p_4 \rightarrow 0} \text{Soft}_A^{(0)}(p_4^{\nu_4}, p_5) V^{g(0)}(q_1, p_5^{\nu_5}, q_3). \quad (\text{G.12})$$

For the equal-helicity vertex eq. (3.4), which comes from a MHV amplitude, this limit is straightforward to verify. In fact, for such an MHV amplitude, the relation at the amplitude level, eq. (G.8), holds exactly in general kinematics without even requiring that $p_4 \rightarrow 0$. For the opposite-helicity vertex, in order to check eq. (G.12) we have found it most convenient to use the representation in eq. (3.22).

As a step towards obtaining the soft limit of the one-loop amplitude, we first consider the rational coefficients. Specifically, for the limit where all components of p_4 tend to zero at the same rate, the minimal variables of eq. (3.10) and eq. (3.11) satisfy

$$X \rightarrow 0, \quad z \rightarrow -\frac{q_{1\perp}}{p_{4\perp}}, \quad w \rightarrow \frac{q_{1\perp}}{p_{5\perp}}, \quad Xz \rightarrow \text{finite}. \quad (\text{G.13})$$

In this limit R_{uv}^A , R_{vw}^A and $R_{\bar{w}\bar{u}}^A$ tend to zero. The others are given by

$$\begin{aligned} R_{wu}^A &\rightarrow \frac{Xz^2(\bar{w}-1)}{w+Xz}, \\ R_{\bar{u}\bar{v}}^A &\rightarrow -\frac{Xz^2|w-1|^2}{(1+Xz)(w+Xz)}, \\ R_{\bar{v}\bar{w}}^A &\rightarrow \frac{Xz^2(\bar{w}-1)}{1+Xz}. \end{aligned} \quad (\text{G.14})$$

Therefore $R_{uv}^A + R_{vw}^A + R_{wu}^A$ and $R_{\bar{u}\bar{v}}^A + R_{\bar{v}\bar{w}}^A + R_{\bar{w}\bar{u}}^A$ tend to the same limit (that of eq. (G.12)). The results for the A' ordering are no longer related to these by $p_4 \leftrightarrow p_5$ because the specific choice of taking $p_4 \rightarrow 0$ breaks the symmetry. We therefore list them here. The rational coefficients $R_{uv}^{A'}$, $R_{\bar{v}\bar{w}}^{A'}$ and $R_{\bar{w}\bar{u}}^{A'}$ tend to zero. The remaining non-zero coefficients are

$$\begin{aligned} R_{\bar{u}\bar{v}}^{A'} &\rightarrow -\frac{wz(1-\bar{w})}{w+Xz}, \\ R_{vw}^{A'} &\rightarrow \frac{wz(1-\bar{w})^2}{w\bar{w}-w-Xz}, \\ R_{wu}^{A'} &\rightarrow \frac{w\bar{w}Xz^2(1-\bar{w})}{(w+Xz)(w\bar{w}-w-Xz)}, \end{aligned} \quad (\text{G.15})$$

such that again $R_{uv}^{A'} + R_{vw}^{A'} + R_{wu}^{A'}$ and $R_{\bar{u}\bar{v}}^{A'} + R_{\bar{v}\bar{w}}^{A'} + R_{\bar{w}\bar{u}}^{A'}$ give the expected tree-level limit:

$$-\frac{wz(1-\bar{w})}{w+Xz} = \text{Soft}_{A'}^{(0)}(p_4^{\nu_4}, p_5) V^{g(0)}(q_1, p_5^\ominus, q_3), \quad (\text{G.16})$$

where, analogous to eq. (G.11), we have introduced the notation

$$\text{Soft}^{(0)}(p_5, p_4^\oplus, p_6) \Big|_{\text{NMRK}} = \text{Soft}_{A'}^{(0)}(p_4^{\nu_4}, p_5) = -\sqrt{\frac{p_5^+}{p_4^+}} \frac{1}{\langle 45 \rangle}. \quad (\text{G.17})$$

Finally, for the B colour ordering $R_{\bar{u}\bar{v}}^B$, R_{vw}^B and R_{wu}^B tend to zero, leaving

$$\begin{aligned} R_{uv}^B &\rightarrow -(\bar{w}-1)z, \\ R_{\bar{v}\bar{w}}^B &\rightarrow -\frac{Xz^2(\bar{w}-1)}{1+Xz-\bar{w}}, \\ R_{\bar{w}\bar{u}}^B &\rightarrow -\frac{z(\bar{w}-1)^2}{\bar{w}-Xz-1}. \end{aligned} \quad (\text{G.18})$$

These then lead to the expected tree-level result where $R_{uv}^B + R_{vw}^B + R_{wu}^B$ and $R_{\bar{u}\bar{v}}^B + R_{\bar{v}\bar{w}}^B + R_{\bar{w}\bar{u}}^B$ both sum to

$$-(\bar{w}-1)z = \text{Soft}_B^{(0)}(p_4) V^{g(0)}(q_1, p_5^\ominus, q_3), \quad (\text{G.19})$$

where as for the other colour orderings we have introduced

$$\text{Soft}^{(0)}(p_1, p_4^\oplus, p_2) \Big|_{\text{NMRK}} = \text{Soft}_B^{(0)}(p_4) = \frac{1}{p_{4\perp}}, \quad (\text{G.20})$$

which does not even depend on the helicity of the soft particle. The three relevant eikonal functions in the NMRK obey

$$\text{Soft}_A^{(0)}(p_4^{\nu_4}, p_5) + \text{Soft}_{A'}^{(0)}(p_4^{\nu_4}, p_5) + \text{Soft}_B^{(0)}(p_4) = 0, \quad (\text{G.21})$$

consistent with the more general eq. (3.31), and the eikonal identity.

We now turn to the colour-ordered amplitudes at one-loop. Beginning with the same-helicity vertex, taking the limit $p_4 \rightarrow 0$ in eqs. (4.26), (4.32) and (4.35), we find

$$\begin{aligned} N_c \kappa_\Gamma \text{Re} [V_6(\sigma_A)|_{\text{NMRK}}] &\xrightarrow{p_4 \rightarrow 0} E(t_1, s_{35}; t_3, s_{56}) + v^{g(1)}(t_1, |p_{5\perp}|^2, t_3) + N_c s_A^{(1)}(p_4^{\nu_4}, p_5) \\ N_c \kappa_\Gamma \text{Re} [V_6(\sigma_{A'})|_{\text{NMRK}}] &\xrightarrow{p_4 \rightarrow 0} E(t_1, s_{35}; t_3, s_{56}) + v^{g(1)}(t_1, |p_{5\perp}|^2, t_3) + N_c s_{A'}^{(1)}(p_4, p_5), \\ N_c \kappa_\Gamma \text{Re} [V_6(\sigma_B)|_{\text{NMRK}}] &\xrightarrow{p_4 \rightarrow 0} E(t_1, s_{35}; t_3, s_{56}) + v^{g(1)}(t_1, |p_{5\perp}|^2, t_3) + N_c s_B^{(1)}(p_4), \end{aligned} \quad (\text{G.22})$$

where $E(t_1, s_{35}; t_3, s_{56})$ is the natural collection of impact factors and Regge trajectories in the absence of p_4 and $v^{g(1)}$ is the one-loop Lipatov vertex correction given in eq. (4.15). The one-loop soft factor [49] is

$$s^{(1)}(p_3, p_4^{\nu_4}, p_5) = -\kappa_\Gamma \left(\frac{\mu^2(-s_{35})}{(-s_{34})(-s_{45})} \right)^\epsilon \left(\frac{1}{\epsilon^2} + \frac{\pi^2}{6} \right) + \mathcal{O}(\epsilon^2), \quad (\text{G.23})$$

which must first be analytically continued to our physical region, discussed in section A.1, and then taken in the NMRK limit. In eq. (G.22) we have used the notation

$$s_A^{(1)}(p_4, p_5) = \text{Re} \left[s^{(1)}(p_3, p_4, p_5) \Big|_{\text{NMRK}} \right], \quad (\text{G.24})$$

$$s_{A'}^{(1)}(p_4, p_5) = \text{Re} \left[s^{(1)}(p_4, p_5, p_6) \Big|_{\text{NMRK}} \right], \quad (\text{G.25})$$

$$s_B^{(1)}(p_4) = \text{Re} \left[s^{(1)}(p_1, p_4, p_2) \Big|_{\text{NMRK}} \right], \quad (\text{G.26})$$

which, as for the analogous tree-level functions, more clearly indicate the simpler kinematic dependence of these one-loop soft functions in the NMRK limit.

Eq. (G.22) exactly matches the expected sum of the one-loop corrections to the non-central pieces, the Lipatov vertex for the single emission of p_5 and the one-loop soft function. From eq. (4.23), these are multiplied by the soft limit of the corresponding tree-level amplitude for that ordering.

Turning now to the opposite-helicity case in eq. (4.61), and starting with the A colour ordering, we find

$$\begin{aligned} S_{wu}^A &\xrightarrow{p_4 \rightarrow 0} \text{Soft}_A^{(0)}(p_4^{\nu_4}, p_5) V^{g(0)}(q_1, p_5^\ominus, q_3), \\ \text{Re} [W_1(\sigma_A) - W_2(\sigma_A)] &\xrightarrow{p_4 \rightarrow 0} 0, \\ \text{Re} [W_3(\sigma_A) - W_2(\sigma_A)] &\xrightarrow{p_4 \rightarrow 0} \log \left(\frac{s_{34} t_3}{s_{35} t_1} \right) \log \left(\frac{|p_{5\perp}|^2}{s_{45}} \right). \end{aligned} \quad (\text{G.27})$$

This allows us to extract a common factor of the tree amplitude multiplying

$$\text{Re} [2W_2(\sigma_A) + (W_3(\sigma_A) - W_2(\sigma_A))].$$

Using eqs. (4.68) and (4.69), we find

$$\begin{aligned}
& \text{Re} [2W_2(\sigma_A) + (W_3(\sigma_A) - W_2(\sigma_A))] |_{\text{NMRK}} \\
&= \text{Re} [V_6(\sigma_A) - \Delta V_A(u_A, v_A, w_A) + \Delta W_A(u_A, v_A, w_A) + (W_3(\sigma_A) - W_2(\sigma_A))] |_{\text{NMRK}} \\
&\xrightarrow{p_4 \rightarrow 0} \text{Re} [V_6(\sigma_A)] |_{\text{NMRK}, p_4 \rightarrow 0},
\end{aligned} \tag{G.28}$$

where the cancellation in the last line arises from the soft limit of eqs. (4.30), (4.70) and (G.27). Eq. (G.22) then immediately gives the expected one-loop structure which equals that found for the same-helicity vertex. The helicity-dependence in the soft limit is contained only in the tree-level factors.

Similarly for the A' -ordering we find

$$\begin{aligned}
S_{uv}^{A'} &\xrightarrow{p_4 \rightarrow 0} \text{Soft}_{A'}^{(0)}(p_4^{\nu_4}, p_5) V^{g(0)}(q_1, p_5^\ominus, q_3), \\
\text{Re} [W_1(\sigma_{A'}) - W_2(\sigma_{A'})] |_{\text{NMRK}} &\xrightarrow{p_4 \rightarrow 0} \log \left(\frac{s_{46} t_1}{s_{56} t_3} \right) \log \left(\frac{|p_{5\perp}|^2}{s_{45}} \right), \\
\text{Re} [W_3(\sigma_{A'}) - W_2(\sigma_{A'})] |_{\text{NMRK}} &\xrightarrow{p_4 \rightarrow 0} 0.
\end{aligned} \tag{G.29}$$

Extracting a common coefficient of the tree amplitude leaves

$$\text{Re} [2W_2(\sigma_{A'}) + (W_1(\sigma_{A'}) - W_2(\sigma_{A'}))] |_{\text{NMRK}} \xrightarrow{p_4 \rightarrow 0} \text{Re} [V_6(\sigma_{A'})] |_{\text{NMRK}, p_4 \rightarrow 0}, \tag{G.30}$$

as expected. Finally for the B ordering,

$$\begin{aligned}
S_{vw}^B + S_{wu}^B &\xrightarrow{p_4 \rightarrow 0} \text{Soft}_B^{(0)}(p_4) V^{g(0)}(q_1, p_5^\ominus, q_3), \\
\text{Re} [W_2(\sigma_B) - W_1(\sigma_B)] |_{\text{NMRK}} &\xrightarrow{p_4 \rightarrow 0} \log \left(\frac{s_{24} s_{56}}{s_{12} t_1} \right) \log \left(\frac{s_{14} s_{35}}{s_{12} t_3} \right), \\
\text{Re} [W_3(\sigma_B) - W_1(\sigma_B)] |_{\text{NMRK}} &\xrightarrow{p_4 \rightarrow 0} \log \left(\frac{s_{24} s_{56}}{s_{12} t_1} \right) \log \left(\frac{s_{14} s_{35}}{s_{12} t_3} \right).
\end{aligned} \tag{G.31}$$

As the final two limits are equal, one again factors out the tree amplitude leaving

$$\text{Re} [2W_1(\sigma_B) + (W_2(\sigma_B) - W_1(\sigma_B))] |_{\text{NMRK}} \xrightarrow{p_4 \rightarrow 0} \text{Re} [V_6(\sigma_B)] |_{\text{NMRK}, p_4 \rightarrow 0}. \tag{G.32}$$

Finally, performing the change of basis of colour structures in eq. (4.42), we collect the

results of this appendix in the following expression for general helicities,

$$\begin{aligned}
& \text{Disp} \left[\mathcal{M}_{\mathcal{N}=4}^{(1)}(p_4^{\nu_4}, p_5^{\nu_5}) \right] \xrightarrow{\text{NMRK}, p_4 \rightarrow 0} \\
& \frac{g_s^6}{(4\pi)^2} s_{12} F^{a_3 a_2 c_1} C^{g(0)}(p_2^{\nu_2}, p_3^{-\nu_2}) \frac{1}{t_1} V^{g(0)}(q_1, p_5^{\nu_5}, q_3) \times \\
& \left\{ (F^{a_4} F^{a_5})_{c_1 c_3} \left[\text{Soft}_A(p_4^{\nu_4}, p_5) \left(3 v^{g(1)}(t_1, |p_{5\perp}|^2, t_3) + N_c \left(2s_A^{(1)}(p_4, p_5) + s_B^{(1)}(p_4) \right) \right. \right. \right. \\
& \quad \left. \left. + 3 E(t_1, s_{35}; t_3, s_{56}) \right) + N_c \text{Soft}_{A'}(p_4^{\nu_4}, p_5) \left(s_{A'}^{(1)}(p_4, p_5) - s_B^{(1)}(p_4) \right) \right] \\
& \quad + (F^{a_5} F^{a_4})_{c_1 c_3} \left[\text{Soft}_{A'}(p_4^{\nu_4}, p_5) \left(3 v^{g(1)}(t_1, |p_{5\perp}|^2, t_3) + N_c \left(2s_{A'}^{(1)}(p_4, p_5) + s_B^{(1)}(p_4) \right) \right. \right. \\
& \quad \left. \left. + 3 E(t_1, s_{35}; t_3, s_{56}) \right) + N_c \text{Soft}_A(p_4^{\nu_4}, p_5) \left(s_A^{(1)}(p_4, p_5) - s_B^{(1)}(p_4) \right) \right] \\
& \quad + d_A^{c_1 a_{\sigma_4} a_{\sigma_5} c_3} \left[\text{Soft}_A(p_4^{\nu_4}, p_5) \left(s_A^{(1)}(p_4, p_5) - s_B^{(1)}(p_4) \right) \right. \\
& \quad \left. \left. + \text{Soft}_{A'}(p_4^{\nu_4}, p_5) \left(s_{A'}^{(1)}(p_4, p_5) - s_B^{(1)}(p_4) \right) \right] \right\} \times \frac{1}{t_3} F^{a_6 a_1 c_3} C^{g(0)}(p_1^{\nu_1}, p_6^{-\nu_1}) .
\end{aligned} \tag{G.33}$$

G.3 Collinear limits

In this appendix we investigate the behaviour of the one-loop amplitude eq. (4.75) in the collinear limit,

$$p_4 \rightarrow z_4 P, \quad p_5 \rightarrow z_5 P, \quad z_4 + z_5 = 1. \tag{G.34}$$

We begin by recalling the collinear limit of the colour ordered six-gluon tree-level amplitude in general kinematics. It factorises into a divergent splitting amplitude, which behaves like $1/\langle 45 \rangle$ or $1/[45]$, and a five-gluon amplitude,

$$M_{6g}^{(0)}(p_1^{\nu_1}, p_2^{\nu_2}, p_3^{\nu_3}, p_4^{\nu_4}, p_5^{\nu_5}, p_6^{\nu_6}) \xrightarrow{p_4 \parallel p_5} \sum_{\nu=\pm} \text{Split}_{-\nu}^{(0)}(p_4^{\nu_4}, p_5^{\nu_5}) M_{5g}^{(0)}(p_1^{\nu_1}, p_2^{\nu_2}, p_3^{\nu_3}, P^\nu, p_6^{\nu_6}), \tag{G.35}$$

where we sum over the helicities of the intermediate state P^ν . For an equal-helicity pair, the tree-level splitting amplitudes are

$$\text{Split}_{\ominus}^{(0)}(p_4^{\oplus}, p_5^{\oplus}) = \frac{1}{\sqrt{z_4 z_5} \langle 45 \rangle}, \quad \text{Split}_{\oplus}^{(0)}(p_4^{\oplus}, p_5^{\oplus}) = 0, \tag{G.36}$$

while for an opposite-helicity pair, they are

$$\text{Split}_{\oplus}^{(0)}(p_4^{\oplus}, p_5^{\ominus}) = \frac{z_5^2}{\sqrt{z_4 z_5} \langle 45 \rangle}, \quad \text{Split}_{\ominus}^{(0)}(p_4^{\oplus}, p_5^{\ominus}) = -\frac{z_4^2}{\sqrt{z_4 z_5} [45]}. \tag{G.37}$$

In the central NMRK limit, eq. (G.35) becomes

$$\begin{aligned}
& M_{6g}^{(0)}(p_1^{\nu_1}, p_2^{\nu_2}, p_3^{\nu_3}, p_4^{\nu_4}, p_5^{\nu_5}, p_6^{\nu_6}) \Big|_{\text{NMRK}} \\
& \xrightarrow{p_4 \parallel p_5} \sum_{\nu=\pm} \text{Split}_{-\nu}^{(0)}(p_4^{\nu_4}, p_5^{\nu_5}) M_{5g}^{(0)}(p_1^{\nu_1}, p_2^{\nu_2}, p_3^{\nu_3}, P^\nu, p_6^{\nu_6}) \Big|_{\text{MRK}},
\end{aligned} \tag{G.38}$$

where the five-gluon amplitude in MRK is given in eq. (G.9), with $q_3 = q_1 - P$. In particular, the two-gluon CEV factorises as

$$A^{gg(0)}(q_1, p_4^{\nu_4}, p_5^{\nu_5}, q_3) \stackrel{p_4 \parallel p_5}{=} \sum_{\nu=\pm} \text{Split}_{-\nu}^{(0)}(p_4^{\nu_4}, p_5^{\nu_5}) V^{g(0)}(q_1, P^\nu, q_3). \quad (\text{G.39})$$

For the equal-helicity vertex eq. (3.4), it is straightforward to verify eq. (G.39). For the opposite-helicity vertex, we have found it more convenient to check eq. (G.39) by starting from eq. (3.22) or eq. (3.24) rather than eq. (3.5), where as we have mentioned in section 3.2, the BCFW representations make clear the collinear singularity structure of the amplitudes. Working in the minimal variables, the collinear limit can be expressed as

$$\begin{aligned} w &\xrightarrow{p_4 \parallel p_5} -\frac{z_4}{z_5} z, \\ X &\xrightarrow{p_4 \parallel p_5} \frac{z_4}{z_5}. \end{aligned} \quad (\text{G.40})$$

For the σ_A ordering we find that four of the six rational terms factorise into a splitting function and Lipatov vertex, while two of the rational terms do not diverge in this limit (unless we move to the further soft-collinear limits of $z_4 \rightarrow 0$ or $z_4 \rightarrow 1$),

$$\begin{aligned} R_{uv}^A &\xrightarrow{p_4 \parallel p_5} V^{g(0)}(q_1, P^\oplus, q_3) \text{Split}_{\ominus}^{(0)}(p_4^\oplus, p_5^\ominus), \\ R_{\bar{u}\bar{v}}^A &\xrightarrow{p_4 \parallel p_5} V^{g(0)}(q_1, P^\ominus, q_3) \text{Split}_{\oplus}^{(0)}(p_4^\oplus, p_5^\ominus), \\ R_{vw}^A &\xrightarrow{p_4 \parallel p_5} -\frac{(z-1)(zz_4+z_5)z_5}{(\bar{z}-1)(\bar{z}z_4+z_5)(|z|^2z_4+z_5)}, \\ R_{\bar{v}\bar{w}}^A &\xrightarrow{p_4 \parallel p_5} -\frac{z^4z_4^2(\bar{z}-1)(\bar{z}z_4+z_5)}{z_5(z-1)(zz_4+z_5)(|z|^2z_4+z_5)}, \\ R_{wu}^A &\xrightarrow{p_4 \parallel p_5} V^{g(0)}(q_1, P^\ominus, q_3) \text{Split}_{\oplus}^{(0)}(p_4^\oplus, p_5^\ominus), \\ R_{\bar{w}\bar{u}}^A &\xrightarrow{p_4 \parallel p_5} V^{g(0)}(q_1, P^\oplus, q_3) \text{Split}_{\ominus}^{(0)}(p_4^\oplus, p_5^\ominus). \end{aligned} \quad (\text{G.41})$$

Analogous results for the $\sigma_{A'}$ ordering can be found by exchanging $p_4 \leftrightarrow p_5$ and taking the complex conjugate, as in eq. (E.12). For the σ_B ordering, as expected, none of the rational terms diverge in this limit,

$$\begin{aligned} R_{uv}^B &\xrightarrow{p_4 \parallel p_5} \frac{|z-1|^2|zz_4+z_5|^2}{z_5((z-1)z_4+z_5)\bar{z}}, \\ R_{\bar{u}\bar{v}}^B &\xrightarrow{p_4 \parallel p_5} 0, \\ R_{vw}^B &\xrightarrow{p_4 \parallel p_5} \frac{z_5(z-1)(zz_4+z_5)}{\bar{z}(|z|^2z_4+z_5)((z+\bar{z}-1)z_4+z_5)}, \\ R_{\bar{v}\bar{w}}^B &\xrightarrow{p_4 \parallel p_5} \frac{z^3z_4^2(\bar{z}-1)(\bar{z}z_4+z_5)}{z_5(|z|^2z_4+z_5)((z+\bar{z}-1)z_4+z_5)}, \\ R_{wu}^B &\xrightarrow{p_4 \parallel p_5} \frac{z_5z_4^2(\bar{z}-1)(\bar{z}z_4+z_5)}{((z-1)z_4+z_5)((z+\bar{z}-1)z_4+z_5)(|z_5+(z-1)z_4|^2+z_4z_5)}, \\ R_{\bar{w}\bar{u}}^B &\xrightarrow{p_4 \parallel p_5} \frac{(z-1)(zz_4+z_5)((\bar{z}-1)z_4+z_5)^3}{z_5((z+\bar{z}-1)z_4+z_5)(|z_5+(z-1)z_4|^2+z_4z_5)}. \end{aligned} \quad (\text{G.42})$$

From these lists of rational terms we can immediately verify that the divergent pieces satisfy the condition in eq. (G.39) from the representations eq. (3.22) or eq. (3.24). We note that in this limit the divergent pieces also satisfy

$$A^{gg(0)}(q_1, p_4^{\nu_4}, p_5^{\nu_5}, q_3) \Big|_{p_4 \parallel p_5} = - A^{gg(0)}(q_1, p_5^{\nu_5}, p_4^{\nu_4}, q_3) \Big|_{p_4 \parallel p_5}. \quad (\text{G.43})$$

In addition to eq. (G.34), the amplitude in eq. (3.3) is divergent in the collinear regions $p_{3\perp} = -q_{1\perp} \rightarrow 0$ or $p_{6\perp} = q_{3\perp} \rightarrow 0$. In those regions, eq. (3.3) must not diverge more rapidly than $1/|q_{i\perp}|$, with $i = 1, 3$, in order for the related cross section not to diverge more than logarithmically. Since eq. (3.3) displays poles as $|q_{1\perp}|^2$ and $|q_{3\perp}|^2$ go to zero, the central-emission vertex must be at least linear in $|q_{i\perp}|$ as $|q_{i\perp}| \rightarrow 0$,

$$A^{gg(0)}(q_1, p_4^{\nu_4}, p_5^{\nu_5}, q_3) \Big|_{q_{i\perp} \rightarrow 0} \mathcal{O}(|q_{i\perp}|), \quad (\text{G.44})$$

with $i = 1, 3$, which is indeed fulfilled by eq. (3.5).

Let us now consider the collinear limit of the one-loop amplitudes in $\mathcal{N} = 4$ SYM in the NMRK limit. It is most convenient if we work at the level of colour-ordered amplitudes, where in general kinematics the colour-ordered one-loop six gluon amplitude has the collinear limit [73],

$$M_{6g}^{(1)}(p_2^{\nu_2}, p_3^{\nu_3}, p_4^{\nu_4}, p_5^{\nu_5}, p_6^{\nu_6}, p_1^{\nu_1}) \xrightarrow{p_4 \parallel p_5} \sum_{\nu=\pm} \left(\text{Split}_{-\nu}^{(0)}(p_4^{\nu_4}, p_5^{\nu_5}) M_{5g}^{(1)}(p_2^{\nu_2}, p_3^{\nu_3}, P^\nu, p_6^{\nu_6}, p_1^{\nu_1}) \right. \\ \left. + \text{Split}_{-\nu}^{(1)}(p_4^{\nu_4}, p_5^{\nu_5}) M_{5g}^{(0)}(p_2^{\nu_2}, p_3^{\nu_3}, P^\nu, p_6^{\nu_6}, p_1^{\nu_1}) \right), \quad (\text{G.45})$$

where the one-loop splitting functions were obtained in [73]. In $\mathcal{N} = 4$ SYM, these splitting functions are proportional to the tree-level splitting function,

$$\text{Split}_{-\nu}^{(1)}(p_4^{\nu_4}, p_5^{\nu_5}) = \kappa_\Gamma \text{Split}_{-\nu}^{(0)}(p_4^{\nu_4}, p_5^{\nu_5}) r_S^{\text{SUSY}}(z_4, s_{45}), \quad (\text{G.46})$$

where the loop factor,

$$r_S^{\text{SUSY}}(z_4, s_{45}) = -\frac{1}{\epsilon^2} \left(\frac{\mu^2}{z_4(1-z_4)(-s_{45})} \right)^\epsilon + 2 \log(z_4) \log(1-z_4) - \frac{\pi^2}{6}, \quad (\text{G.47})$$

is independent of the helicities. In the central NMRK limit we expect to obtain

$$M_{6g}^{(1)}(p_2^{\nu_2}, p_3^{\nu_3}, p_4^{\nu_4}, p_5^{\nu_5}, p_6^{\nu_6}, p_1^{\nu_1}) \Big|_{\text{NMRK}} \xrightarrow{p_4 \parallel p_5} \sum_{\nu=\pm} \left(\text{Split}_{-\nu}^{(0)}(p_4^{\nu_4}, p_5^{\nu_5}) M_{5g}^{(1)}(p_2^{\nu_2}, p_3^{\nu_3}, P^\nu, p_6^{\nu_6}, p_1^{\nu_1}) \Big|_{\text{MRK}} \right. \\ \left. + \text{Split}_{-\nu}^{(1)}(p_4^{\nu_4}, p_5^{\nu_5}) M_{5g}^{(0)}(p_2^{\nu_2}, p_3^{\nu_3}, P^\nu, p_6^{\nu_6}, p_1^{\nu_1}) \Big|_{\text{MRK}} \right). \quad (\text{G.48})$$

Let us check this first for the same-helicity case. As we are working at the level of colour-ordered amplitudes, we consider the three representative orderings of eq. (4.23). For the σ_A colour ordering, we find

$$s_{234} \xrightarrow{p_4 || p_5} z_5 t_1 + z_4 t_3, \quad (\text{G.49})$$

so that in the collinear limit,

$$v_A + w_A \xrightarrow{p_4 || p_5} 1. \quad (\text{G.50})$$

In particular, this allows us to use the identity,

$$\text{Li}_2(1-x) + \text{Li}_2(x) = \frac{\pi^2}{6} - \log(1-x) \log(x). \quad (\text{G.51})$$

to write

$$\begin{aligned} \Delta V_A(u_A, v_A, w_A) \xrightarrow{p_4 || p_5} N_c \kappa_\Gamma & \left(-\frac{1}{4} \log^2 \left(\frac{s_{45}}{|P_\perp|^2} \right) - \frac{1}{2} \log \left(\frac{s_{45}}{|P_\perp|^2} \right) \log \left(\frac{t_1 t_3 z_4 z_5}{s_{234}^2} \right) \right. \\ & \left. + \log \left(\frac{z_4 t_3}{s_{234}} \right) \log \left(\frac{z_5 t_1}{s_{234}} \right) \right). \end{aligned} \quad (\text{G.52})$$

For the full transcendental function of this colour ordering we find

$$\begin{aligned} N_c \kappa_\Gamma \text{Re} [V_6(\sigma_A)|_{\text{NMRK}}] \xrightarrow{p_4 || p_5} & E(t_1, p_3^+ P^-; t_3, P^+ p_6^-) + v_{\mathcal{N}=4}^{g(1)}(t_1, |P_\perp|^2, t_3) \\ & + N_c \text{Re} [r^{\text{SUSY}}(z_4, s_{45})], \end{aligned} \quad (\text{G.53})$$

which is invariant under $p_4 \leftrightarrow p_5$. After manipulating the colour factors to obtain the natural association of one adjoint generator with each three-point tree-level factor, we obtain

$$\begin{aligned} \text{Re} \left[\mathcal{M}_{\mathcal{N}=4}^{(1)}(p_4^\oplus, p_5^\oplus) \right] \xrightarrow{\text{NMRK}, p_4 || p_5} & \frac{g_S^6}{(4\pi)^2} \kappa_\Gamma s_{12} \left[F^{a_3 a_2 c_1} C^{g(0)}(p_2^\nu, p_3^{-\nu_2}) \right] \frac{1}{t_1} \\ & \times \left[F^{c_1 c_3 c_2} V^{g(0)}(q_1, P^\oplus, q_3) \right] \left[F^{c_2 a_5 a_4} \text{Split}_\ominus^{(0)}(p_4^\oplus, p_5^\oplus) \right] \\ & \times \frac{1}{t_3} \left[F^{a_6 a_1 c_3} C^{g(0)}(p_1^\nu, p_6^{-\nu_1}) \right] \times \left\{ N_c \text{Re} [V_6(\sigma_A)]|_{\text{NMRK}, p_4 || p_5} \right\}. \end{aligned} \quad (\text{G.54})$$

The opposite-helicity case proceeds similarly. From eq. (G.41) we see that in the collinear limit, both S_{uv}^A and S_{wu}^A are equal to the tree-level amplitude, and these terms combine with the ΔW_A term to play the same role as ΔV_A in this limit,

$$\begin{aligned} A^{gg(0)}(q_1, p_4^\oplus, p_4^\ominus, q_3) \Delta W_A(u_A, v_A, w_A) + S_{uv}^A \log(v_A) \left(\frac{w_A}{u_A} \right) + S_{wu}^A \log(w_A) \left(\frac{v_A}{u_A} \right) \\ \xrightarrow{p_4 || p_5} \left(\sum_{\nu=\pm} V^{g(0)}(q_1, P^\nu, q_3) \text{Split}_{-\nu}^{(0)}(p_4^\oplus, p_5^\ominus) \right) \Delta V_A(u_A, v_A, w_A)|_{p_4 || p_5} \end{aligned} \quad (\text{G.55})$$

This means we can straightforwardly write

$$\begin{aligned}
& \text{Re} \left[\mathcal{M}_{\mathcal{N}=4}^{(1)}(p_4^\oplus, p_5^\ominus) \right] \xrightarrow{\text{NMRK}, p_4 || p_5} \\
& \frac{g_s^6}{(4\pi)^2} \kappa_\Gamma s_{12} \left[F^{a_3 a_2 c_1} C^{g(0)}(p_2^{\nu_2}, p_3^{-\nu_2}) \right] \frac{1}{t_1} \\
& \times \sum_{\nu=\pm} \left(\left[F^{c_1 c_3 c_2} V^{g(0)}(q_1, P^\nu, q_3) \right] \left[F^{c_2 a_5 a_4} \text{Split}_{-\nu}^{(0)}(p_4^\oplus, p_5^\ominus) \right] \right) \\
& \times \frac{1}{t_3} \left[F^{a_6 a_1 c_3} C^{g(0)}(p_1^{\nu_1}, p_6^{-\nu_1}) \right] \times \left\{ N_c \text{Re} [V_6(\sigma_A)]|_{\text{NMRK}, p_4 || p_5} \right\}.
\end{aligned} \tag{G.56}$$

References

- [1] L.N. Lipatov, *Reggeization of the Vector Meson and the Vacuum Singularity in Nonabelian Gauge Theories*, *Sov. J. Nucl. Phys.* **23** (1976) 338.
- [2] E.A. Kuraev, L.N. Lipatov and V.S. Fadin, *Multi - Reggeon Processes in the Yang-Mills Theory*, *Sov. Phys. JETP* **44** (1976) 443.
- [3] E.A. Kuraev, L.N. Lipatov and V.S. Fadin, *The Pomeron Singularity in Nonabelian Gauge Theories*, *Sov. Phys. JETP* **45** (1977) 199.
- [4] I.I. Balitsky and L.N. Lipatov, *The Pomeron Singularity in Quantum Chromodynamics*, *Sov. J. Nucl. Phys.* **28** (1978) 822.
- [5] V.S. Fadin and L.N. Lipatov, *BFKL pomeron in the next-to-leading approximation*, *Phys. Lett.* **B429** (1998) 127 [[hep-ph/9802290](#)].
- [6] M. Ciafaloni and G. Camici, *Energy scale(s) and next-to-leading BFKL equation*, *Phys. Lett.* **B430** (1998) 349 [[hep-ph/9803389](#)].
- [7] A.V. Kotikov and L.N. Lipatov, *NLO corrections to the BFKL equation in QCD and in supersymmetric gauge theories*, *Nucl. Phys.* **B582** (2000) 19 [[hep-ph/0004008](#)].
- [8] A.V. Kotikov and L.N. Lipatov, *DGLAP and BFKL equations in the $\mathcal{N}=4$ supersymmetric gauge theory*, *Nucl. Phys.* **B661** (2003) 19 [[hep-ph/0208220](#)].
- [9] A.H. Mueller and H. Navelet, *An Inclusive Minijet Cross-Section and the Bare Pomeron in QCD*, *Nucl. Phys. B* **282** (1987) 727.
- [10] V. Del Duca and C.R. Schmidt, *Dijet production at large rapidity intervals*, *Phys. Rev. D* **49** (1994) 4510 [[hep-ph/9311290](#)].
- [11] W.J. Stirling, *Production of jet pairs at large relative rapidity in hadron hadron collisions as a probe of the perturbative pomeron*, *Nucl. Phys. B* **423** (1994) 56 [[hep-ph/9401266](#)].
- [12] J.R. Andersen, V. Del Duca, S. Frixione, C.R. Schmidt and W.J. Stirling, *Mueller-Navelet jets at hadron colliders*, *JHEP* **02** (2001) 007 [[hep-ph/0101180](#)].
- [13] D. Colferai, F. Schwennsen, L. Szymanowski and S. Wallon, *Mueller Navelet jets at LHC - complete NLL BFKL calculation*, *JHEP* **12** (2010) 026 [[1002.1365](#)].
- [14] J.R. Andersen and J.M. Smillie, *Multiple Jets at the LHC with High Energy Jets*, *JHEP* **06** (2011) 010 [[1101.5394](#)].

- [15] B. Ducloue, L. Szymanowski and S. Wallon, *Confronting Mueller-Navelet jets in NLL BFKL with LHC experiments at 7 TeV*, *JHEP* **05** (2013) 096 [[1302.7012](#)].
- [16] J. Bartels, L.N. Lipatov and A. Sabio Vera, *BFKL Pomeron, Reggeized gluons and Bern-Dixon-Smirnov amplitudes*, *Phys. Rev. D* **80** (2009) 045002 [[0802.2065](#)].
- [17] L.J. Dixon, C. Duhr and J. Pennington, *Single-valued harmonic polylogarithms and the multi-Regge limit*, *JHEP* **10** (2012) 074 [[1207.0186](#)].
- [18] B. Basso, S. Caron-Huot and A. Sever, *Adjoint BFKL at finite coupling: a short-cut from the collinear limit*, *JHEP* **01** (2015) 027 [[1407.3766](#)].
- [19] V. Del Duca, S. Druc, J. Drummond, C. Duhr, F. Dulat, R. Marzucca et al., *Multi-Regge kinematics and the moduli space of Riemann spheres with marked points*, *JHEP* **08** (2016) 152 [[1606.08807](#)].
- [20] V. Del Duca, S. Druc, J.M. Drummond, C. Duhr, F. Dulat, R. Marzucca et al., *All-order amplitudes at any multiplicity in the multi-Regge limit*, *Phys. Rev. Lett.* **124** (2020) 161602 [[1912.00188](#)].
- [21] S. Caron-Huot, D. Chicherin, J. Henn, Y. Zhang and S. Zoia, *Multi-Regge Limit of the Two-Loop Five-Point Amplitudes in $\mathcal{N} = 4$ Super Yang-Mills and $\mathcal{N} = 8$ Supergravity*, *JHEP* **10** (2020) 188 [[2003.03120](#)].
- [22] S. Caron-Huot, *When does the gluon reggeize?*, *JHEP* **05** (2015) 093 [[1309.6521](#)].
- [23] S. Caron-Huot, E. Gardi and L. Vernazza, *Two-parton scattering in the high-energy limit*, *JHEP* **06** (2017) 016 [[1701.05241](#)].
- [24] S. Caron-Huot, E. Gardi, J. Reichel and L. Vernazza, *Infrared singularities of QCD scattering amplitudes in the Regge limit to all orders*, *JHEP* **03** (2018) 098 [[1711.04850](#)].
- [25] S. Caron-Huot, E. Gardi, J. Reichel and L. Vernazza, *Two-parton scattering amplitudes in the Regge limit to high loop orders*, *JHEP* **08** (2020) 116 [[2006.01267](#)].
- [26] G. Falcioni, E. Gardi, N. Maher, C. Milloy and L. Vernazza, *Scattering amplitudes in the Regge limit and the soft anomalous dimension through four loops*, *JHEP* **03** (2022) 053 [[2111.10664](#)].
- [27] V. Del Duca, L.J. Dixon, C. Duhr and J. Pennington, *The BFKL equation, Mueller-Navelet jets and single-valued harmonic polylogarithms*, *JHEP* **02** (2014) 086 [[1309.6647](#)].
- [28] V. Del Duca, C. Duhr, R. Marzucca and B. Verbeek, *The analytic structure and the transcendental weight of the BFKL ladder at NLL accuracy*, *JHEP* **10** (2017) 001 [[1705.10163](#)].
- [29] V. Del Duca, C. Duhr and V.A. Smirnov, *An Analytic Result for the Two-Loop Hexagon Wilson Loop in $\mathcal{N} = 4$ SYM*, *JHEP* **03** (2010) 099 [[0911.5332](#)].
- [30] V. Del Duca, C. Duhr and V.A. Smirnov, *The Two-Loop Hexagon Wilson Loop in $\mathcal{N} = 4$ SYM*, *JHEP* **05** (2010) 084 [[1003.1702](#)].
- [31] L.J. Dixon and M. von Hippel, *Bootstrapping an NMHV amplitude through three loops*, *JHEP* **10** (2014) 065 [[1408.1505](#)].
- [32] J.M. Henn and B. Mistlberger, *Four-Gluon Scattering at Three Loops, Infrared Structure, and the Regge Limit*, *Phys. Rev. Lett.* **117** (2016) 171601 [[1608.00850](#)].
- [33] S. Caron-Huot, L.J. Dixon, A. McLeod and M. von Hippel, *Bootstrapping a Five-Loop Amplitude Using Steinmann Relations*, *Phys. Rev. Lett.* **117** (2016) 241601 [[1609.00669](#)].

- [34] O. Almehid, C. Duhr, E. Gardi, A. McLeod and C.D. White, *Bootstrapping the QCD soft anomalous dimension*, *JHEP* **09** (2017) 073 [[1706.10162](#)].
- [35] S. Caron-Huot, L.J. Dixon, F. Dulat, M. von Hippel, A.J. McLeod and G. Papathanasiou, *Six-Gluon amplitudes in planar $\mathcal{N} = 4$ super-Yang-Mills theory at six and seven loops*, *JHEP* **08** (2019) 016 [[1903.10890](#)].
- [36] F. Caola, A. Chakraborty, G. Gambuti, A. von Manteuffel and L. Tancredi, *Three-loop gluon scattering in QCD and the gluon Regge trajectory*, [2112.11097](#).
- [37] V. Fadin, *Chapter 4: BFKL — Past and Future*, in *From the Past to the Future*, J. Bartels, V. Fadin, E. Levin, A. Levy, V. Kim and A. Sabio-Vera, eds., pp. 63–90 (2021), DOI [[2012.11931](#)].
- [38] V.S. Fadin, R. Fiore, M.G. Kozlov and A.V. Reznichenko, *Proof of the multi-Regge form of QCD amplitudes with gluon exchanges in the NLA*, *Phys. Lett. B* **639** (2006) 74 [[hep-ph/0602006](#)].
- [39] V.S. Fadin, M.G. Kozlov and A.V. Reznichenko, *Gluon Reggeization in Yang-Mills Theories*, *Phys. Rev. D* **92** (2015) 085044 [[1507.00823](#)].
- [40] V.S. Fadin, M.I. Kotsky and R. Fiore, *Gluon Reggeization in QCD in the next-to-leading order*, *Phys. Lett. B* **359** (1995) 181.
- [41] V.S. Fadin, R. Fiore and M.I. Kotsky, *Gluon Regge trajectory in the two loop approximation*, *Phys. Lett. B* **387** (1996) 593 [[hep-ph/9605357](#)].
- [42] V.S. Fadin, R. Fiore and A. Quartarolo, *Reggeization of quark quark scattering amplitude in QCD*, *Phys. Rev. D* **53** (1996) 2729 [[hep-ph/9506432](#)].
- [43] J. Blumlein, V. Ravindran and W.L. van Neerven, *On the gluon Regge trajectory in $O(\alpha_s^{*2})$* , *Phys. Rev. D* **58** (1998) 091502 [[hep-ph/9806357](#)].
- [44] V. Del Duca and E.W.N. Glover, *The High-energy limit of QCD at two loops*, *JHEP* **10** (2001) 035 [[hep-ph/0109028](#)].
- [45] V.S. Fadin and L.N. Lipatov, *Radiative corrections to QCD scattering amplitudes in a multi - Regge kinematics*, *Nucl. Phys. B* **406** (1993) 259.
- [46] V.S. Fadin, R. Fiore and A. Quartarolo, *Quark contribution to the reggeon - reggeon - gluon vertex in QCD*, *Phys. Rev. D* **50** (1994) 5893 [[hep-th/9405127](#)].
- [47] V.S. Fadin, R. Fiore and M.I. Kotsky, *Gribov's theorem on soft emission and the reggeon-reggeon - gluon vertex at small transverse momentum*, *Phys. Lett. B* **389** (1996) 737 [[hep-ph/9608229](#)].
- [48] V. Del Duca and C.R. Schmidt, *Virtual next-to-leading corrections to the Lipatov vertex*, *Phys. Rev. D* **59** (1999) 074004 [[hep-ph/9810215](#)].
- [49] Z. Bern, V. Del Duca and C.R. Schmidt, *The Infrared behavior of one loop gluon amplitudes at next-to-next-to-leading order*, *Phys. Lett. B* **445** (1998) 168 [[hep-ph/9810409](#)].
- [50] V.S. Fadin and L.N. Lipatov, *High-Energy Production of Gluons in a QuasimultiRegge Kinematics*, *JETP Lett.* **49** (1989) 352.
- [51] V. Del Duca, *Real next-to-leading corrections to the multi - gluon amplitudes in the helicity formalism*, *Phys. Rev. D* **54** (1996) 989 [[hep-ph/9601211](#)].
- [52] V.S. Fadin and L.N. Lipatov, *Next-to-leading corrections to the BFKL equation from the gluon and quark production*, *Nucl. Phys. B* **477** (1996) 767 [[hep-ph/9602287](#)].

- [53] V. Del Duca, *Quark - anti-quark contribution to the multi - gluon amplitudes in the helicity formalism*, *Phys. Rev. D* **54** (1996) 4474 [[hep-ph/9604250](#)].
- [54] V. Del Duca, *Next-to-leading corrections to the BFKL equation*, *Frascati Phys. Ser.* **5** (1996) 463 [[hep-ph/9605404](#)].
- [55] J. Bartels, D. Colferai and G.P. Vacca, *The NLO jet vertex for Mueller-Navelet and forward jets: The Quark part*, *Eur. Phys. J. C* **24** (2002) 83 [[hep-ph/0112283](#)].
- [56] J. Bartels, D. Colferai and G.P. Vacca, *The NLO jet vertex for Mueller-Navelet and forward jets: The Gluon part*, *Eur. Phys. J. C* **29** (2003) 235 [[hep-ph/0206290](#)].
- [57] V.S. Fadin and R. Fiore, *Quark contribution to the gluon-gluon - reggeon vertex in QCD*, *Phys. Lett. B* **294** (1992) 286.
- [58] V.S. Fadin, R. Fiore and A. Quartarolo, *Radiative corrections to quark quark reggeon vertex in QCD*, *Phys. Rev. D* **50** (1994) 2265 [[hep-ph/9310252](#)].
- [59] V. Del Duca and C.R. Schmidt, *Virtual next-to-leading corrections to the impact factors in the high-energy limit*, *Phys. Rev. D* **57** (1998) 4069 [[hep-ph/9711309](#)].
- [60] C. Duhr, *New techniques in QCD*, Ph.D. thesis, Louvain U., CP3, 2009.
- [61] N. Gromov, F. Levkovich-Maslyuk and G. Sizov, *Pomeron Eigenvalue at Three Loops in $\mathcal{N}=4$ Supersymmetric Yang-Mills Theory*, *Phys. Rev. Lett.* **115** (2015) 251601 [[1507.04010](#)].
- [62] V.N. Velizhanin, *BFKL pomeron in the next-to-next-to-leading approximation in the planar $\mathcal{N}=4$ SYM theory*, [1508.02857](#).
- [63] V.N. Velizhanin, *NNLLA BFKL pomeron eigenvalue in the planar $\mathcal{N}=4$ SYM theory*, [2106.06527](#).
- [64] V. Del Duca, G. Falcioni, L. Magnea and L. Vernazza, *Analyzing high-energy factorization beyond next-to-leading logarithmic accuracy*, *JHEP* **02** (2015) 029 [[1409.8330](#)].
- [65] V.S. Fadin and L.N. Lipatov, *Reggeon cuts in QCD amplitudes with negative signature*, *Eur. Phys. J. C* **78** (2018) 439 [[1712.09805](#)].
- [66] G. Falcioni, E. Gardi, C. Milloy and L. Vernazza, *Climbing three-Reggeon ladders: four-loop amplitudes in the high-energy limit in full colour*, *Phys. Rev. D* **103** (2021) L111501 [[2012.00613](#)].
- [67] V.S. Fadin, *Three-Reggeon Cuts in QCD Amplitudes*, *Phys. Atom. Nucl.* **84** (2021) 100.
- [68] G. Falcioni, E. Gardi, N. Maher, C. Milloy and L. Vernazza, *Disentangling the Regge Cut and Regge Pole in Perturbative QCD*, *Phys. Rev. Lett.* **128** (2022) 132001 [[2112.11098](#)].
- [69] V. Del Duca, R. Marzucca and B. Verbeek, *The gluon Regge trajectory at three loops from planar Yang-Mills theory*, *JHEP* **01** (2022) 149 [[2111.14265](#)].
- [70] V. Del Duca, A. Frizzo and F. Maltoni, *Factorization of tree QCD amplitudes in the high-energy limit and in the collinear limit*, *Nucl. Phys. B* **568** (2000) 211 [[hep-ph/9909464](#)].
- [71] E.N. Antonov, L.N. Lipatov, E.A. Kuraev and I.O. Cherednikov, *Feynman rules for effective Regge action*, *Nucl. Phys. B* **721** (2005) 111 [[hep-ph/0411185](#)].
- [72] Z. Bern, L.J. Dixon and D.A. Kosower, *One loop corrections to five gluon amplitudes*, *Phys. Rev. Lett.* **70** (1993) 2677 [[hep-ph/9302280](#)].

- [73] Z. Bern, L.J. Dixon, D.C. Dunbar and D.A. Kosower, *One loop n point gauge theory amplitudes, unitarity and collinear limits*, *Nucl. Phys. B* **425** (1994) 217 [[hep-ph/9403226](#)].
- [74] Z. Bern, L.J. Dixon, D.C. Dunbar and D.A. Kosower, *Fusing gauge theory tree amplitudes into loop amplitudes*, *Nucl. Phys. B* **435** (1995) 59 [[hep-ph/9409265](#)].
- [75] V. Del Duca, *Equivalence of the Parke-Taylor and the Fadin-Kuraev-Lipatov amplitudes in the high-energy limit*, *Phys. Rev. D* **52** (1995) 1527 [[hep-ph/9503340](#)].
- [76] L.N. Lipatov, *High-energy scattering in QCD and in quantum gravity and two-dimensional field theories*, *Nucl. Phys. B* **365** (1991) 614.
- [77] V. Del Duca, C. Duhr and E.W. Nigel Glover, *The Five-gluon amplitude in the high-energy limit*, *JHEP* **12** (2009) 023 [[0905.0100](#)].
- [78] V. Del Duca, C. Duhr, E.W. Nigel Glover and V.A. Smirnov, *The One-loop pentagon to higher orders in epsilon*, *JHEP* **01** (2010) 042 [[0905.0097](#)].
- [79] B.A. Kniehl and O.V. Tarasov, *Analytic result for the one-loop scalar pentagon integral with massless propagators*, *Nucl. Phys. B* **833** (2010) 298 [[1001.3848](#)].
- [80] M.G. Kozlov and R.N. Lee, *One-loop pentagon integral in d dimensions from differential equations in ϵ -form*, *JHEP* **02** (2016) 021 [[1512.01165](#)].
- [81] N. Syrrakos, *Pentagon integrals to arbitrary order in the dimensional regulator*, *JHEP* **06** (2021) 037 [[2012.10635](#)].
- [82] V. Del Duca, C. Duhr, E. Gardi, L. Magnea and C.D. White, *An infrared approach to Reggeization*, *Phys. Rev. D* **85** (2012) 071104 [[1108.5947](#)].
- [83] V. Del Duca, C. Duhr, E. Gardi, L. Magnea and C.D. White, *The Infrared structure of gauge theory amplitudes in the high-energy limit*, *JHEP* **12** (2011) 021 [[1109.3581](#)].
- [84] V. Del Duca, G. Falcioni, L. Magnea and L. Vernazza, *High-energy QCD amplitudes at two loops and beyond*, *Phys. Lett. B* **732** (2014) 233 [[1311.0304](#)].
- [85] V.S. Fadin, *Particularities of the NNLLA BFKL*, *AIP Conf. Proc.* **1819** (2017) 060003 [[1612.04481](#)].
- [86] V. Del Duca, C. Duhr, E. Gardi, L. Magnea and C.D. White, *An infrared approach to Reggeization*, *Phys. Rev. D* **85** (2012) 071104 [[1108.5947](#)].
- [87] S. Mandelstam, *Non-Regge Terms in the Vector-Spinor Theory*, *Phys. Rev.* **137** (1965) B949.
- [88] P.D.B. Collins, *An Introduction to Regge Theory and High-Energy Physics*, Cambridge Monographs on Mathematical Physics, Cambridge Univ. Press, Cambridge, UK (5, 2009), [10.1017/CBO9780511897603](#).
- [89] M. Canay and V. Del Duca, *One-loop impact factor for the emission of two gluons*, *JHEP* **06** (2021) 034 [[2103.16593](#)].
- [90] R. Britto, F. Cachazo and B. Feng, *New recursion relations for tree amplitudes of gluons*, *Nucl. Phys. B* **715** (2005) 499 [[hep-th/0412308](#)].
- [91] R. Britto, F. Cachazo, B. Feng and E. Witten, *Direct proof of tree-level recursion relation in Yang-Mills theory*, *Phys. Rev. Lett.* **94** (2005) 181602 [[hep-th/0501052](#)].
- [92] F. Cachazo, P. Svrcek and E. Witten, *MHV vertices and tree amplitudes in gauge theory*, *JHEP* **09** (2004) 006 [[hep-th/0403047](#)].

- [93] M.L. Mangano, S.J. Parke and Z. Xu, *Duality and Multi - Gluon Scattering*, *Nucl. Phys. B* **298** (1988) 653.
- [94] J.M. Drummond, J. Henn, G.P. Korchemsky and E. Sokatchev, *Conformal Ward identities for Wilson loops and a test of the duality with gluon amplitudes*, *Nucl. Phys. B* **826** (2010) 337 [[0712.1223](#)].
- [95] J.M. Drummond, J. Henn, G.P. Korchemsky and E. Sokatchev, *Dual superconformal symmetry of scattering amplitudes in $\mathcal{N}=4$ super-Yang-Mills theory*, *Nucl. Phys. B* **828** (2010) 317 [[0807.1095](#)].
- [96] V. Del Duca, *Parke-Taylor amplitudes in the multi - Regge kinematics*, *Phys. Rev. D* **48** (1993) 5133 [[hep-ph/9304259](#)].
- [97] J.H. Weis, *Factorization of multi-regge amplitudes*, *Phys. Rev. D* **4** (1971) 1777.
- [98] G. Veneziano, *Origin and intercept of the Pomeron singularity*, *Phys. Lett. B* **43** (1973) 413.
- [99] F.A. Berends and W.T. Giele, *Multiple Soft Gluon Radiation in Parton Processes*, *Nucl. Phys. B* **313** (1989) 595.
- [100] Z. Bern and D.A. Kosower, *Color decomposition of one loop amplitudes in gauge theories*, *Nucl. Phys. B* **362** (1991) 389.
- [101] R. Kleiss and H. Kuijf, *Multi - Gluon Cross-sections and Five Jet Production at Hadron Colliders*, *Nucl. Phys. B* **312** (1989) 616.
- [102] V. Del Duca, L.J. Dixon and F. Maltoni, *New color decompositions for gauge amplitudes at tree and loop level*, *Nucl. Phys. B* **571** (2000) 51 [[hep-ph/9910563](#)].
- [103] V. Del Duca, C. Duhr and E.W.N. Glover, *Iterated amplitudes in the high-energy limit*, *JHEP* **12** (2008) 097 [[0809.1822](#)].
- [104] D.A. Kosower and P. Uwer, *One loop splitting amplitudes in gauge theory*, *Nucl. Phys. B* **563** (1999) 477 [[hep-ph/9903515](#)].
- [105] Z. Bern, V. Del Duca, W.B. Kilgore and C.R. Schmidt, *The infrared behavior of one loop QCD amplitudes at next-to-next-to leading order*, *Phys. Rev. D* **60** (1999) 116001 [[hep-ph/9903516](#)].